COLLAGEN FILMS AS SUBSTRATES FOR FLEXIBLE ELECTRONICS

by

Salvador Moreno

APPROVED BY SUPERVISORY COMMITTEE:

_____

Dr. Majid Minary, Chair

_____

Dr. Manuel Quevedo-Lopez

_____

Dr. Shalini Prasad

_____

Dr. Walter Voit

To my parents

COLLAGEN FILMS AS SUBSTRATES FOR FLEXIBLE ELECTRONICS

by

SALVADOR MORENO, BS, MS

DISSERTATION

Presented to the Faculty of

The University of Texas at Dallas

in Partial Fulfillment

of the Requirements

for the Degree of

DOCTOR OF PHILOSOPHY IN

MECHANICAL ENGINEERING

THE UNIVERSITY OF TEXAS AT DALLAS

May 2019

ACKNOWLEDGEMENTS

To venture out into unexplored areas of science, it is important to be in environment with freedom and tools to explore ideas. I would like to thank Dr. Majid Minary for providing me with that environment over the course of my graduate school career. It is not a simple task to take a chance on an unproven senior undergraduate. I would like to thank the members of my committee, Dr. Manuel Quevedo, Dr. Walter Voit, and Dr. Shalini Prasad, for seeing the potential in my work and offering me their advice and support. It is also important to acknowledge the team I was a part of, who served not only as collaborators and coauthors, but also as mentors and a source of support and encouragement. I would like to acknowledge Dr. Mahmoud Baniasadi and Dr. Zhe Xu serving as the senior members of our lab when I started. Thanks to Dr. Soheil Daryadel, Dr. Reza Morsali, Dr. Ali Behroozfar, Dr. Jiacheng Huang, and Dr. Enlong Yang, all of whom were part of the lab during my studies as well as Andrea Rivera, Samantha Smith and the almost dozen undergraduate students who came through my mentorship. I would also like to acknowledge the members of Dr. Quevedo's team who also helped with my development such as Dr. Martha Serna, Dr. Israel Mejia, and other members of his team such as Rodolfo Rodriguez and Javad Keshtkar. I would also like to acknowledge Dr. Brian Rodriguez's team at University College Dublin who expanded my knowledge base such as Arwa Bazaid and Hossam Ibrahim. The cleanroom staff, the Mechanical Engineering staff, and the McDermott Fellowship staff led by Mrs. Reena Schellenberg proved to be invaluable. I would also like acknowledge the National Science Foundation Graduate Research and McDermott Fellowships for funding my research.

April 2019

COLLAGEN FILMS AS SUBSTRATES FOR FLEXIBLE ELECTRONICS

Salvador Moreno, PhD
The University of Texas at Dallas, 2019

Supervising Professor: Majid Minary

With fast progress in the field of implantable electronics, pushing towards an integration of technology with humans, the biocompatibility of these electronics is a key issue. Collagen, one of the most abundant proteins in mammalian tissues, is a well-known biomaterial used in tissue engineering and bone scaffolds. Our preliminary studies showed that collagen could be used as a substrate for flexible electronics made using with E-Beam (electron beam) deposition by shadow mask. This allows you to make passive sensors with electrodes such as temperature sensors and strain sensors as well as active devices such as antennas and heaters. However, in order to make more advanced electronic devices, manufacturing strategies need to be developed in order to overcome limitations of collagen for these applications, namely processing temperature and mechanical stability in water. Transfer printing of electronics is one such strategy, using sacrificial layers of plastics, which also have their own temperature limitations. Germanium oxide is presented in this dissertation as novel water based sacrificial layer, which is amenable to high temperature processes such as the annealing and doping of Zinc Oxide (ZnO) via Pulse Laser Deposition (PLD). A number of devices presented in this dissertation include capacitors, transistors, and an integrated inverter transistor circuit. After etching in water overnight, devices

made on wafers are lifted off and transferred to collagen films. By using crosslinkers, devices built on collagen films can be programmatically enhanced to resist enzymatic digestion. Cross-linked collagen was shown to have enhanced mechanical and thermal properties Encapsulated integrated electrical devices transferred onto collagen were shown to have minimal effects on cell viability on assays on MC3T3 osteoblast and A549 epithelial cells. Together, this dissertation demonstrates a manufacturing strategy of developing biocompatible integrated electrical devices on collagen.

TABLE OF CONTENTS

LIST OF FIGURES

LIST OF ABBREVIATIONS AND ACRONYMS

A549	Adenocarcinomic human alveolar basal epithelial cell line
AFM	Atomic Force Microscopy
ARG	Argenine
BOE	Buffered Oxide Etch
CVD	Chemical Vapor Deposition
DAPI	4′,6-diamidino-2-phenylindole stain
DGEA	Aspertate-Glycine-Glutamate-Alanine
DSC	Differential Scanning Calorimetry
ECM	Extracellular matrix
EDAC	(1-ethyl-3-(3-dimethylaminopropyl)carbodiimide hydrochloride)
EDC	(1-ethyl-3-(3-dimethylaminopropyl)carbodiimide hydrochloride)
FBR	Foreign Body Reaction
FDA	Food and Drug Administration
FTIR	Fourier-transform infrared spectroscopy
GATR	Grazing angle attenuated total reflectance
GFOGER	Glycine-Phenylalanine-Hydroxyproline-Glycine-Glutamate-Arginine
GLY	Glycine
GTA	Glutaraldehyde
HBSS	Hank’s Balanced Salt Solution
HCL	Hydrogen Chloride
IDVG	Drain Current vs. Gate Voltage

IGZO	Indium Gallium Zinc Oxide
IR	Infrared
ITO	Indium Tin Oxide
IV	Current vs Voltage
LED	Light Emitting Diode
LYS	Lysine
MC3T3	Mouse Calvaria osteoblastic cell line
MEA	Multielectrode Array
MIM	Metal Insulator Metal
MTS	(3-[4,5,dimethylthiazol-2-yl]-5-[3-carboxymethoxy-phenyl]-2-[4- sulfophenyl]-2H-tetrazolium
PBS	Phosphate Buffered Saline
PECVD	Plasma Enhanced Chemical Vapor Deposition
PET	Polyethylene terephthalate
PI	Polyimide
PLGA	Poly(lactic-co-glycolic acid)
PMMA	Poly(methyl methacrylate)
PVA	Poly(vinyl alcohol)
RF	Radio Frequency
RMS	Root mean square
SEM	Scanning electron microscopy
TFT	Thin film transistor

TNBS	Trinitrobenzensulfonic acid
TRITC	Tetramethylrhodamine
UV-Vis	Ultraviolet-visible
UNT	Untreated
Vin	Voltage In
Vout	Voltage Out
ZnO	Zinc Oxide

CHAPTER 1

INTRODUCTION

Background

Sensing of biological phenomena in situ and in vivo requires a unique strategy for both device design and choice of materials. Such strategy must include device and materials that are biocompatible, biodegradable and environmentally benign. Novel applications in biomedical areas demand development of wearable and implantable electronic devices that interface efficiently and seamlessly with biological systems [1-6].There are several characteristics that are deemed essential for functional implantable devices: a) the substrate should be flexible and conformal to the target tissue; b) the elastic mismatch between the device and the tissue should be minimal; c) the devices must be biocompatible and preferably biodegradable; d) the devices should be amenable to minimally invasive implantation; and e) the materials used for the device should have a high chance to be approved by the FDA and other similar institutions.

Various materials have been used as substrates for fabrication of devices for biomedical applications and in particular for implantation purposes [7, 8]. In particular, substrates based on organic materials offer several advantages when they interface with living biological systems, and might potentially satisfy several of the criteria given above. Thus, synthetic polymers such as poly (ethylene terephthalate) (PET) [9-11], poly (imide) PI [12] and poly (ether sulfone) [13] have been used as substrates as seen in Figure 1D. Other organic materials have been also used as active layers in operational amplifiers [14], ferroelectric memories [15], and digital circuits [16]. Poly

(L-lactide-co-glycolide) (PLGA), as one of the most common biodegradable polymers used in temporary medical implants has been a frequent component in biomedical devices and drug delivery systems [17, 18]. Water soluble polymers, such as dextran and poly (vinyl alcohol), have also been used as tissue engineering scaffolds [19]. Cellulose and silk fibroin are the only polymers derived from living systems that have been evaluated as components in bioelectronics as transistors, sensors and photovoltaic cells [20, 21] as seen in Figure 1C and 1E.

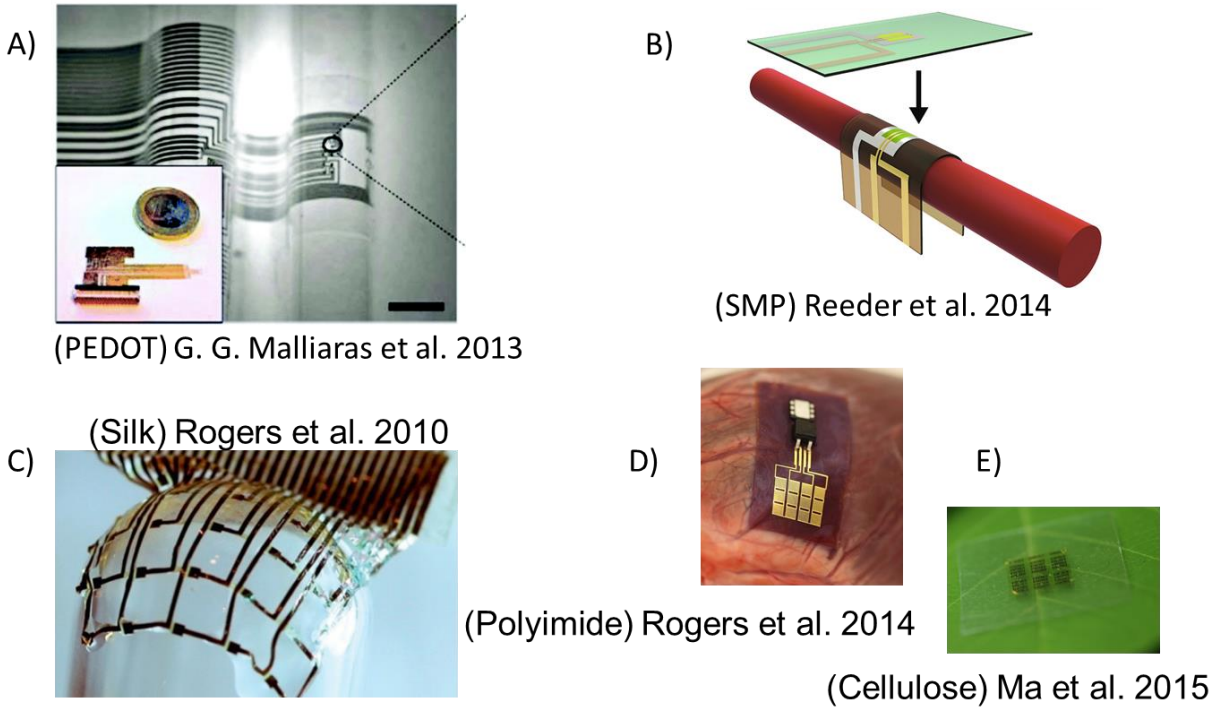

Figure 1. *(A) PEDOT Multielectrode Array (MEA) [22], (B) Shape memory polymer neuroelectrode [23], (C) Silk MEA neurostimulator [1], (D) Kapton energy harvester [24], (E) Cellulose Integrated Circuit [25].*

Flexible electronics requires different strategies depending on the area of application. Wearable electronics for example need be flexible and conformal to the area of their application and further benefit from being stretchable as demonstrated by Lu and Kim [26] on silicone and rubber. Other considerations include the interface between the skin and the substrate which can cause rashes

depending on the interaction. Epidermal electronics demonstrated flexible conformable devices on polyester using polyvinyl alcohol (PVA), which is biocompatible, to stick them onto skin conformably similar to a tattoo [27] showing no adverse effects to the substrate.

Implantable electronics, however, have to deal with a completely different environment in addition to the previously mentioned constraints of flexibility, elastic mismatch, conformality, and stretch ability depending on the application to avoid direct physical damage. Implantable electronics also have to take into consideration the immune response to the device. Upon implantation [28], devices first acquire a layer of proteins (including collagen, fibronectin, among others) from interstitial fluids such as blood. Through this absorbed layer, cells sense foreign surfaces [29] and this process determines the immune response and by extension the foreign body response (FBR). Macrophages and monocytes are attracted to the implant site by chemokines and inflammatory molecules due to tissue injury that releases them through the blood clotting system as demonstrated by Roberto Weigert in Figure 2 [30], A cascading series of signals trigger the fusion of macrophages into foreign-body giant cells which cannot phagocytose the large implant and begin damaging it by releasing reactive oxygen species (ROS) and degradative enzymes (including granules such as collagenase) leading to an acidic environment and potentially leading to device failure. Over the course of the foreign body response, the immune protection is compromised due to immune cell apoptosis, leading to an infection and the formation of a film around the implant called fibrotic encapsulation to isolate the implant from its surrounding environment.

Timescales for this process can vary depending on the variation of the FBR and the extent of the injury. In the case of an infarction, i.e. the blocking of blood supply, leading to tissue death, acute inflammatory events occur within the first week, with chronic effects such as the formation of a fibrotic scar resulting after two weeks [31]. In the case of injuries due to implantation in the central nervous system, such as brain electrodes, inflammation after the trauma can last two to four weeks with scarring forming by 6 weeks [32]. With the variation in timescales, it is therefore important to take into account that they vary by tissue to tissues when designing implants.

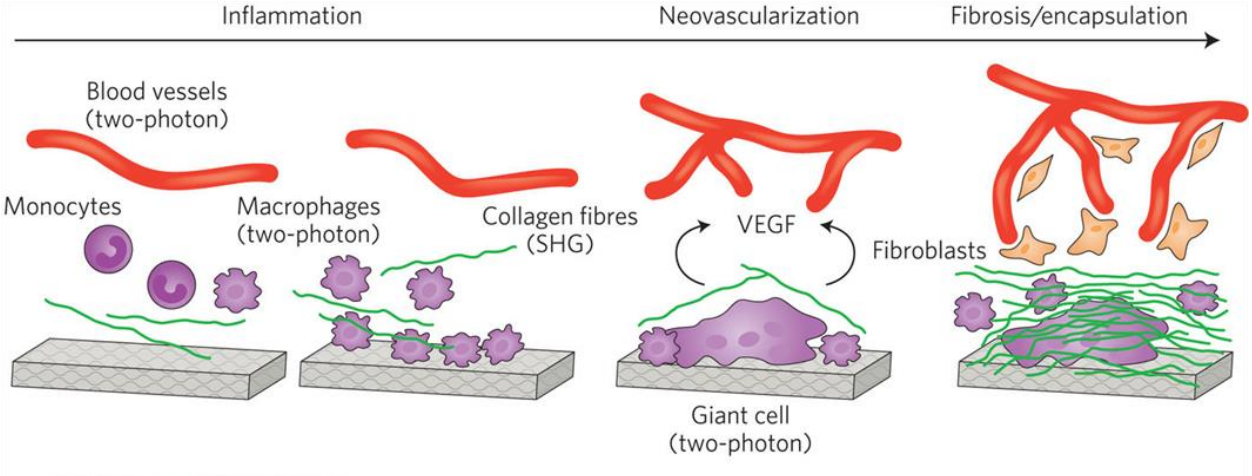

Figure 2. *The Foreign Body Response multistep process* [30].

The premise of biopolymers as substrates is that they are biodegradable, as in the body can degrade them because of their composition. Silk is a prominent material in this field because it is easy to process and flexible [1]. Silk is bioresorbable because it degrades into amino acids that the body can absorb. The mechanical properties of silk can be changed by reducing the Beta-sheet content in the fibroin which also affects the degradation rate. In this manner, the lifetime of devices encapsulated with silk can be modulated for different applications. Although it is possible to fabricate directly on silk since it withstands organic solvents, transfer printing is the primary

method used to fabricate devices on silk [33]. By fabricating on a carrier substrate with a sacrificial layer and then transferring to silk, it is possible to fabricate complex devices with a variety of semiconductor processes, without limitations. However, while the substrate is biocompatible, biodegradable, and bioresorbable, what about the electronics? Electronic components (such as conductors including gold and copper, semiconductors such as doped silicon, dielectrics such as aluminum oxide), have to be biocompatible as well. To account for this requirement, the field of flexible electronics evolved to include transient electronics that are fully bioresorbable including the components of the electronics. As demonstrated by Rogers et al. [33], electronics including conductors such as magnesium (Mg) and zinc (Zn) were demonstrated on silk as opposed to inert gold. Other electronic layers demonstrated were devices using semiconductors of magnesium oxide and zinc oxide as well as silicon oxide. Each individual layer was studied as to what chemical reactions occurred in the physiological chemical environment with precise amount of layer material in each device determines dissolution rate to show fully transient electronics. Devices demonstrated in by Rogers et al. on silk include antennas with rectifying circuits, transistors, multielectrode arrays, wireless heaters, and drug delivery systems.

The focus of this dissertation is one of the most extensively studied biopolymers, collagen. It is also one of the oldest biopolymers, as the word “collagen” is derived from the Greek words for glue [34]. This is because tissues that contained the protein collagen were boiled to make the first glues. The word collagen evolved to define the constituent of connective tissues or the biological glue that held cells together as in 1838 collagen was properly discovered by Payen [35]. The

modern view of collagen from the scientific perspective is that it is a major component of the extracellular matrix (ECM).

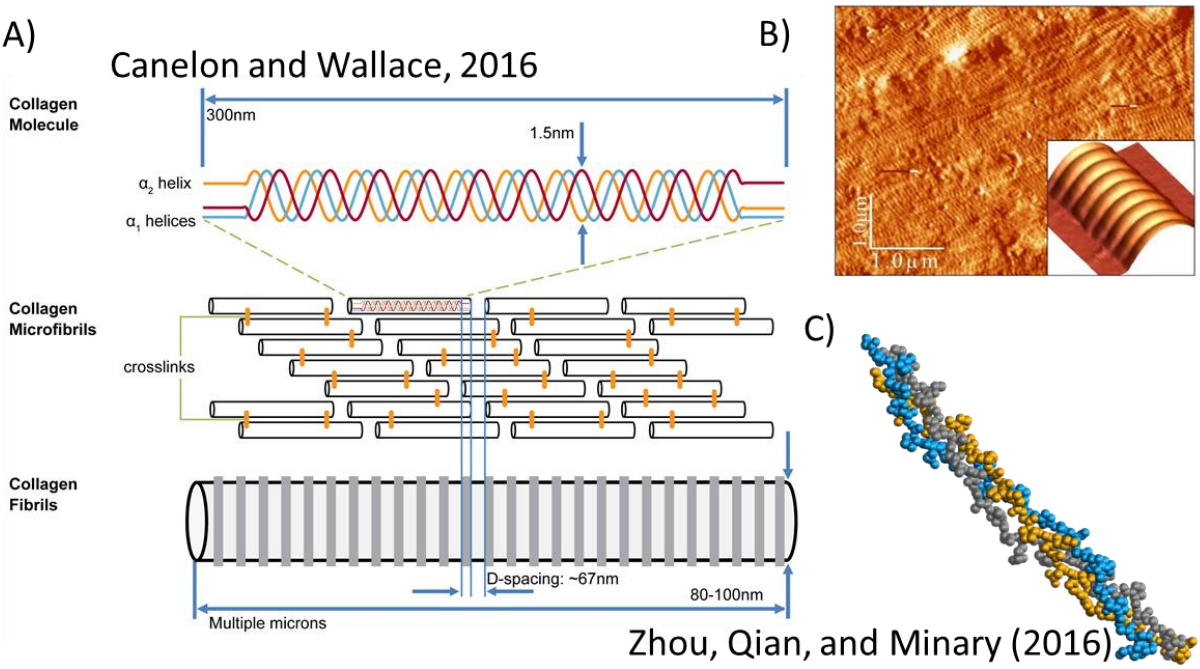

Figure 3. *(A) Collagen fibrillar structure hierarchy* [36], *(B) collagen fibers in bone* [37], *and (C) collagen molecule triple helix* [38].

Collagen belongs to a family of over 20 proteins that are the major constituents of all vertebrates, all of which have amino acid sequences of $[Gly\text{-}X\text{-}Y]_{n.}$ Collagen types differ in the pattern of this sequence of Glycine (GLY) and other amino acids. In particular, collagen type I (Col-I), a variant that forms higher order structures [36] called fibrils, and which is the focus of this dissertation. Collagen Type I consists of three peptide chains forming a triple helical molecule (α_1,α_1,α_2) called tropocollagen which is held together by hydrogen bonds as shown in Figure 3C. Collagen type I is an important component of extracellular matrix (ECM) and is found in all tissues, particularly in connective tissue such as dermal skin compartment, tendon, cornea and bone [39, 40, 41]. Fibroblasts are the major cell type that synthesizes collagen type I and secrete it into the

extracellular domain as single triple helical molecule. In the prevailing physiological environment, the collagen self assembles into micro-fibrils and fibrils, then as fibers or various sizes/thicknesses and finally as bundles of fibers [36]. Collagen is insoluble in physiological environment, water and saline solutions of certain ionic strength, however, it is soluble in acidic solutions with a pH range of 2-4. It should be noted that gelatin is an irreversibly hydrolyzed form of collagen. In gelatin, the triple helical peptides structure "unwinds" into single peptide chains, and hence is distinctly different than collagen, since it is soluble in water.

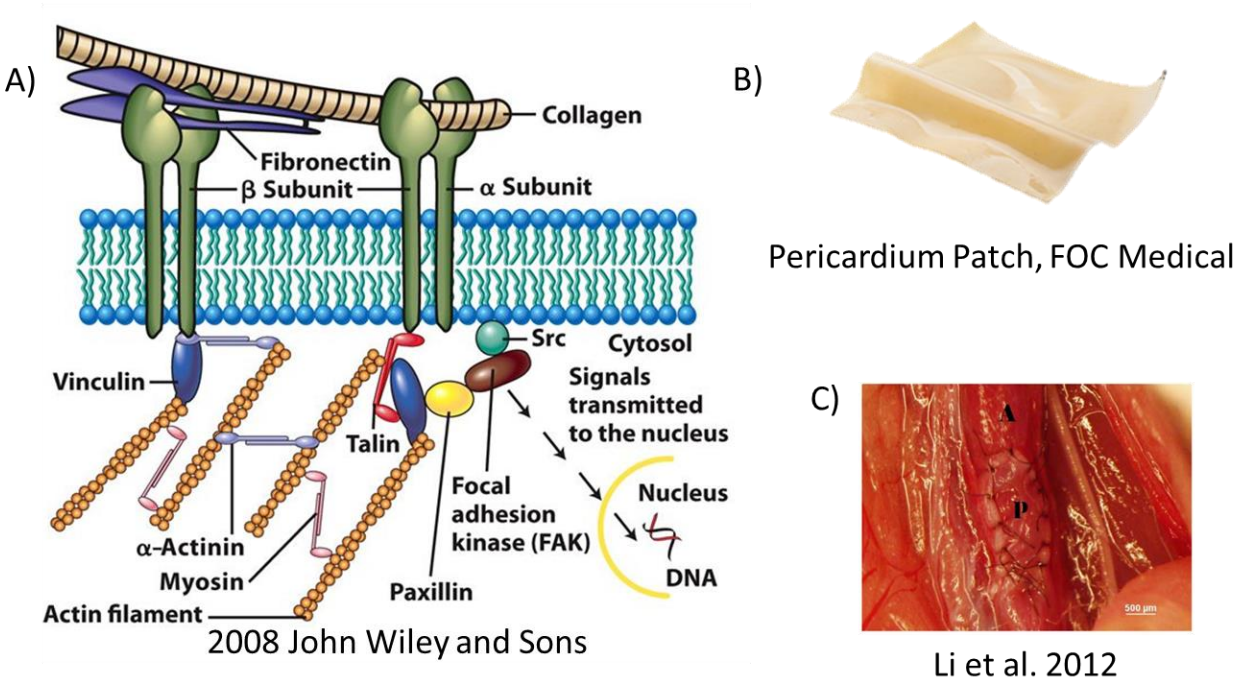

Figure 4. *(A) Focal Adhesion of cells onto collagen* [42], *(B) Pericardium Patch* [43], *(C) Pericardial Patch Angioplasty where P is the pericardial patch and A is the aorta* [44].

Collagen Type I, as a major component of the extracellular matrix, provides a 3D scaffold for cell growth and plays a major role in cellular behavior [34]. Cells attach to the ECM via focal adhesions as shown in Figure 4A using integrins labeled α and β subunits. Integrins are used by cells to

recognize specific amino acid sequences (DGEA/GFOGER) on collagen. Actin, the structural components of cells that are also used in cell movement bind to integrins. This focal adhesion or lack thereof plays a major role in the foreign body response as previously mentioned [29] which promotes coagulation activation. Focal adhesion plays a central role in cell migration and proliferation since adhesion through integrin/actin is necessary for movement. In this sense, forces exerted through focal adhesion are a biomechanical sensor since Focal adhesion kinase (FAK) transmits signals to the nucleus.

Inspired by the role collagen has in the body, devices made from collagen include collagen scaffolds for tissue grafts in areas such as the skin or the heart [34]. Other devices include hydrogels for cell assays, freeze-dried sponges for 3D cell scaffolds, extruded collagen fibers, films, and tubes. Among commercial products, there are a variety of pericardium patches needed to help wound healing after heart surgery as seen in Figure 4B and C. According to the US Patent 6,599,526 by Dr. Dan Dimitrijevich (who collaborated in this dissertation) [45], pericardial patches can be made using Type I collagen resulting in a film with a density is amenable to cell invasion, which allows for the formation of tissues and blood vessels, and becomes vascularized 4-8 weeks after surgery. This vascularization can assist biodegradation as it makes the area accessible to macrophages and lymphocytes, allowing for wound healing/tissues remodeling to being. Experiments for the mentioned patent did not show any foreign body reaction in vivo. Cell infiltration studies by Li X et al. [44], further confirmed this finding as arterial remodeling of the patches showed growth of endothelial tissues (endothilization). Early infiltration of the patch by cells show how quickly the patch adapts the arterial environment. Patches have a monolayer of

cells by day seven and by day 30 develop a neointima or the innermost lining of a blood vessel due to the proliferation of smooth muscle cells. The minimal foreign body response can be attributed to collagen's ability modulate innate immunity [46]. Amelia Thomas et al. were the first to demonstrate the direct link between collagen fragments and human monocyte cytokine production showing that collagen is an active player in the inflammatory process.

Motivation

The development of bioelectronics is booming, fueling the development of flexible electronics for medical applications to monitor physical phenomena and other body processes Protein materials such as elastin, keratin, reflectin, and in particular silk, demonstrate favorable properties for bioelectronics such as enhanced biocompatibility [47]. As mentioned in the Background section, transient electronics, for implantable electronics in particular, are designed (from the substrate to electronic components) to have a controllable degradation and be bioresorbable. Collagen shows biocompatibility that is difficult to match because it has innate amino acid sequences that play a role in cell adhesion and the foreign body response. This amino acid sequence is a frequent point of biomimicry studies, functionalizing other biopolymers such as silk in attempt to further enhance biocompatibility [48]. The ability to promote vascularization plays a major role in FBR. Collagen also shows biodegradation and bioresorption as fibroblasts and other cells have been shown to secrete, remodel and degrade collagen using enzymes known as collagenases [34]. Collagen is particularly interesting since there is a significant number of FDA approved biomedical devices that utilize various forms of mammalian (bovine and porcine) collagen. Thus, implantable devices based on collagen type I are unlikely to face regulatory rejection. Collagen is a dynamic material

with various ways to form it into different objects such as fibers, films, sponges among other possibilities as well as various ways to change its properties through a library of cross linkers and the ability to functionalize it with different chemicals [34]. This is demonstrated by the wide variety of applications that are only limited by a researcher's creativity as shown in Figure 5B and C which include tilapia skin used to heal skin burns, given the high collagen content, and a collagen heart valve. In this dissertation, we demonstrate for the first time [47] the use of collagen films as substrate for flexible electronic applications.

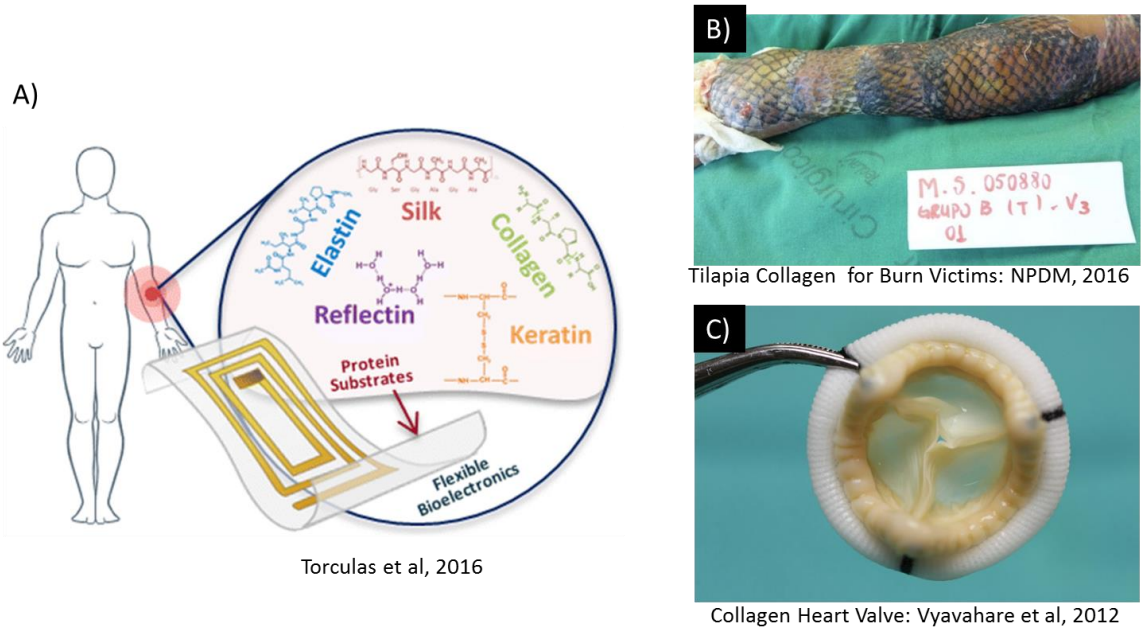

Figure 5. *(A) Protein Based Electronics* [47], *(B) Tilapia collagen for burn victims* [49], *and (C) Collagen Heart Valve* [50].

In this dissertation, it is hypothesized that collagen film degradation can be controlled by degree of crosslinking, which demonstrates collagen is a suitable substrate for flexible transient electronics. This study explores the fabrication and properties of collagen films for flexible electronics in Chapter 2, where the fabrication and characterization of flexible electronics directly on collagen are explored. In Chapter 3, the shortcomings of direct fabrication on collagen and an

alternate process (transfer printing) for fabrication of electronics on collagen are explored. Further discussion is made on the biodegradable properties of these devices and their biocompatibility. In Chapter 4, the controllable biodegradation of collagen by first demonstrating controllable crosslinking is explored. We correlate this % crosslinking with changes in collagen's various properties and finally demonstrate how this affects biodegradation via collagenase. In Chapter 5, the concluding statements and outlooks for research in collagen as a substrate for flexible electronics are presented.

CHAPTER 2

DEVICES BUILT DIRECTLY ON COLLAGEN

Authors- Salvador Moreno, Mahmoud Baniasadi, Shakil Mohammed, Israel Mejia, Yuanning Chen, Manuel Angel Quevedo-Lopez, Nalin Kumar, Slobodan Dimitrijevich, Majid Minary-Jolandan

The Department of Mechanical Engineering, EC 38
The University of Texas at Dallas
800 West Campbell Road
Richardson, Texas 75080-3021

The Department of Materials Science and Engineering, RL 10
The University of Texas at Dallas
800 West Campbell Road
Richardson, Texas 75080-3021

The Alan G. MacDiarmid NanoTech Institute, BE 26
The University of Texas at Dallas
800 West Campbell Road
Richardson, Texas 75080-3021

UHV Technologies Inc.
450 South Freeway
Fort Worth, TX 76104-3503

Previously published as "Biocompatible Collagen Films as Substrates for Flexible Implantable Electronics" in Advanced Electronic Materials. DOI:10.1002/aelm.201500154 Copyright license 4546600558325

2.1 Introduction

For the variety of biomedical applications developed from collagen, connective tissues such as tendon and skin from bovine, porcine and ovine in origin serve as the primary source of collagen type I [34]. Waste material from fish such as fins, skin, bones, and scales have also been used for this purpose [51]. Early work with collagen used rat tail tendon because of its purity and ease of extraction [52]. Collagen varies in mechanical properties and denaturation temperature depending on the extraction protocol as well as the tissue origin. As detailed by Holista CollTECH [53], their patented process starts by placing the tissue in a dilute acidic solution such as acetic acid (pH 4-4.2) to break down the aldimine crosslinks between triple helices which are loosely held together. Other salts such as sodium bicarbonate are included in the buffer. Tissue acid solution is incubated in temperatures up to 30 °C for up to 27 hours. To break the more stable ketoimine bonds holding together more mature fibers, proteases such as pepsin are added to the buffer. This protease treatment cleaves the N and C terminal regions of the triple helix, which can affect collagen's properties. The collagen buffer is centrifuged and the soluble components of collagen are filtered out with the precipitate dissolved in 0.1M Acetic acid. The solution can be frozen and stored. Although in general, it is better to extract collagen from a source with DNA as close to possible as humans, farmed animals provide an abundant source as there is little variation in the amino acid sequence among mammals. For example, humans and ovine share a 90% amino acid sequence homology compared to 88% in mice and 93% in horses. Ovine collagen is favored by Hollista CollTECH because traditional sources of collagen such as cow and pig can result in issues due to Mad Cow disease. Sheep sourced from Australia do not have these issues, since the sheep population isolated on an island with strict restrictions in regards to animal importations thus

protecting herds from Mad Cow disease [53]. In this chapter, electronics are fabricated directly onto collagen, with the goal of demonstrating collagen as a substrate for transient electronics.

2.2 Collagen Film Fabrication and Topography

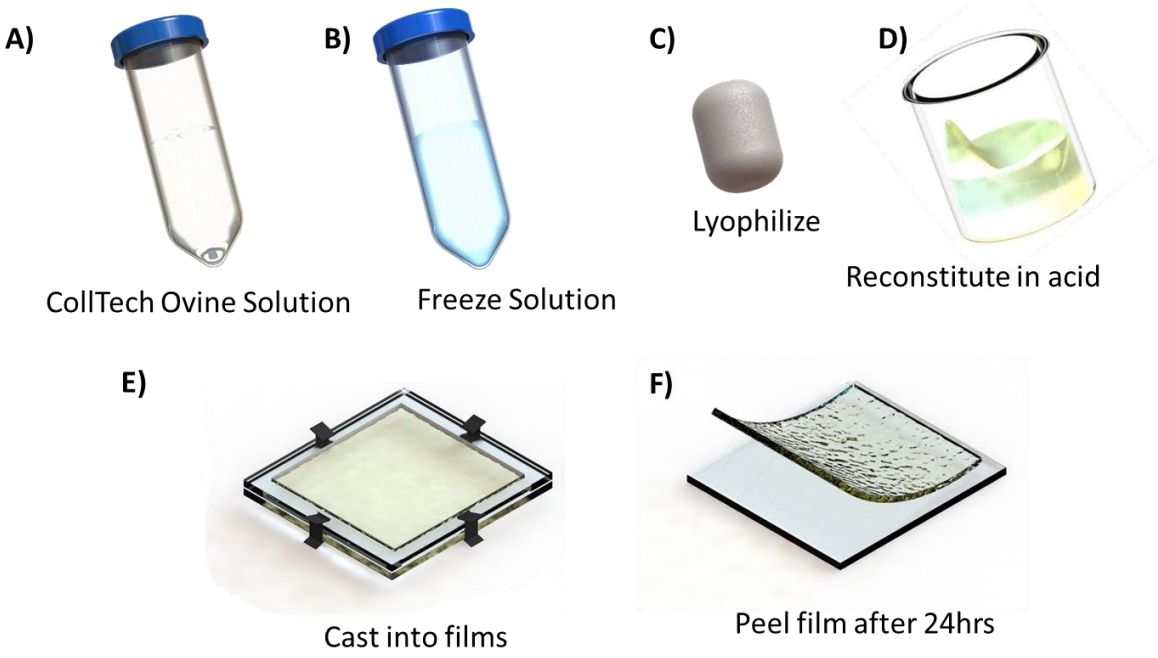

Figure 6. *(A) CollTECH Ovine stock concentrated collagen solution, (B) Solution is frozen and stored, (C) Freeze dried or Lyophilized collagen sponge, (D) Collagen is reconstituted in weak acid solution, (E) Collagen acid solution is poured into a plastic frame cast, (F) Collagen film can be peeled from frame after drying for 24 hours.*

For this study, collagen films were fabricated from stock concentrated ovine collagen provided from Holista CollTECH (Amino acid profile Figure A19) in the form of uniform thickness and transparent films (Figures 7A and A1). The process starts by freeze drying the frozen solution resulting in a lyophilized collagen sponge (still in triple helix form) which is also known as dehydrated collagen. It is then reconstituted in a weak acid at 4 °C and poured into a plastic frame. It is important that this frame is hydrophobic so that a film can be peeled after 24 hours drying.

The frame can be designed to be any shape and can be even cast onto silicon wafers. The collagen film is stable in air and at room temperature for long periods of time. It is highly hydroscopic and responds to change in moisture. In water, collagen expands in size and decreases in thickness, which can affect its mechanical properties. Films are also stable in organic solvents such as alcohol and acetone.

Metallic patterns were deposited on collagen films using E-beam evaporation through a shadow mask laser cut to shape. Depositions are kept at room temperatures using a large chamber such as in the CHA MARK 50 E-Beam evaporator. Metals such as gold, chromium and magnesium are shown to be deposited. Since the depositions are made at room temperature, the shadow masks can be made from plastic or metal. Figure 7C shows a folded collagen film with gold patterns that can be used as electrodes, interconnections, localized heaters or strain gauges. Figure 7D shows a 10μm×10μm Atomic force microscopy (AFM) amplitude image of the surface of the collagen film. Surface roughness of the films are less than 100 nm, as determined from the AFM topography images (Figure A2). Figures 7E and F show plan-view and cross-sectional Scanning Electron Microscope (SEM) images of the collagen films coated with a thin layer of platinum and gold, respectively. The thickness of the collagen films can be controlled by changing the initial concentration of the dehydrated collagen sponge in weak acid solution or recasting in the same frame. Solutions with a concentration of 5 mg/ml result in collagen films with thickness of ~8 μm. The figure to the right in Figure 7F shows a zoomed-in view of the red-boxed area. Collagen shows a filamentous microstructure, as apparent from the SEM results and consistent with the AFM images. The surface morphology of collagen film shows a uniform pattern of several microns that

result from the assembly of collagen filaments. This fibrous microstructure of collagen makes it insoluble in physiological environment, a major difference between collagen and gelatin.

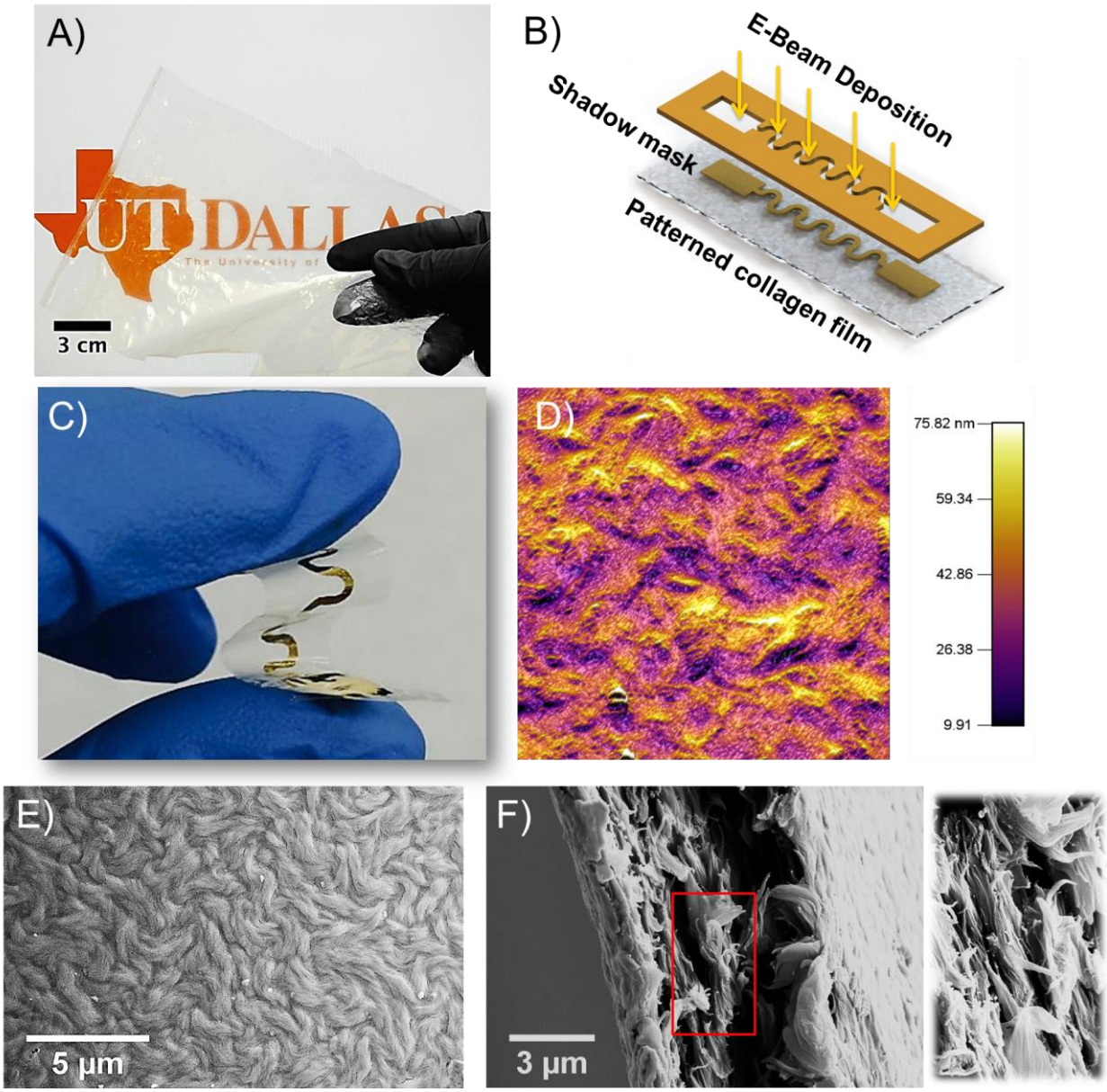

Figure 7. *(A) Photograph of a large-area transparent collagen film. (B) Metallic patterns were deposited onto collagen film using E-beam evaporation through a shadow mask. (C) Shows a folded collagen substrate with gold deposited patterns. (D) 10µm×10µm AFM amplitude image of collagen film surface. Figures (E) and (F) show SEM surface morphology for plan-view (E) and cross-sectional view (F) of collagen films. The figure to the right in (E) shows a zoomed in-view of the red-boxed area. The filamentous microstructure of collagen is apparent in this view.*

2.3 Material Properties of Collagen

FTIR spectra of collagen films are shown in Figure 8A (The full FTIR spectrum is given in Figure. A3). The main peaks at 1654 cm^{-1}, 1555 cm^{-1} and 1238 cm^{-1} correspond to the Amide I, II and III bands, respectively [54, 55, 56]. The Amide I band (between 1600 and 1700 cm^{-1}) is associated with the stretching vibration of $C=O$ and is directly related to the backbone conformation of collagen. The Amide II band is conformationally sensitive and results from the N-H bending vibration and from the C-N stretching vibration. The Amide III bands are complex bands that result from a mixture of several coordinated displacements. An amino acid profile provided by Holista CollTECH seen in Figure A19 shows that the Glycine content is roughly 1/3.

Collagen, similar to other bio-derived proteins, is stable under physiological conditions (~37˚C). Therefore, higher processing temperatures should be limited to maintain collagen's material integrity. The collagen films were subjected to temperatures of up to 70 ˚C in increments of 10 ˚C from room temperature for durations of 45 minutes. FTIR spectrum of the heat-treated collagen film does not change significantly as the temperature increases, i.e., the Amide peaks remain unchanged (Figures A4 A, B). In addition, SEM images of heat-treated collagen film show filamentous microstructure similar to the control collagen films (Figures A4 C, D). These results show a stable collagen substrate with enough endurance for temperature-dependent applications up to at least 70˚C

Mechanical integrity of the substrate is an important factor for functional and reliable electronics. Mechanical properties of collagen films were characterized using a custom-built micro-tensile

tester (Figure A5). A typical stress-strain response from tensile test of the collagen film is shown in Figure 8B. Collagen films offer comparable or favorable mechanical properties compared to other similar substrates. The collagen film exhibits an elastic modulus of E=2.04±0.26 GPa, a tensile strength of σ_f=90.71 ± 12.91 MPa, and sustains failure strains of up to ε_f=16.8±2 % (n=5) (See Figure A6 and Table S1). The elastic modulus of collagen is in the range reported in the literature for collagen [57]. At a strain of 3.3%, the film yields and finally ruptures, with a tensile toughness of over 8 J/g. The elastic modulus of collagen is comparable to that of polyethylene terephthalate (PET), which is a common substrate for flexible electronics E_{PET} ~ 2.43 GPa [4]. These properties for collagen are comparable to silk films (E=2.8 GPa) [1], and nano-cellulose based substrates (E ~ 2.25 GPa, σ_f~25 MPa, and ε_f < 3.5% [4]). For a typical sample of 5 mm in width and 8 μm in thickness, the flexural rigidity of the collagen film is EI ~ 4.35 ×10^{-13} N.m^2, where I is the second moment of area of the cross-section. By increasing the concentration of the initial collagen solution from 5 mg/ml, stronger samples could be obtained for applications where tuning mechanical properties is imperative. For example, 10 mg/ml collagen films, as seen in Table S1, achieve a failure strain of 32%, almost twice the value of 5mg/ml samples. The mechanical properties of bare collagen films with the films were compare to films with a metal deposited layer. The results show that the elastic modulus was relatively unchanged (Figure A6, E= 2.1 GPa), i.e. metal patterns do not compromise mechanical properties of the collagen films. If desired, the elasticity of collagen films can be improved upon by incorporation of elastin-like matrices [58] for a platform of stretchable collagen based electronics.

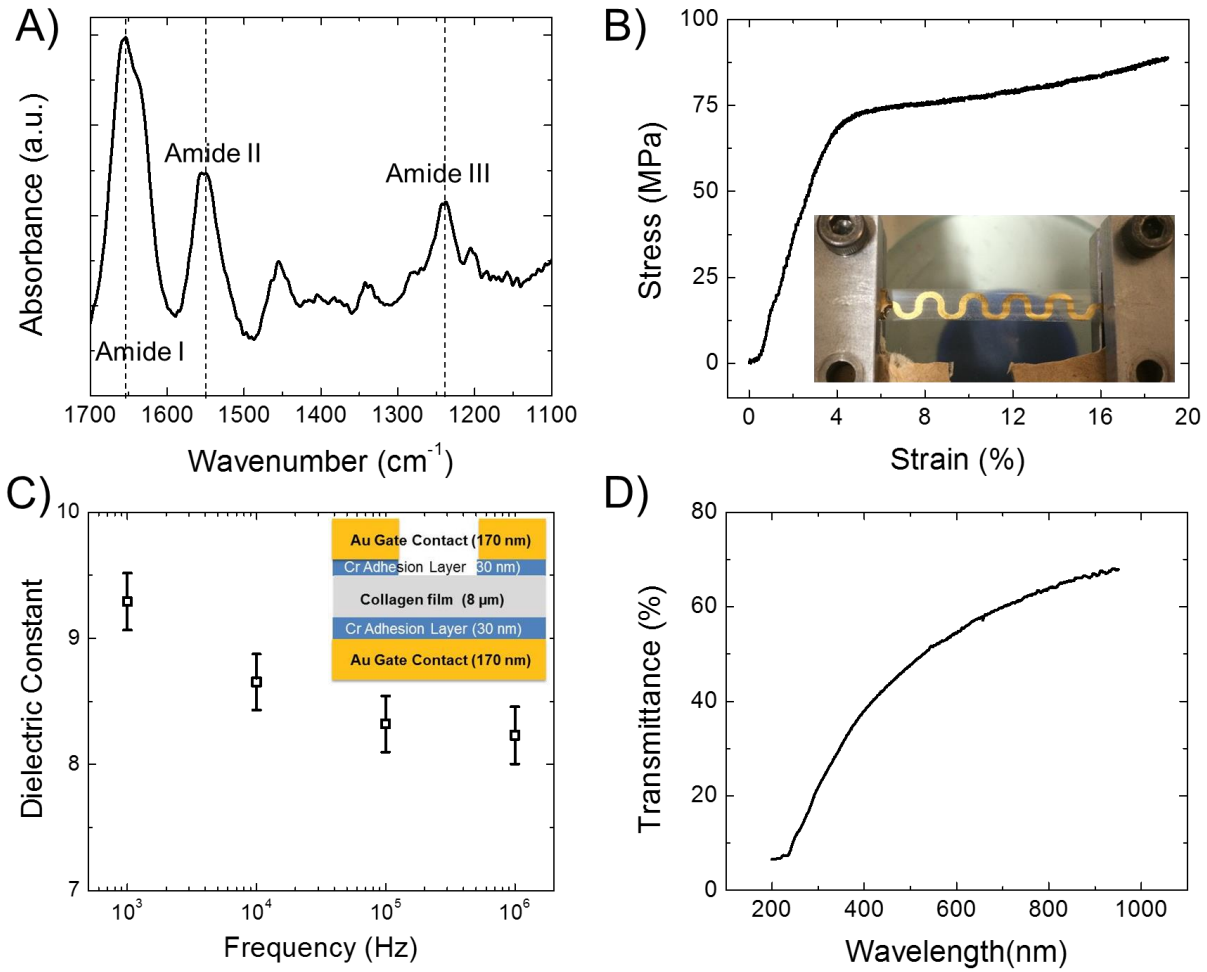

Figure 8. *Material properties of collagen films. (A) FTIR spectrum. (B) A representative stress-strain mechanical response form tensile test. Inset shows a collagen film with metal electrode under tension. (C) Dielectric constant vs. frequency. Error bars show standard deviation (n=4). (D) UV-Vis transmittance spectra of the collagen film.*

The dielectric constant of the collagen films was measured by fabricating metal-insulator-metal capacitors, in which the collagen film functions as the insulating layer (Figure A7). Dielectric constant (k_i) was obtained from the experimentally measured capacitance (C_i) using $C_i = (\varepsilon_0 \cdot k_i \cdot A)/x_o$, where x_o is the thickness of the collagen film, ε_0 is the vacuum permittivity and the area A is calculated using the diameter of the circular pattern defining the capacitor. The collagen films showed a dielectric constant of 8.2 – 9.3 in the frequency range of 10^3 – 10^6 Hz (Figure 8C). Most

common ceramics and polymers have dielectric constant in the range of 2 to 10 [59]. For comparison, the dielectric constant of collagen is similar to the dielectric constant of PVDF (polyvinylidene fluoride k_i ~8.5), and almost three times larger than PMMA (Poly (methyl methacrylate) k_i ~ 2.6). This large dielectric constant is appealing for several applications, for example fabricating high frequency antennas.

UV-Vis transmittance spectra of collagen film is shown in Figure 8D. A significant advantage of collagen film is its transparency in the visible spectrum (400 nm-700 nm) (Figure 7A). This property is attractive for its application for example in artificial cornea or in bionic contact lenses, given that collagen is the main component of natural cornea. The low transmittance of collagen in the UV range can be used for applications requiring filtering or reducing UV exposure.

2.4 Flexible Electrode Deposition and Encapsulation

Electron beam evaporation was used to deposit metal electrodes on collagen films as shown in Figure 9A i. Shadow masks with various patterns were fabricated using a laser engraver (Figure A16). The metal deposition (30nm Cr/170nm Au) was performed at low deposition rates (0.1 nm/s) in order to maintain a chamber temperature below 30˚C and prevent any damage to the collagen substrate. As seen in Figure 9A ii, Magnesium (Mg) was deposited on collagen, which demonstrates collagen as a promising platform for biodegradable electronics [33, 60]. Figure A8 shows SEM images of the collagen film surface after metal deposition. Metal layer is conformal onto collagen film and the microstruture of collagen film is unaffected by metal depostion. Micro-

fractures in metal layer are apparent in high magnification image Figure A8 C, which do not significantly affect the overall conductivity of the metal layer, as seen in Figures 9B and C.

In addtion to metal evaporation, ink-jet printing was also used to deposit regular inks (office printer) and metals (laboratory printer) on the collagen films, as seen in Figures A12 and A13. The printed characters on collagen using an office printer were stable in water and PBS buffer and did not show any apparent peeling. Such findings suggest that many of the techniques developed for paper-based electronics can be used on collagen films [61]. From E-beam deposition to ink-jet printing, collagen film shows to be a versatile platform on which devices can be affordabily fabricated for various applications.

In contrast to gelatin, collagen is not soluble in aqueous media, which is the main advantage for implantable electronics. For example, when placed in PBS buffer or DI water, the film hydrates and swells (Figure A10) and after drying, it returns to its initial state. Collagen films with an Au/Cr metal electrode were encapsulated by overlaying another moist collagen film on top it, so that the metal electrode was sandwiched between two collagen films (Figures 9 iii-v). When the encapsulated electrode was placed in PBS solution there was only small amount of micro-fracture of the gold electrode observed after 2 hours at high magnification (inverted microscope) that did not affect the conductive properties. This state can remain stable up to a tested four weeks (Figure 9 v and Figure A12). Once removed from the PBS and allowed to dry, the sandwiched electrode maintained its integrity and returned to its initial state. Without encapsulation the rate of hydration and swelling of the collagen film results in fractures in the metal electrodes deposited on the film,

which can completely peel off from the film in 10-20 minutes (Figure A11). These results show that with proper encapsulation, electrodes fabricated on collagen could be implanted without their integrity being compromised.

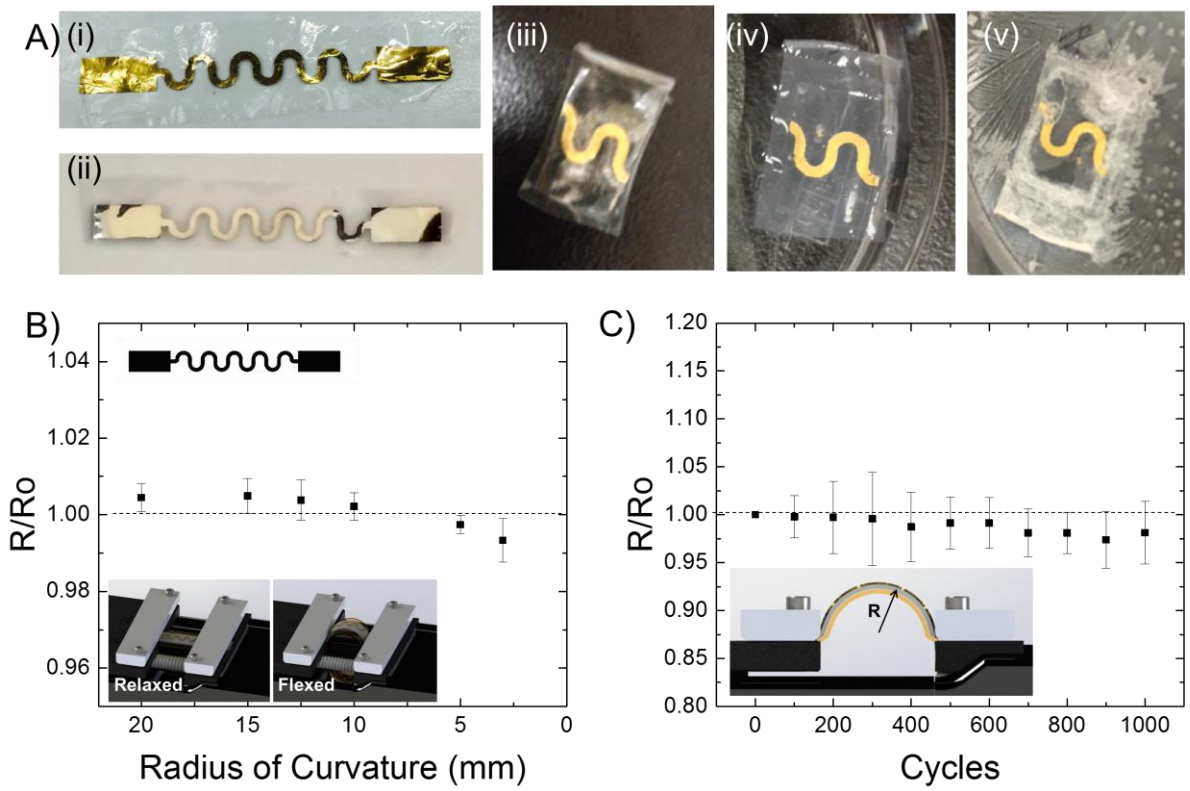

Figure 9. *(A) (i) Au/Cr and (ii) Mg conductive strips on collagen substrates. (iii-v) Encapsulated Au/Cr film between two collagen films: as prepared sample, after two hour in PBS buffer, and after four weeks, respectively. (B) Changes in resistance vs. radius of curvature. The horizontal dash line shows the resistance for zero curvature. Change in resistance vs. radius of curvature is less than ~1%. (C) Flexure experiments for resistance vs. number of cycles. After 1,000 cycles, the resistance changes less than ±5%.*

Serpentine resistors built on collagen substrates were shown to be highly flexible as shown in Figure 9B with a change in resistance less than 1% for radius of curvature down to 2.5 mm. Crossheads pushed the collagen substrate inwards, making the radius of curvature sharper as detailed in Section 2.7 Materials and Methods. Flexibility of the films can be further improved by

deposition of thinner metals layers. The resistors on collagen film showed less than ±5% change in resistance after 1000 cycles of flexure to a flexure radius of 13.5 mm, see Figure 9C.

2.5 Device Applications

Several applications of collagen film were demonstrated in in the following sections. These applications include strain gauges, wireless antenna, temperature sensor and heater.

2.5.1 Strain gauge:

Strain gauges are the main component in many sensor designs such as pressure and force sensors. The application of collagen film in strain gauges is demonstrated, which have potential as implantable strain sensors with further development. Using shadow mask with a pattern based on commercial strain gauges, the strain gauge was deposited on collagen film (Figure 10A i, inset). This strain gauge functions based on the piezoresistivity phenomena. The strain gauge was calibrated using a cantilevered beam (Figure A14). The calibration results show a linear relation between strain and resistance change up to 0.15% strain, well within the elastic range of collagen film. This limit is attributed to the existing experimental setup of the cantilever flexure frame in the laboratory, and not the collagen film since the elastic strain of the film was shown to be > 3%. The experimental gauge-factor (GF) for this strain gauge design was calculated to be ~1.6.

To demonstrate possible applications of collagen-based strain sensors, the sensor was placed on a cylindrical shaped balloon as shown in Figure 10A(ii), for example as a model for the aorta. The balloon was tied at its ends, and squeezed from left and right of the sensor simultaneously. This action increased the pressure at the sensor and caused a slight increase of balloon radius. This

increase in the radius strains the device (hoop stress) resulting in the peaks shown in Figure 10A (iii). With further development, such a device would be useful for example in monitoring the size of an aneurysm in the abdominal aorta, the rapid increase in which could lead to a fatal rupture. With future improvement toward wireless communication capability and downsizing, a collagen substrate strain sensor would be ideal for applications requiring long term implantations.

2.5.2 RF Antenna:

The application of collagen film as a substrate for receiver antennas was demonstrated in Figure 10B which shows the patterned antenna on collagen film. This is a hook-shaped dual frequency antenna that is capable of receiving frequencies at 915 MHz and 2.4 GHz. The antenna pattern was deposited onto the collagen film by E-beam evaporation. The antenna was connected to a circuit that has a PowerCast P1110 IC, which harvests RF energy and converts it to DC voltage. The circuit was powered wirelessly using an external transmitter (PowerCast) placed in the proximity of the antenna that transmits at 915 MHz with 3W power. Figures 10B ii), and iii) show an LED (~1 mW) is wirelessly powered by the antenna fabricated on the collage substrate at a distance of 10 cm from the transmitter. As the separation increases between the transmitter and receiver, the brightness of the LED decreases until it is completely turned off at a distance of 1 m. This application showcases the ability to wirelessly power devices fabricated on a collagen substrate. Further development would be needed to build the individual components of an AC-to-DC energy conversion on collagen film. By encapsulating the AC-to-DC converter and fabricating an antenna on collagen, it would be possible to power biocompatible devices implanted in sensitive environments with an external power source in a nonintrusive manner.

2.5.3 Temperature sensor and heater:

Heat is an important area of exploration for sensing since many of the human body's functions are temperature expressive (for example, inflammation, and infections). Tissue temperature monitoring is important for the diagnosis of possible diseases whether it is fever or infectious diseases. There are several strategies used in temperature sensor development such as resistance, which was used in this study for demonstration of a temperature sensor. The same design as the strain sensor was used with 2X scale-up in order to increase the measurement accuracy. As Figure 10C i shows, the temperature sensor has a fairly linear relation between temperature and resistance between room temperature to 55˚C, which is a reasonable range for biological temperature sensing. The slope of the linear response was 0.0008 K^{-1} or 0.1322 Ohm/˚C. The temperature sensor was calibrated as described in the experimental section. Details of the setup are shown in Figure A9. A comparable study showed a 0.00423 K^{-1} temperature coefficient for gold among other metals, suggesting a more conductive design with a different metal could result in a higher sensitivity [62].

Resistors can also generate heat through "Joule heating," in which resistor releases heat as current passes through it. This should be observable in any resistor. The initial experiments with thin evaporated metal elements showed very small heat release before the device burnt out. Due to the nanometer metal thickness, the power rating of the deposited metals was low. Larger heat gradients required a thicker conductor and slow deposition rate; for this reason silver ink (~14 μm thick) was employed as a more efficient alternative to slow deposition rates. As shown in Figure 10C iii, the element heated up to 36.4 ˚C at 6V. The inset IR image shows heat radiating from the metal element. The heater performance was fairly linear between 3V and 6V with a slope of ~3.7 ˚C/V.

As a future direction, collagen substrate skin patches bearing a heater element could be used as a drug delivery platform [63] or for localized heating of cell cultures [3].

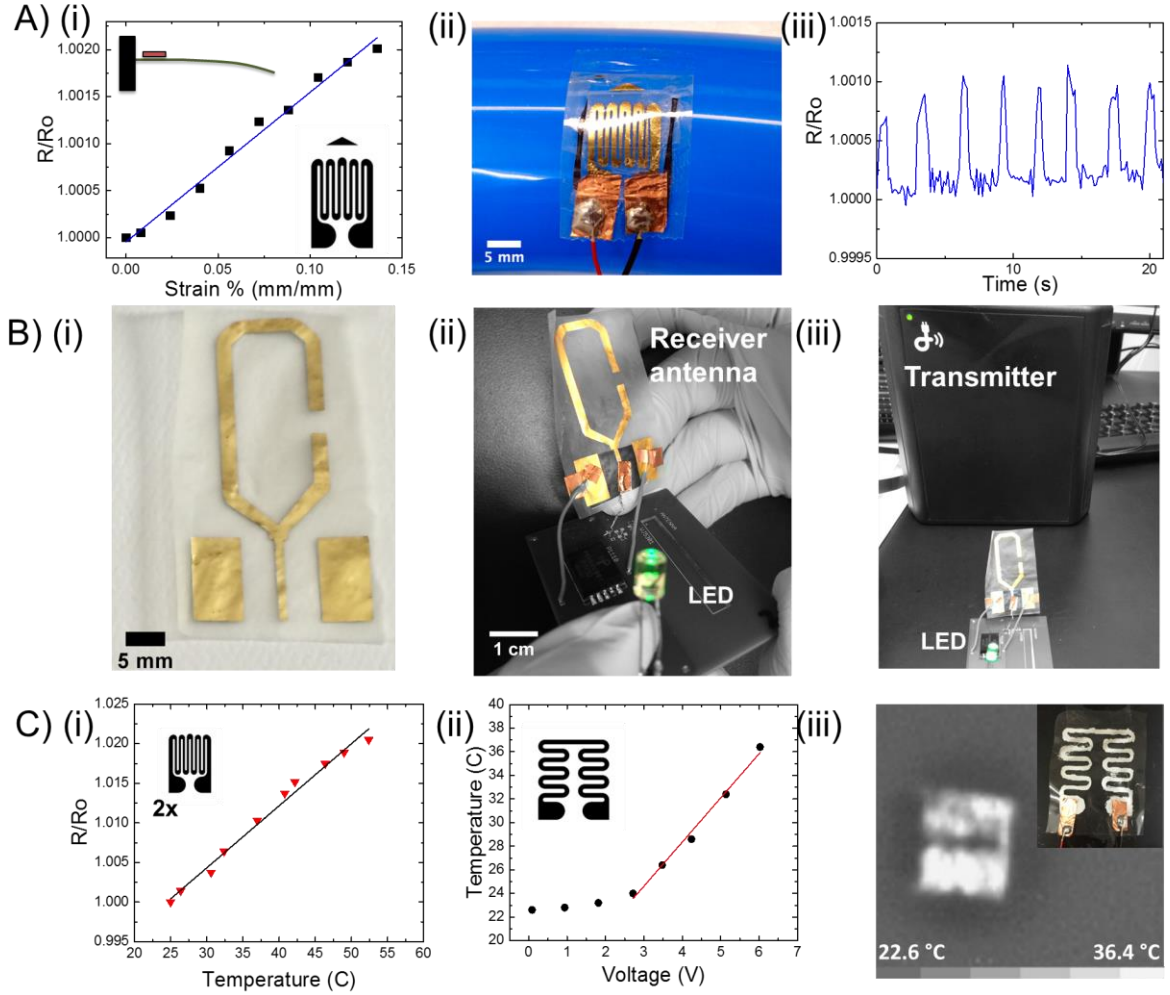

Figure 10. *(Ai-iii) shows applications of strain sensors fabricated on collagen films. i) shows calibration of the sensor using a cantilevered beam. ii) and iii) show the same strain sensor design mounted along the circumference of a balloon. When the balloon is squeezed, the increase in pressure results in an increase in resistance as shown in iii). (Bi-iii) show an RF antenna fabricated on collagen film. An LED is lit up using the wireless power from a transmitter in ii) and iii). (Ci-iii) shows thermal applications of collagen film in a (Ci) temperature sensor and a (Cii-iii) heater. (Ciii) shows an IR camera image of the heated metal on collagen. The inset shows the actual heater on collagen film.*

2.6 Conclusion

In summary, first demonstration of collagen films for substrate in flexible electronics is reported. Large area and transparent collagen-based substrates were fabricated and characterized morphologically, mechanically, electrically, and chemically. Collagen is a biocompatible and biodegradable protein, and the most abundant protein in mammals. The demonstrations including strain gauges, wireless antenna, heater, and temperature sensor are promising for future applications of this substrate for implantable biomedical devices for long-term monitoring of physiological environment. Collagen encapsulated devices hold well for extended periods of time (four weeks), but without being able to measure them it is difficult to ascertain as to how well they function. Collagen bonds to itself through hydrogen bonds which will hold until they are interfered with such as with alcohol. Devices fabricated are essentially electrodes since only metals were deposited by E-beam. Other processes with different materials are needed to determine the limitations of direct fabrication on collagen towards the development of collagen based transient electronics. Implantation *in vivo* or collagenase degradation experiment are needed to determine how the electronics on collagen degrade. Furthermore, controllable degradation of collagen is not clear at this stage.

2.7 Materials and Methods

2.7.1 FTIR spectroscopy:

FTIR spectroscopy was performed using a Nicolet iS50 Spectrometer (Thermo Scientific) using a GATR grazing angle accessory (Harrick) with a 65° incident angle and germanium crystal. Collagen film samples were mounted on cardboard frames with a 10 mm ×10 mm cutout. The absorbance/transmittance and background signals were measured using 32 scans over a spectral range of 4000 cm^{-1} to 650 cm^{-1} and a spectral resolution better than 0.07 cm^{-1}. FTIR spectra were also collected from collagen film sample after E-beam deposition of metal electrodes to examine the possible effect of the process on collagen films. Several collagen films were also exposed to temperature up to 70 ˚C inside an oven and FTIR spectra were obtained for each sample to determine stability of the films in this temperature range.

2.7.2 UV-Vis spectra:

The transmittance spectra of collagen films were acquired in the wavelength range of 200 nm to 1000 nm. The UV−Vis spectra were measured using an Ocean Optics QE65 Pro spectrometer with a DT-mini-2-GS light source.

2.7.3 Characterization of mechanical properties:

Tensile tests were conducted using a custom-built micro-tensile tester. Collagen films were prepared on a cardboard frame to protect the sample from the grips. The experiments were conducted at a quasi-static strain rate of 1% strain/min. Force-displacement data was acquired using a LabVIEW program. The length and width of each sample was measured before the

experiment using a digital caliper. The engineering strain was obtained by dividing the extension of the gauge length of the sample by the original gauge length. The thickness of each sample was measured using a digital micrometer as well as using cross-section SEM images. Engineering stress was obtained by dividing the force by the cross-sectional area of the film. The tensile toughness of the films was derived from the area under the force-displacement response curve up to the point of failure. The elastic modulus (E) of the film was obtained from the initial linear portion of the stress-strain response. The bending modulus of the film is defined as $E \times I$, where I is the moment of inertial of the cross-section.

2.7.4 Atomic force microscopy:

Surface topography of collagen films was imaged using a MFP-3D Asylum AFM. Collagen films were mounted on an AFM sample holder using a double sided tape. Images were acquired in air and in tapping mode. Surface roughness of the films was obtained by image analysis using the instrument software (Igor Pro 6.34).

2.7.5 Metal electrode deposition:

Au/Cr electrodes were deposited using a CHA Mark 50 E-beam evaporator at deposition pressures of less than 5×10^{-6} torr while keeping temperature under 30˚C. Various devices including resistors, RF antenna, etc. were fabricated using shadow masks. The shadow masks were fabricated using a Gravograph LS 100 laser engraver. Au/Cr deposition rate was 1-1.5 A/s. Ag and Mg deposition was performed at 1 A/s and 10 A/s, respectively.

2.7.6 Flex experiments:

Collagen films with deposited serpentine metal electrodes were subjected to dynamic flexure tests on a modified Sigma Koki SGSP26 series translation motorized stage. A collagen film was flexed for 1000 cycles at 1 Hz. The resistance across the electrodes was measured with an Agilent Multimeter 34410a. The stage was controlled via LabVIEW VI, which counted the number of cycles while acquiring data from the multimeter. The stage was set to a ΔL amplitude of 7 mm, which subjected the collagen film to an out of plane displacement of 13.5 mm resulting in radius of curvature of 5 mm for a sample of length 30 mm (See Supplementary Information). By moving the crossheads inward while measuring displacement or ΔL and the resistance of the metal electrodes with the multimeter, the change in resistance as a function of radius of curvature was obtained.

2.7.7 Measurement of dielectric properties of the collagen films:

The dielectric constant of the collagen films was measured using a Cascade Microtech nanoprobe station with a Microchamber attached to a Keithley 4200 Semiconductor Characterization System and an Agilent 4284A Precision LCR Meter. Parallel plate capacitors (metal-insulator-metal) were fabricated on collagen films using e-beam evaporation on which capacitance-voltage (C-V) curves were measured from 1000 Hz to1 MHz. The top metal electrodes were circular shapes with various diameters; the 0.55 mm diameter was used for calculation of the dielectric properties. The electrodes were deposited on the top-side of the collagen film and on the entire bottom side of the collagen film. In this configuration, collagen film functions as the dielectric layer. The dielectric constant was calculated by the method reported for organic dielectrics [64].

2.7.8 Strain sensor fabrication and calibration:

The strain sensor was fabricated via E-beam evaporation and a shadow mask. Copper tape soldering terminals were attached to connect thin wires for measurement. The fabricated strain sensor was calibrated using a cantilevered beam under a controlled beam deflection. The sensor was attached to an Aluminum 6061-T6 cantilever using double-sided tape (3M) and single-sided tape on top to assure profile uniformity. The beam was deflected using a cantilever flexure frame (Vishay) while measuring the deflection with a micrometer (Starrett) and 4-wire resistance using a multimeter. Using deflection measurements and elastic beam theory, calculated strain vs. resistance was calibrated. The strain sensor was then attached along the circumference of a cylindrical-shaped balloon to demonstrate possible application as an arterial pressure sensor. First the double sided tape was placed on the balloon, and then the single sided tape already on the sensor was used to align the sensor. The balloon was squeezed and then released on both sides of the sensor to induce an increase in pressure at the sensor.

2.7.9 Temperature sensor fabrication and calibration:

Au/Cr metal electrodes were deposited using E-beam evaporation onto collagen substrate. The mask used was the same as the strain sensors, scaled 2X to increase sensitivity. To calibrate the sensitivity of the temperature sensor, it was placed on an aluminum heat sink block on a hot plate. Double-sided copper tape was used between the sensor and the heat sink to ensure that good thermal contact was established as well as to make sure the flexible substrate was uniformly in contact with the block. Temperature of the hot plate was increased from 30˚C to 60˚C while its surface temperature was measured using a handheld IR (Infra-red) thermometer (CEN-TECH).

The temperature-dependent resistance of the metal electrode was registered using an Agilent 33410a multimeter in the 4-probe configuration.

2.7.10 Fabrication and characterization of the heater:

To fabricate a heater on collagen film, a mask design based on commercial etched metal foil heaters was used as a stencil. Pelco silver conductive paint (Ted Pella) was used as the conductive material. The paint was necessary to achieve thick conductive material on the collagen film. Once the silver paint was dried, copper solder tabs with wires were added. The heater was powered using a Keithley 2200 DC Power supply. Voltage was slowly increased from 0 to 6V using constant current (CC) mode to prevent damage to the heater. The increase in heat emitted due to increased voltage was observed using a long-wave IR camera (Bendix Night Vision) modified to focus on closer objects. A temperature gradient was observed and calibrated with a handheld IR thermometer (CEN-TECH).

2.7.11 Ink-Jet printing:

An OmniJet 100 Mini Inkjet Printing System from UniJet was used to print Silver ink patterns on collagen films. In addition, printing was performed using an office inkjet printer (HP Photosmart Plus B209a-m). Pieces of collagen films were taped onto printer papers and were fed into the printer to print letters on the collagen films.

CHAPTER 3

TRANSFER PRINTING ONTO COLLAGEN

3.1 Introduction

Collagen, in its many shapes and forms, is difficult to classify and compare with traditional substrates for flexible electronics when it comes applications. Collagen's elastic modulus for example, can vary a lot depending on its crystalline form, crosslinking, level of hydration, leading to an order of magnitude of range in reported values from ~46.MPa [65] to ~1 GPa [66]. In chapter 2's published work [67], collagen film membranes had an elastic modulus of 2.04 GPa when tested dry at room temperature. However, due to its amorphous structure (without crystalline fibers), with relatively little crosslinking, the films have high water retention, changing the film from a flexible plastic to a hydrogel when put in liquids. Changes in humidity can also affect the film. This can be explained by the complex protein structure with many amino acids with a high degree of hydrogen bonding available. Although this can be ameliorated by crosslinking [68], it is an inherent property of collagen; it will still swell to some degree. This makes manufacturing of electrical devices challenging when compared to other plastics such as PET or Kapton (PI) especially for applications such as wearable electronics, making collagen altogether a less competitive candidate in this field. However, it is these exact properties that make collagen an ideal candidate for implantable electronics. Rigid implanted electrodes in a complex mechanical environment with soft tissues are an elastic mismatch, which can cause irritation and inflammation. Other strategies have been employed to address this such as PDMS (silicone), shape memory polymers that soften in physiological environments, or natural polymers such as silk or PLGA.

3.2 Issues with Biocompatibility

The use of natural polymers or biopolymers is an interesting strategy as plays on the body's foreign body response (FBR) and not elicit fibrotic encapsulation of the device [28], which ultimately cuts down on the performance and ultimate elimination of any implanted device. During implantation, devices will immediately be covered in interstitial fluids which contain a layer of proteins such as laminins, fibronectins, and other system dependent complements that ultimately is picked up by the immune system, which determines if/how FBR, and the immune response will occur. One of the components of the encapsulation layer is collagen [28]. If the FBR proceeds, immune cells are called to the implantation site due to chemokines, eventually the cells attach to the biomaterial and attempt to phagocytose the biomaterial using enzymes. With immune cells overpopulating the area, they undergo apoptosis at which point the encapsulation begins to occur, isolating the device from the environment. However, if the device is made on collagen, one of the components of the initial coating layer, then the majority of this drawback can be avoided. Ultimately, metal electrodes on collagen will have be exposed to the environment, so even if the immune cells start attaching to the collagen, the collagen based device can be broken down by phagocytosis using enzymes. However, collagen has another advantage, cells recognize collagen and attach to it in the extra cellular matrix (ECM) via focal adhesions using integrins. These integrins bind to ECM proteins via short amino acid sequences such as DGEA/GFOGER motifs on collagen [69]. Collagen integrin/receptors control cell migration, proliferation, adhesion, ECM regulation, and the activation of coagulation. Due to these properties, cells can readily form vascular networks that is why collagen has been shown to be successfully used for long term implants such as heart valves [70], as cell scaffolds for burn victims [71], and absorbable pericardial patches [45].

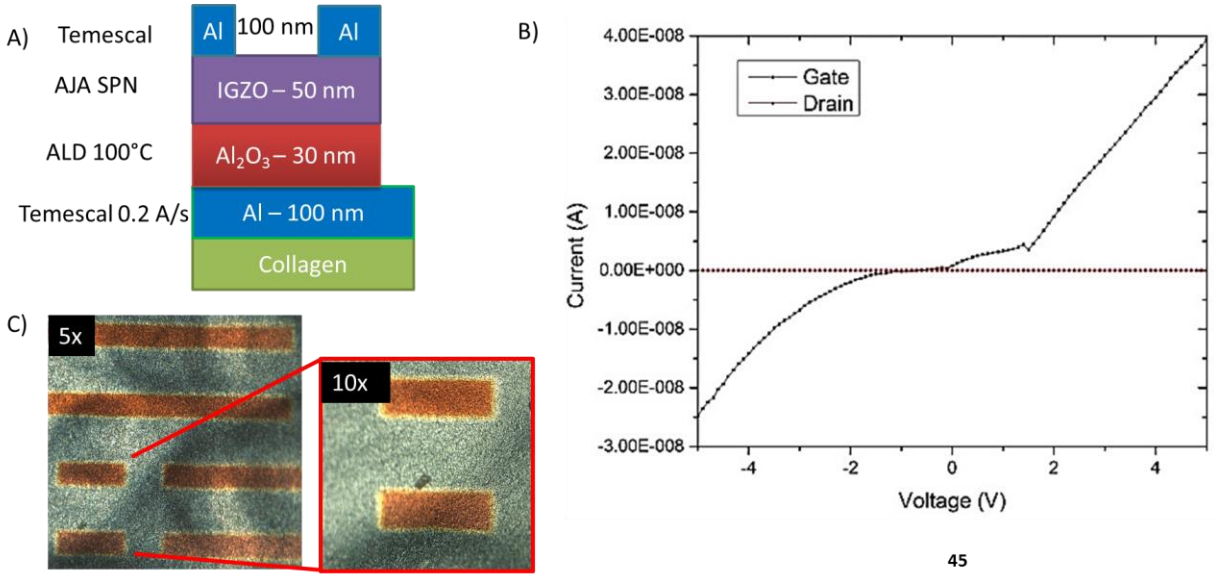

Figure 11. *(A) Transistor built directly on collagen, (B) IDVG Curve, (C) Device Topography.*

3.3 Fabrication Strategies

In order to develop an implantable biomedical device on collagen, such as the wireless devices demonstrated on silk [72], cellulose [25], and polyvinyl alcohol (PVA) [73], a more complex processing method needs to developed to overcome collagen's susceptibility to swelling. Although it was demonstrated that it is possible to deposit metal electrodes by e-beam deposition at room temperature, depositing semiconductor/dielectric layers has proven challenging as changes in temperature and pressure cause the deposited layers to form cracks due to collagen hygroscopic nature as seen in Figure 11. In addition, lithography would be needed to design complex devices, which would also prove difficult on collagen. Transfer printing is a strategy that has been shown to work on a number of substrates as seen on silk using PMMA [1], which is a process limited by temperature. Other sacrificial layers demonstrated include silicon oxide [25], nickel [74, 75], which can use harsh etchants to remove the sacrificial layer. On the other hand, there exist water dissolvable sacrificial layers such as PVA [76] and germanium oxide [77].

3.4 Germanium Oxide as a Sacrificial Layer

Germanium has long been a desirable material in the semiconductor industry because of its high mobility and small band gap [78], but it readily oxidizes into Germanium oxide that can interfere with the performance of devices. However, it is relatively easy to remove Germanium oxide as shown in this equation: $GeO_2(s) + H_2O\ (l) \leftrightarrow H_2GeO_3\ (aq)$

This process can be pH and temperature dependent as it has been shown by Sameshima et al. that higher temperature water can accelerate the etching time [79]. Sameshima et al. showed it is possible to sputter germanium in the presence of oxygen and argon gas to form germanium oxide that is the process used in this dissertation. It is also possible to oxidize germanium after deposition as demonstrated by Nam et al. [79], which showed that the process is not limited by temperature owing to its ceramic nature, allowing for annealing steps that can help semiconductor performance. Since Germanium oxide dissolves in water, it is therefore important to determine the proper encapsulation.

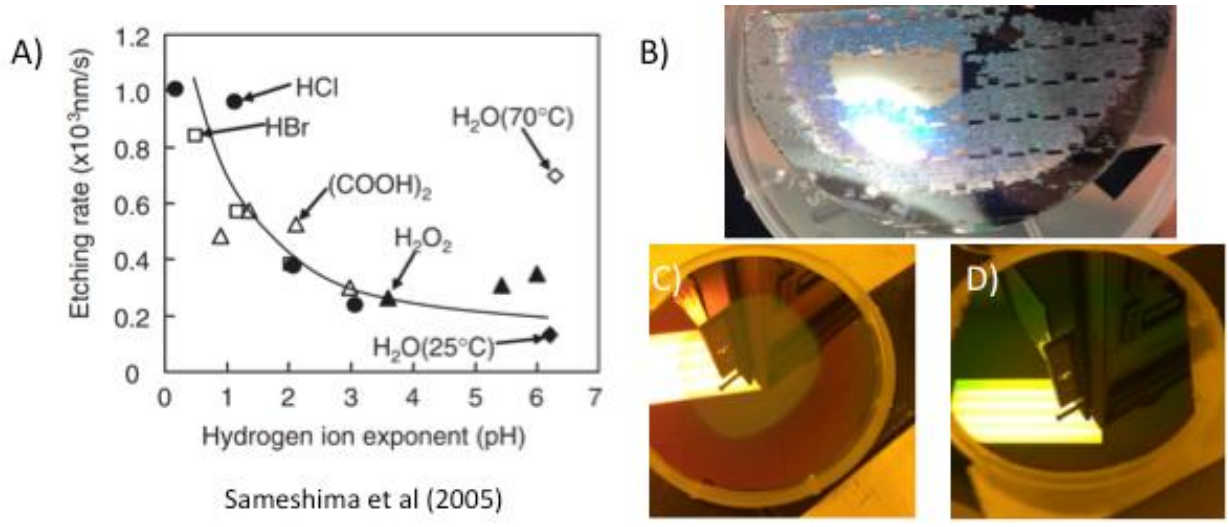

Figure 12. *(A) Germanium oxide etching, (B) Poor encapsulation, (C) degraded wafer, (D) properly encapsulated wafer.*

Silicon oxide deposited by Plasma Enhanced Chemical Vapor Deposition (PECVD) was used to encapsulate the germanium oxide and protect the layer from water during processing. In general, thicker layers dissolve faster, however, they are also more sensitive to the humidity in the air. Generally, the wafers are stored in an inert environment such as a nitrogen box, but over time they can degrade as shown in Figure 12C. The thicker the germanium layer, the thicker the encapsulation layer may need to be, as thicker layers may not be as uniform and are more likely to have pinholes which can lead to accidental lift during fabrication as shown in Figure 12B.

3.5 Transfer Printing Strategy

The following process was developed to transfer devices from wafers onto collagen:

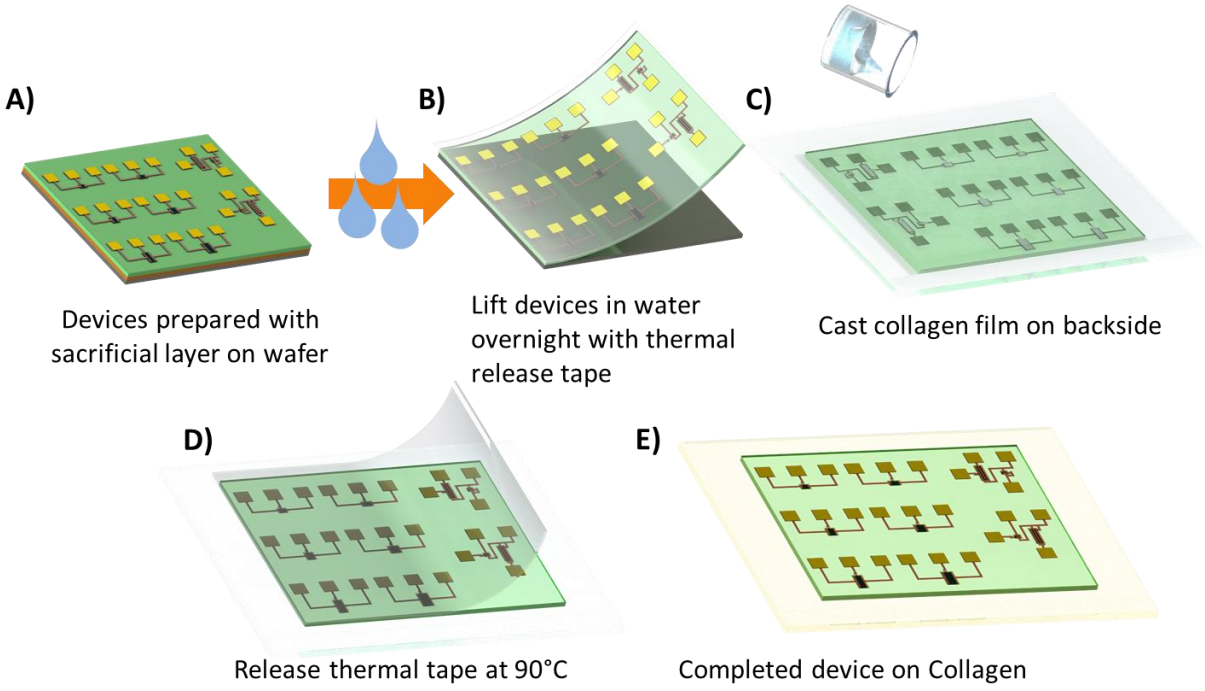

Figure 13. *(A) A wafer with sacrificial layer, (B) lift devices with water, (C) cast collagen on backside of the tape carrying devices, (D) thermal release, (E) completed device on collagen.*

Silicon oxide by PECVD was used as the encapsulation layer. Varying the silicon oxide thickness from 200nm to 500nm, there was minimal change in roughness with RMS roughness values ranging from 1-4nm. Compared to a wafer without germanium oxide, there is a less than ~6% change in roughness when holding the silicon oxide thickness constant as seen in Figure 14.

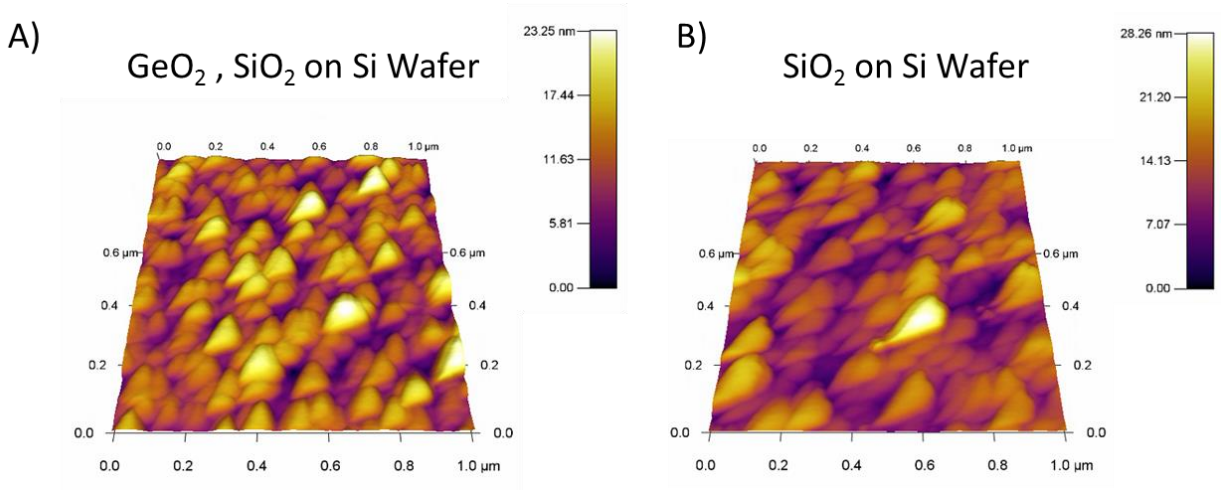

Figure 14. *(A) An AFM scan of silicon oxide encapsulation of Germanium oxide, (B) An AFM scan of Silicon oxide on a Si wafer.*

Once the device is prepared on the carrier wafer with silicon oxide encapsulating germanium oxide, the device is lifted in warm water (50 °C) overnight covering the device with a thermal release tape as seen in Figure 13B, once the device is lifted, it is flipped over and collagen can be cast on the backside using a frame using a collagen solution as described in the Methods section. Once dried (typically 24 hours), the devices can be released from the thermal tape at 90 °C. Flipped over the devices are then transferred to collagen. The device can now be encapsulated with a collagen film (crosslinked or not) as described in the Materials and Methods section. Devices need to be measured before collagen encapsulation makes it difficult to access the contacts.

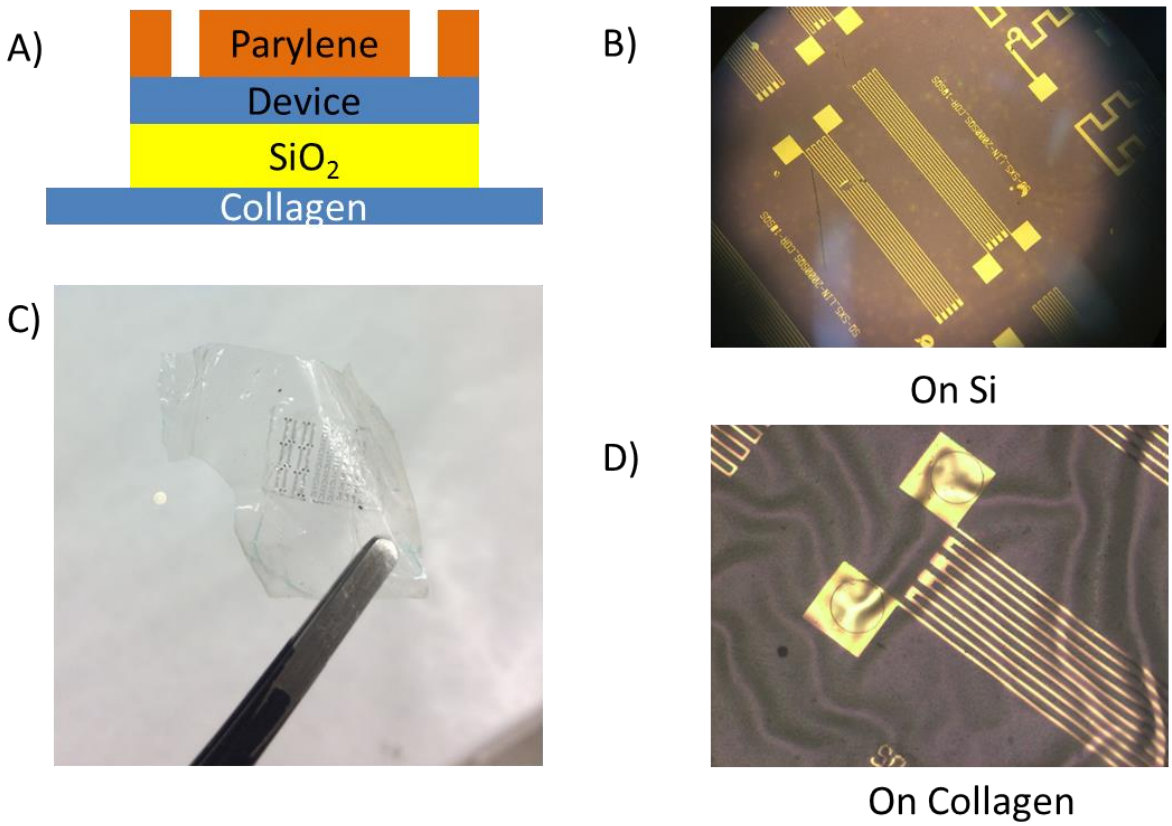

***Figure 15**. (A) Device layout, (B) Serpentines on silicon, (C) serpentines on collagen, (D) optical microscope image of serpentine on collagen taped onto a glass slide.*

3.6 Serpentine Resistors, Capacitors, Transistors, and Inverters

Serpentines were used in initial studies to examine the sacrificial layer parameters, and also as the process stack got more complex, useful to study how the process affects each layer type. Gold was deposited onto the carrier wafer with chromium as an adhesion layer and transferred onto collagen as previously described. These serpentines showed no significant changes in morphology and also no significant changes in resistance (<1%). Although this was demonstrated for an array of small devices, this observation extends to larger area devices such as a Multielectrode array (MEA) used for neural stimulation and measurements [80] as seen in Figure 16 which also shows an actual devices being transferred from the wafer onto a collagen film.

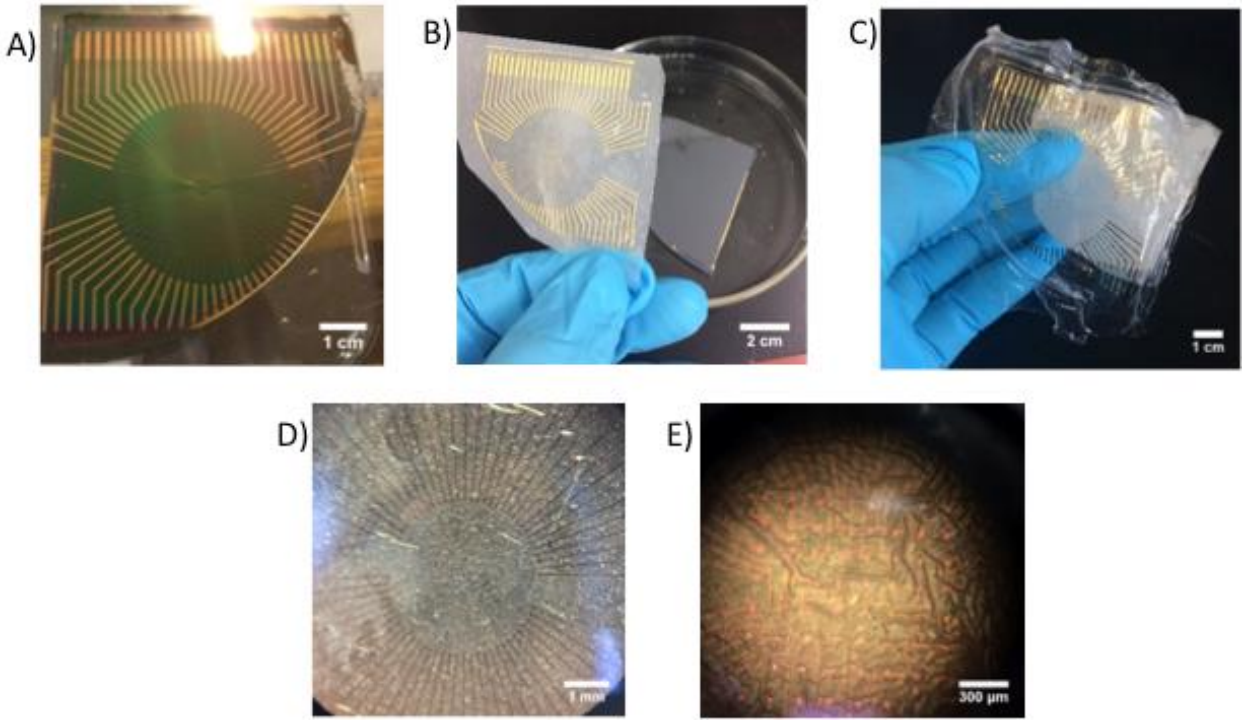

Figure 16. *(A) Multielectrode Array (MEA) neural pattern on carrier wafer, (B) Pattern lifted onto transfer tape, (C) Collagen cast and peeled from transfer tape, (D)the inner portion of MEA pattern, (E)the innermost portion of MEA pattern.*

Capacitors were transferred from a carrier wafer onto collagen as seen in Figure 17. The dielectric in the capacitors deposited on top of the entire area, including the bottom electrode, was aluminum oxide (~19 nm) by Atomic Layer Deposition (ALD). Vias were etched through the dielectric layer to access the bottom electrode. Au/Cr was deposited as the top electrode with an additional pad to access the bottom electrode through the via. Parylene was deposited to encapsulate the entire device array with vias opened to access only the pad and protect the device array during transfer. Devices were measured and showed slight changes across capacitor area size and stability up to 1 MHz as seen in Figure 17. The changes can be attributed to deformations affecting the dielectric during the transfer process.

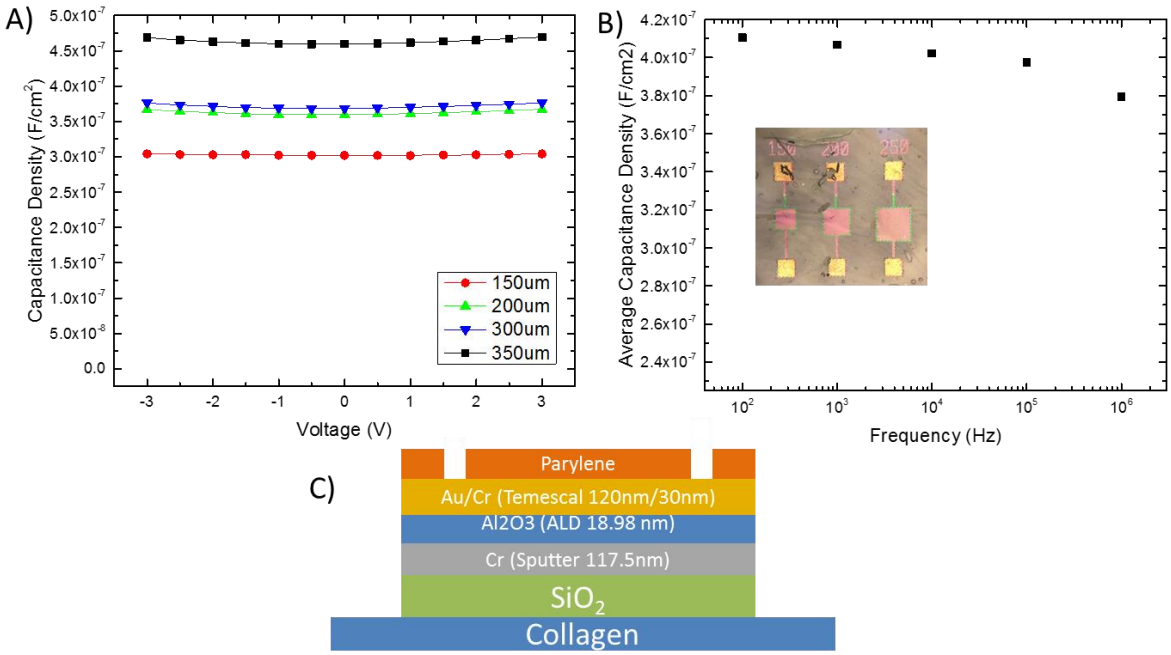

Figure 17. *(A) Capacitance density vs. voltage, (B) capacitance density vs. frequency, (C) process stack for capacitor.*

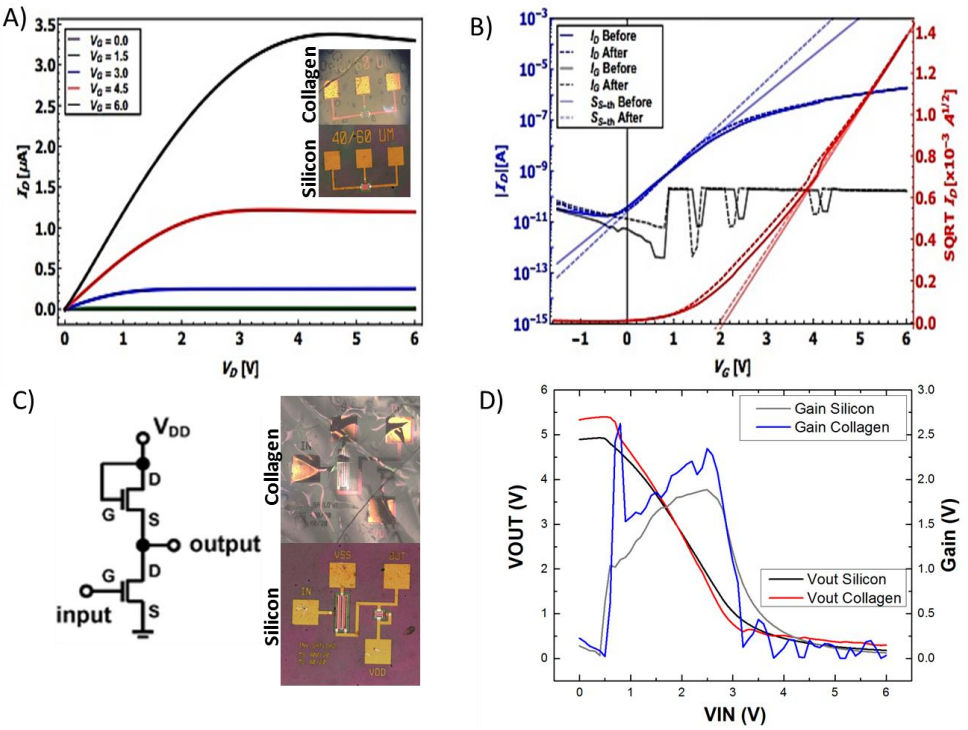

Figure 18. *(A) An IDVD curve for a transistor on collagen, (B) An IDVG before and after for a transistor on collagen, (C) an Inverter on Collagen, (D) Inverter Vout vs Vin.*

Transistors were fabricated on a carrier wafer and transferred onto collagen with a process stack as described in Figure 19 using the architecture described by Chapman et al. [81]. Figure 18A shows the device on both silicon and collagen with minimal changes in morphology, as well as the drain voltage vs the gate current from the range of the gate voltage from 0 to 6V. Figure 18B shows the gate voltage vs. the drain current before and after sweeping from -1V to 6V. From this results the mobility was calculated to be ~0.48 with a threshold voltage of ~2.4, a 59% and 18 % decrease compared to their counterparts on silicon. These changes can be attributed to stresses experienced during the transfer, which may affect the gate/dielectric interface. The low values can be attributed to a change in the gate material from ITO to Cr when compared to the architecture described by Chapman et al. A saturated load was demonstrated on collagen that showed the same behavior on collagen, as on silicon, which demonstrates logic processing is feasible on collagen.

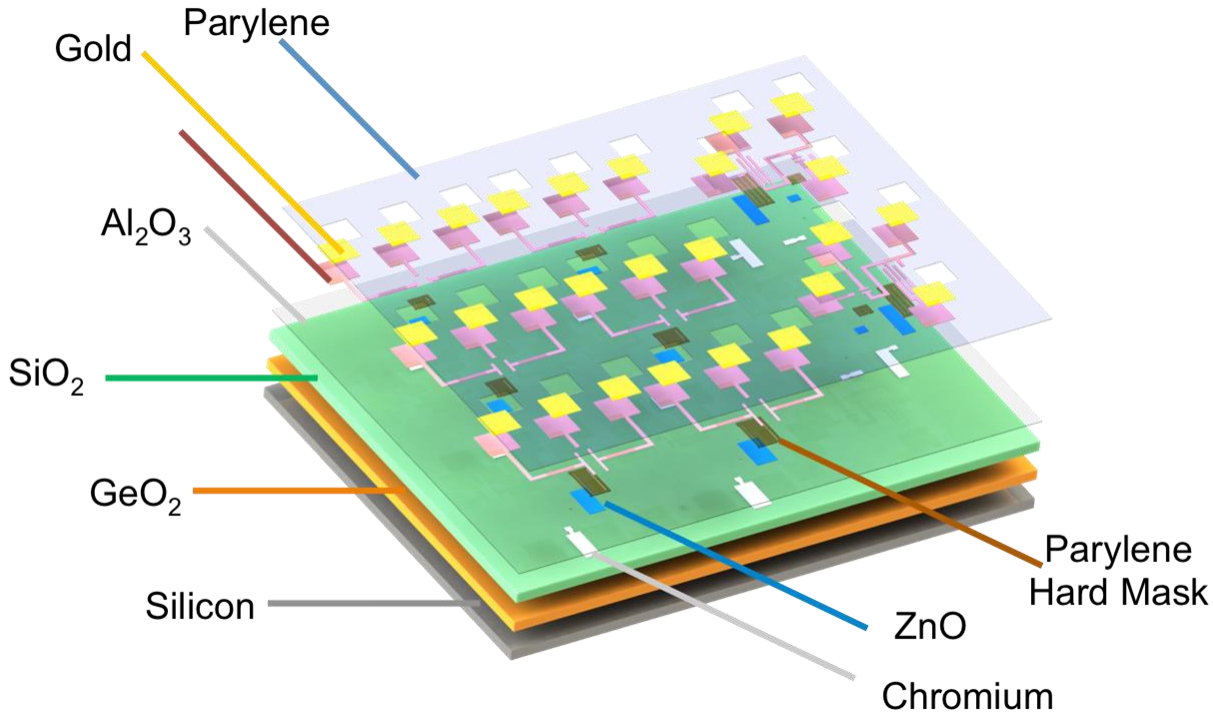

Figure 19. *The process stack for transistor and inverter.*

3.7 Cell Culture Studies on Fabricated Devices

In order to study *in vitro* cell response to implantation of devices on collagen substrates described in this dissertation, A549 epithelial cells and MC3T3 Osteoblasts were seeded and grown on encapsulated devices on collagen. Osteoblasts are fibroblasts that have differentiated into a cell that synthesizes bone. Fibroblasts in general play an immune response role when tissue injury occurs. A549 is a lung tissue epithelia cell, which is widely used as a cell model for drug metabolism, tissue engineering, and as a transfection host. Generally, cells can be counted using a trypan blue staining kit, however, this staining involves detaching cells using trypsin. When counting cells on a hemocytometer, it is difficult to ascertain as to which cells were growing on the collagen or on the cell plate within the same cell well. MTS Cell proliferation kits offer an alternative that measures cell metabolism. MTS tetrazolium is bioreduced into the colored formazan by active cells, the absorbance of which can be measured as proportional to the number of living cells. The cell assay was conducted on collagen-encapsulated devices as described in the Methods section 3.11. Cells without collagen were used as the positive control, wells with dead cells were used as the negative control, and the cell media with MTS was used as the background for measurement. Cell viability results are summarized in Figure 20, with 70% and 85% viabilities for epithelial and osteoblast cells respectively after an eight day incubation. This value can be attributed to the shock cells experience when they are growing in a new environment, as cells can grow on top and below the encapsulated device as well as along the cell plate walls. Overtime from one to eight days incubation, cell viability increased as the cells acclimated, possibly increasing further outside the experiment window of eight day incubation. Epithelial cells in general proliferated at a higher rate than osteoblasts, however, might be explained by how the

squamous cells grow attached to each other helping proliferation to accelerate, while the osteoblasts are more spaced out as seen in Figure 20.

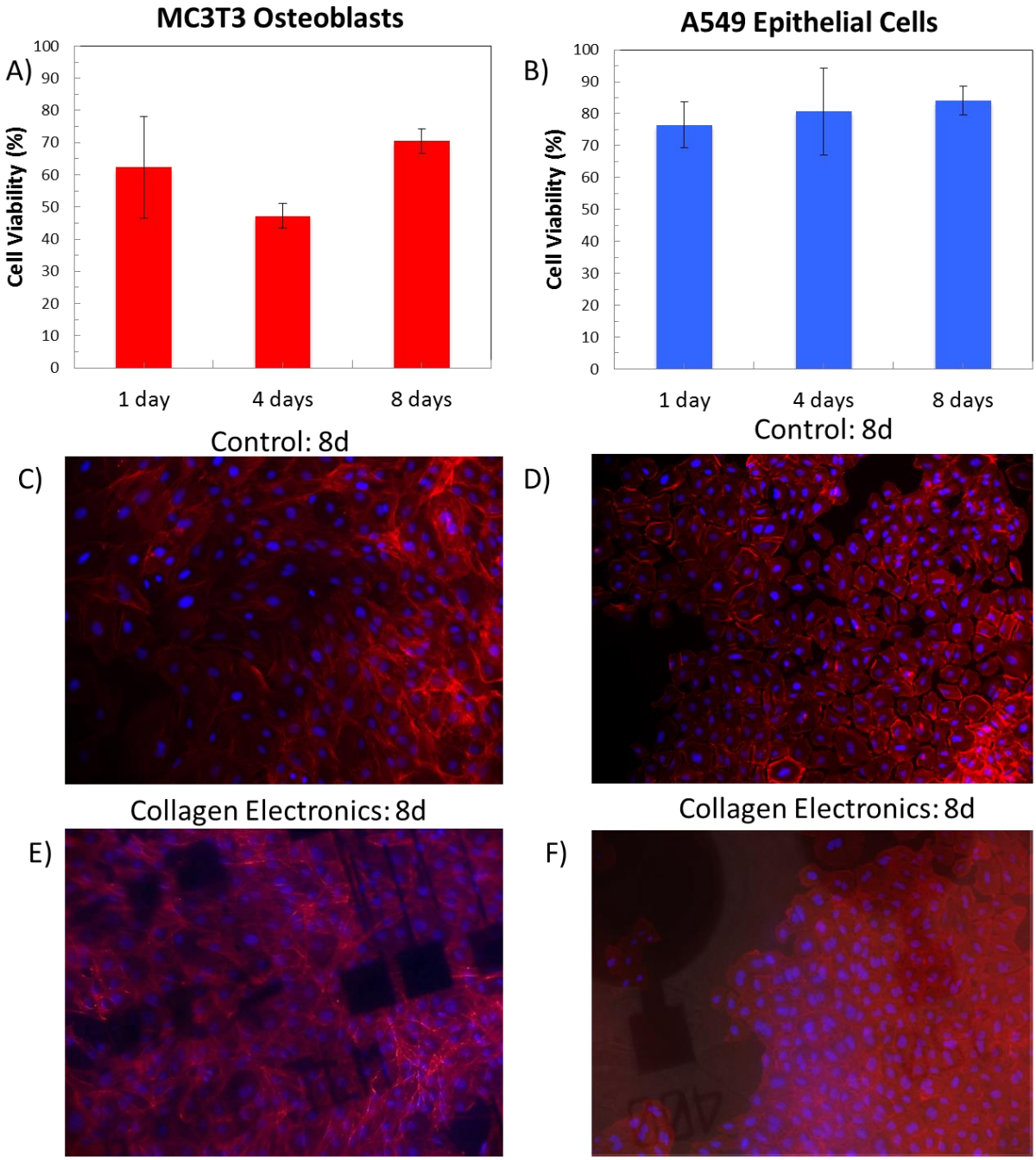

Figure 20. *(A) MC3T3 osteoblast cell viability, (B) A549 epithelial cell, (C) osteoblasts after 8 day incubation control, (D) after 8 day incubation on fabricated devices, (E) Epithelial cells after 8 day incubation control, (F) after 8 day incubation on fabricated devices.*

Cell staining was also performed on the cells seeded on the collagen-encapsulated devices in order to observe cell adhesion. Cellular integrins are the means by which cells recognize and interact with collagen. Therefore, both cell lines were stained with TRITC and DAPI in order to observe the actin and nuclei of the cells as described in the respective Methods sections 3.11. Actin staining helps visualize how the cells attach to the films and also if the cells have the correct morphology. Figure 20 shows that the cells have a healthy morphology compared to their control in both the control and the device cell wells for both epithelial and osteoblast cell lines. This demonstrates that cells are recognizing the collagen and attaching to it.

3.8 Collagenase Degradation

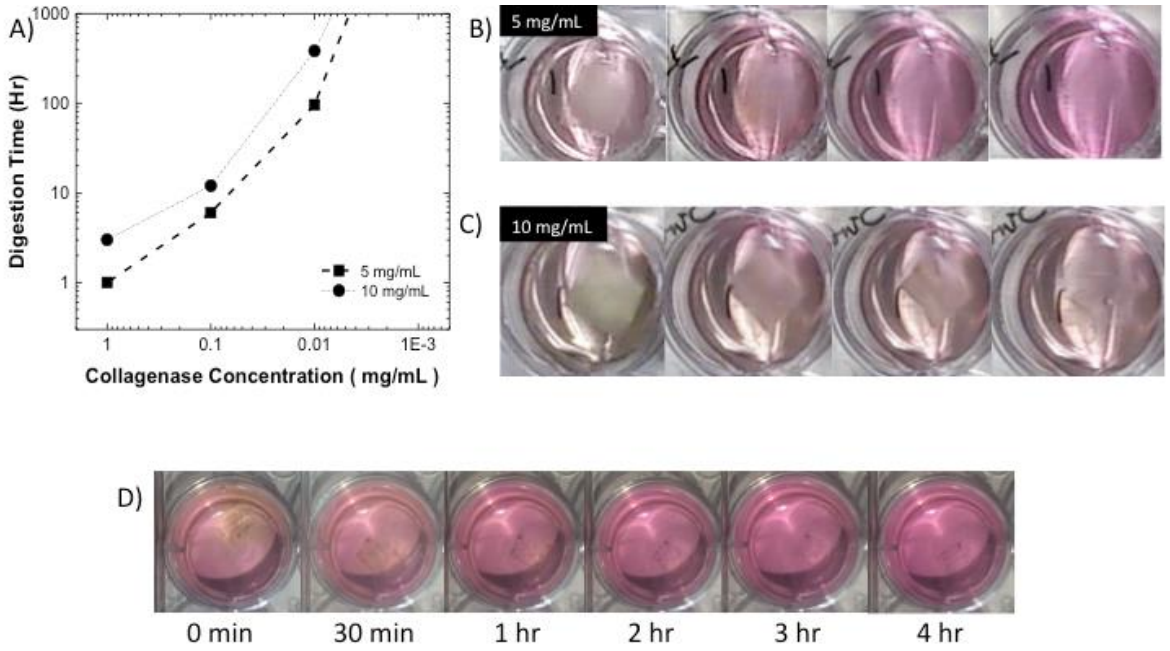

Figure 21. *(A) Collagen digestion time, (B) 5 mg/mL film digestion, (C) 10 mg/mL film digestion, (D) Collagen encapsulated device digestion.*

Collagenases are a family of enzymes that break the peptide bonds that hold collagen together. Cells such as osteoblasts and fibroblasts secrete collagenases as part of the normal immune

response or to remodel collagen in different tissues. Although its exact mechanism is not completely understood, it is believed that collagenase unzips the triple helix. When designing devices encapsulated in collagen that will be implanted long-term, it is important to understand how to control collagen degradation as it may be important to have devices last longer depending on the intended therapy. In order to better understand this, collagen films were placed in a collagenase D solution in order to measure the digestion time. As shown in Figure 21, it is possible to increase the degradation time of collagen films simply by increasing the concentration of the collagen solution from which the film is made of. Digestion was observed at less than 1 hr and 4 hrs for 5 mg/mL and 10 mg/mL films for 1 mg/mL collagenase solution concentration. Since it is difficult to determine how much collagenase is secreted during an immune response, this test was run at decreasing logarithmic concentrations for which the trend was similar to 10 mg/mL films lasting longer than 5 mg/mL. When placing the encapsulated device in collagenase, we see the device was dissolved after 4 hrs.

3.9 Device Encapsulation

While in Chapter 2, it was demonstrated that electrodes encapsulated between two collagen sheets are relatively stable when placed in PBS, it was difficult to measure how the functionality of the encapsulated device changed without compromising the encapsulation. Using the transfer printing method, it was possible to selectively encapsulated and have access to the electrodes. This was done by opening the contacts via lithography. However, this still necessitated a large electrode area to solder wires and seal shut the connection. The electrode encapsulation design for this experiment is shown in Figure 22A. A device stack of silicon oxide, aluminum oxide, gold chrome

electrode, and parylene overcoat was transferred onto collagen taped using scotch double-sided tape to a glass slide for stability, with the electrode terminals open. Then collagen was placed on the interdigital portion of the electrode, leaving the terminals open.

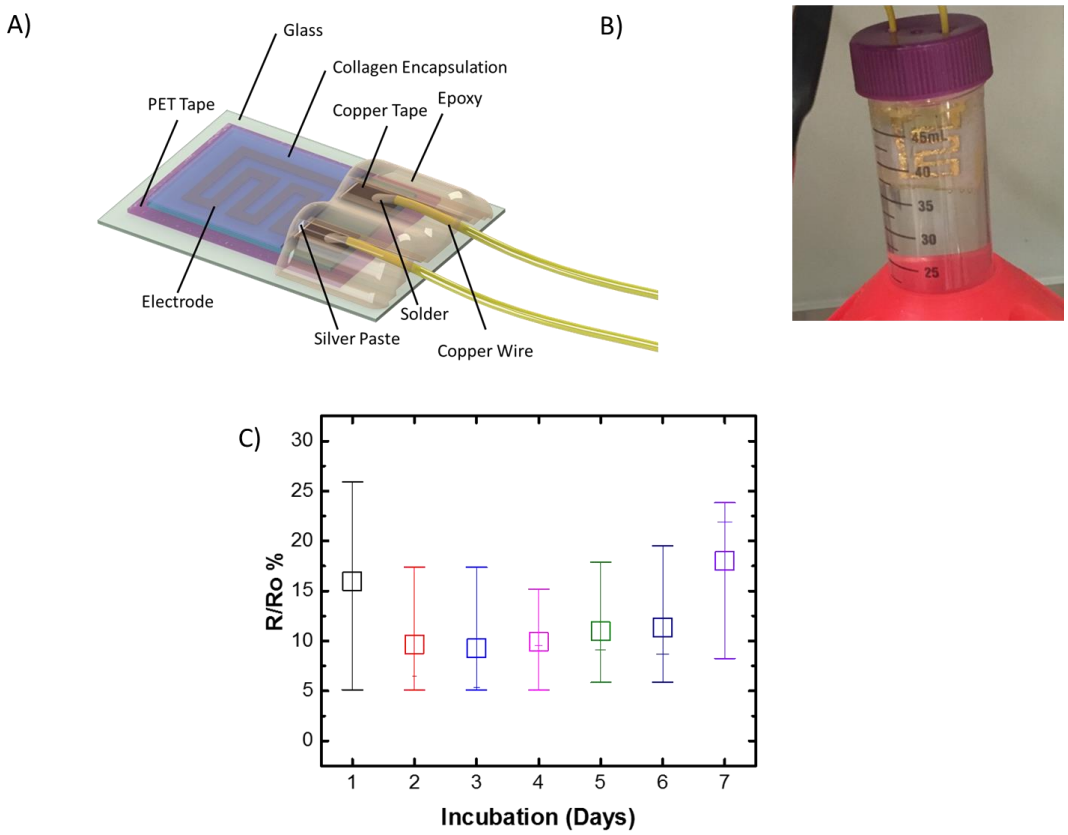

Figure 22. *(A) Electrode encapsulation, (B) Electrode encapsulation setup, (C) Change in resistance over 7 days in 37.5°C, (D) Change in resistance simulated over 28 weeks at 37.5°C.*

Wires soldered onto the copper tape tabs were placed and glued using silver pasted on the electrode terminals, and finally fully encapsulated with epoxy. In this manner, it is possible to observe the functionality of an encapsulated device while incubated in PBS at 37.5°C. This design, however, is not without faults. The epoxy/tape fixing the collagen device onto glass fails first in that it starts detaching from the glass slide as seen in Figure 23A. This is important because like a stent on a broken bone, it keeps the collagen device in place since the collagen will float. As it floats, it bends around the epoxy/collagen interface, which forms a sharp edge, another point of failure. Finally,

excessive movement during resistance measurements via multimeter can result in the silver paste/electrode interface separating after the tape/glass separation as seen in Figure 23B.

Incubated over a period of 7 days, samples averaged 18% change in resistance with large enough variation (8.5% standard deviation) to suggest the change is constant throughout the incubation period as shown in Figure 22C). The large variation can be attributed to the tape, glue, and glass used to fix the collagen device in place during the incubation. The collagen device itself remains encapsulated with no visible damage to the electrode regardless of the loss of contact between the silver paste and electrode contact. A sample was also placed in a simulated 28 week encapsulation of 37.5°C as demonstrated by Garcia Sandoval et al [82] as seem in Figure A18. Using the following equation $t_{37}=t_T \, x \, Q_{10}^{dT/10}$, where t_T is two weeks, Q_{10}, the aging factor, is equal to 2, and dT is $T\text{-}37.5°C$, where T is 75°C. By incubating at a higher temperature for a set time, it is possible to simulate aging over a longer period of time at a lower temperature. This experiment showed a 13% simulated change in resistance after 28 weeks, within the variation of the one week experiment, showing that the sample change minimally over an extended incubation time, ideal for implantable electronics

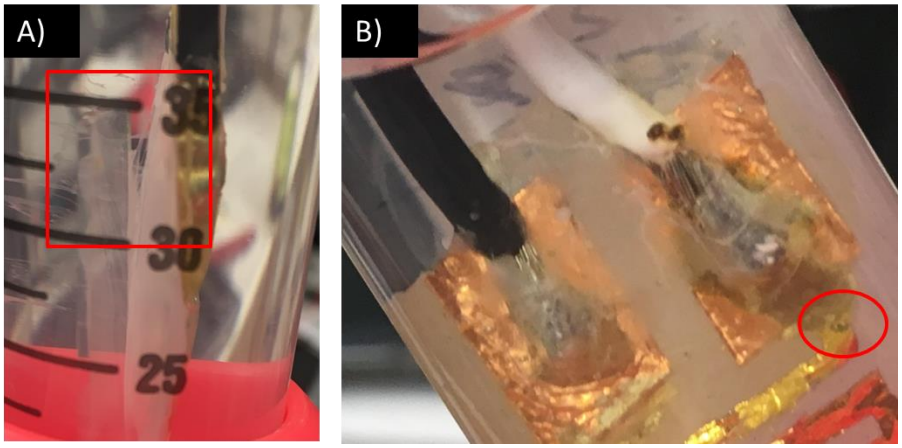

Figure 23. *(A) Sample separating from the tape (B) Silver paste/electrode interface fracture.*

3.10 Conclusion

In regard to the thesis hypothesis, various milestones have been hit towards demonstrating collagen as a substrate for transient electronics. In this section, it is show that it is possible to transfer devices fabricated on a silicon wafer onto collagen with minimal changes to biocompatibility. This process allows for a universality of semiconductor processes compatible with collagen with the added benefit of high temperature processing due to the sacrificial layer's ceramic nature. Germanium oxide was demonstrated to be compatible with processes of at least 650 °C opening the possibility of various annealing treatment that are not available to processes using polymers as sacrificial layers. Although there are some changes in performance in regards to capacitors and transistors, improvements can be made with the silicon oxide and parylene outer layers to better protect the fabricated device throughout the transfer process as seen in S21. Cracks in optical images are mainly on the parylene layer.

Additionally, although the transistor shows low mobility, this mostly originated from the original transistor on the silicon wafer before the process. Improvements of the transistor on silicon will be passed to transistors on collagen. Simple circuits such as an inverter were demonstrated on collagen, considering that transfer printing was demonstrated on collagen, more complex circuit designs can be transferred as well. MC3T3 and A549 cell lines showed no changes in cell morphology with slight decreases in cell proliferation on devices built on. It was also demonstrated that devices built on collagen can be digested by enzyme collagenase, which enables us to postulate that devices built on collagen can be bioresorbable if designed with transient metals, dielectrics, and semiconductors. A process to control degradation rate of collagen based devices was

demonstrated. Increasing the collagen solution concentration that was used to make films results in films that take longer to degrade in collagenase solution. Together, transfer printing, cell viability on collagen, and collagenase degradation show collagen's viability as a substrate for transient electronics. Incubation experiments demonstrated that encapsulated devices are functional, however, there are still limitations with measuring as it is difficult to isolate whether the changes are inherent to the device or the measurement methods. This uncertainty demonstrates the need to move towards an all wireless platform to isolate these issues where devices are fully encapsulated. Chapter 2 demonstrated that collagen has a dielectric constant ideal for RF applications, however, further studies need to be done to quantify changes in the dielectric constant while incubated in aqueous environments.

3.11 Materials and Methods

3.11.1 Preparation of Collagen:

Ovine collagen type I solution (OV-CL, CollTech Perth, Australia) was frozen (-20 °C) and lyophilized/freeze-dried (Labconco FreeZone 2.5 L, <1 Pa, <-50 °C). Collagen solutions were prepared using lyophilized ovine collagen sponge at 5 mg/mL and 10 mg/mL concentrations in 0.1 M acetic acid. Amino acid profile as provided by CollTECH is in Figure A18.

3.11.2 Preparation of silicon wafer for transfer:

A Silicon wafer with <100> orientation was prepared for sputtering by washing with Buffered Oxide Etch (BOE) with 7:1 concentration for 30 seconds to eliminate any surface oxides and was immediately placed in the sputtering chamber. Using a germanium target (N-type, 5-40 ohm-cm,

99.999% pure), a germanium oxide layer was deposited onto the silicon wafer by RF Sputtering (Ar 40 sccm, O_2 20 sccm, 120 W, 6 torr, 60min, AJA International 1500-V Sputter System). The wafer was immediately encapsulated by plasma enhanced chemical vapor deposition (PECVD) of SiO_2 (~300 nm) at 250 °C via Plasma-Term 190 PECVD (2%SiH4/He). Additional annealing can be done prior to PECVD encapsulation at 650 °C in N_2 gas. An additional layer of Al_2O_3 (~15 nm, UltraTech ALD Savannah) can be deposited on the SiO_2 encapsulated wafer to eliminate any possible pinholes due to debris that can affect the transfer. The prepared wafer is then stored in a nitrogen glovebox to prevent degradation of the sacrificial germanium oxide by air humidity.

3.11.3 Fabrication of ZnO TFTs:

The gate metal chromium (Cr) was deposited onto the prepared wafer via electron beam evaporation (~100 nm) via Temescal e-beam evaporator and etched after photolithography. Aluminum oxide (Al2O3) was deposited as the dielectric (150 °C, ALD, ~15 nm). Zinc Oxide (ZnO) was the semiconductor deposited by Pulse Laser Deposition (PLD, 100 C, 20mtorr, ~ 45 nm). Parylene was used as both a protection layer and hard mask layer to protect the active area (~250 nm) by Chemical Vapor Deposition (CVD) using a Specialty Coating Systems Parylene Labcoater. Source and Drain Aluminum (Al) metal contacts were deposited by e-beam (200 nm). Additionally, Gold/Chrome (200 nm, 30 nm) was deposited on the contact pads to prevent tip penetration during measuring and prevent oxidation during plasma etching. A final protective encapsulation layer of parylene was deposited via CVD (~ 500 nm) and the contact pads were opened with photolithography via RIE plasma.

3.11.4 Fabrication of Aluminum Oxide MIM Capacitors:

Bottom contacts were made from Chromium, deposited (~100 nm) using e-beam evaporation. Aluminum oxide was used as the dielectric layer (~15 nm) by ALD. Vias were etched through the aluminum oxide using phosphoric acid and BOE. Top contacts were made by depositing Gold Chrome (200 nm, 10 nm) using e-beam evaporation.

3.11.5 Transfer printing of Devices onto Collagen:

Completed devices were transferred using a temporary substrate (Nitto Thermal Release Tape, 90 °C) by placing tape on the devices fabricated on prepared silicon and then placing them in water overnight at 37 °C. Once lifted, collagen was film cast onto the silicon oxide exposed backside of the device on thermal release tape using a frame. One mL of collagen solution was cast on a 15 × 15 mm area. Once cast, the collagen/device/thermal release tape was placed on a hot plate at 90 °C to release the completed device onto a collagen film. To facilitate measurements, the stack was taped onto a glass slide before releasing the thermal tape. Devices were encapsulated using a hydrated collagen film (treated or as-made), sandwiching the device between the film cast collagen and the hydrated collagen film.

3.11.6 Measurement of MIM Capacitors and TFTs:

Capacitors on collagen/silicon were measured using a Cascade Microtech nanoprobe station with a Keithley 4200 Semiconductor Characterization System. The capacitance was measured using an attached Agilent 4284A Precision LCR meter. Capacitance-voltage (C-V) curves were conducted at frequencies ranging from 100 Hz to 1 MHz with voltage sweeps from -3 V to 3 V.

3.11.7 Cell Culture Assay:

MC3T3 osteoblast and A549 alveolar basal epithelial cell lines were cultured for assays. one mL of 104 cells/mL was used to seed collagen devices (covering the bottom of a 24 cell well plates). 100 µL of MTS tetrazolium was added to the 24 cell well plates maintaining a 1:10 vol. ratio and incubated at 37 °C. 100 µL of the supernatant was transferred onto a 96 cell well plate after 4 hr incubation. Absorbance was measured using a Thermo Scientific Varioskan Flash. Cells without collagen were used as positive control. Wells without cells and wells with dead cells were used as a negative control. Cell media with MTS was used as a background baseline for measurements. Prior to seeding onto collagen films with devices, the films were sterilized by washing in IPA/water 70% and placed under UV light for 30 minutes.

3.11.8 Cell Culture Staining:

Devices with cells were stained with an Actin Cytoskeleton and Focal Adhesion Staining kit with the following protocol: Cells were fixed with a 4% PFA in 1X PBS for 15-20 min at room temperature (2X wash with wash buffer). 0.1%v Triton X-100 in 1X PBS was used to permeabilize cells for 5 min at room temperature, after which cells were washed 2X with wash buffer. Cells were placed in blocking solution for 30 min at room temperature in dark ambient conditions. Cells were incubated in primary antibody solution (anti-vinculin 1:1000 vol in blocking solution) with a 2X buffer wash afterwards. Cells were placed in dilute secondary antibody solution (TRITC, 1:1000 vol in 1x PBS). Nuclei counterstaining was done in DAPI (1 µL: 1 mL PBS) for 5 min at room temperature. Imaging was done on a Zeiss Axiovert 200M at 10X magnification.

3.11.9 Collagen Degradation via Collagenase:

One cm^2 untreated collagen films were placed in 1, 0.1, 0.01, 0.001 mg/mL concentrations of Collagenase D in 1X HBSS solution and monitored over a period of seven days with a time-lapse photo capture (IPhone 5s, Lapse it Pro) for 5 mg/mL collagen films and 10 mg/mL films.

CHAPTER 4

CROSSLINKING OF COLLAGEN

4.1 Introduction

The collagen extraction process using pepsin de-polymerizes collagen and can damage the amino/carboxyl terminals that contain intermolecular cross-links as described by S. Gorgieva et al. [83].

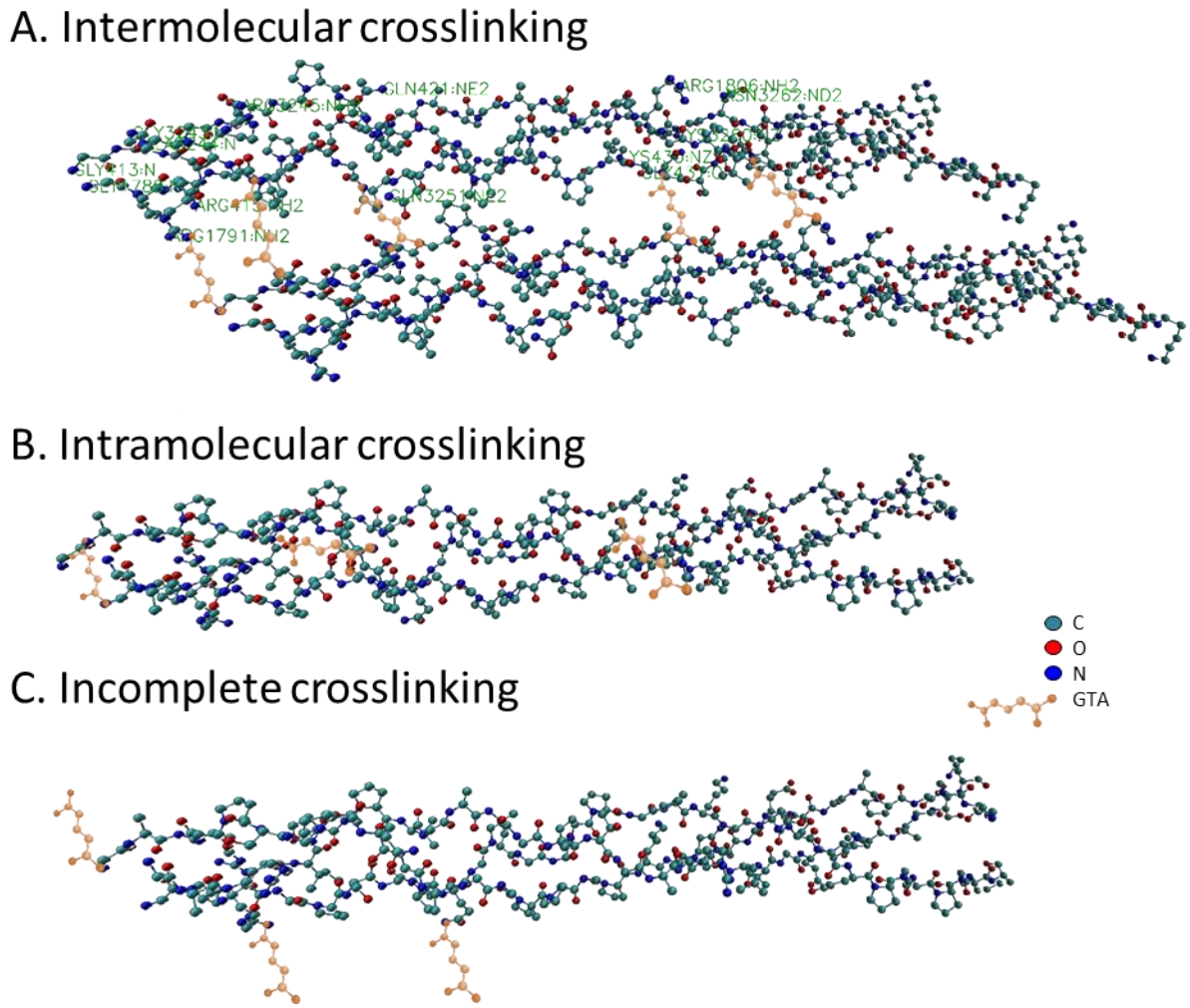

Figure 24. *(A) Glutaraldehyde (GTA) Intermolecular crosslinking between collagen molecules with highlighted amine crosslinking sites, (B) Intramolecular crosslinking within a collagen molecule, (C) Incomplete crosslinking of collagen with hanging GTA molecules.*

This process affects all of collagen's properties resulting in poor thermal stability, high water swelling ratio, antigenicity, and lower mechanical strength. Due to all these effects, there is a significant interest in a variety of crosslinking methods to abate these changes in properties. Crosslinking methods of collagen are expansive, ranging from chemical crosslinking using aldehydes like Glutaraldehyde (GTA) [84] and Carbodiimides (EDC) [84, 85] to enzymatic (Transglutaminase) [86] to physical crosslinking using UV [87] and Gamma radiation [88].

Each crosslinking method have with their own drawbacks, however, GTA is well understood and in particular has fast, controllable, tunable reactions. GTA crosslinking occurs between carboxyl groups on the GTA molecule and the free amine groups of lysine (LYS) and arginine (ARG) as seen in Figure 24A, forming a Schiff-base [89]. Using a previously developed atomistic model of the collagen molecule by Zhou et al. [90], and a GTA pdb (protein data bank) model (T3D4359), Figure 24 shows three different GTA crosslinking scenarios: Intermolecular crosslinking between two collagen molecules is shown in Figure 24A. Intramolecular crosslinks within collagen [91] between two amine sites within the collagen molecule is shown in Figure 24B. Incomplete crosslinking is also possible whereby GTA molecules are left hanging or GTA is left unreacted, which can cause local incompatibility and result in cytotoxicity. All of these scenarios can occur at the same time at varying degrees. Regardless of possible cytotoxic effects, GTA has become the standard cross linker for the production of collagen-based heart valves [83], as patent protected protocols minimize uncross linked GTA residues. Standard alcohol based sterilization methods will not work with GTA, since it will react with residual GTA and form a more unstable collagen crosslinked compound [92].

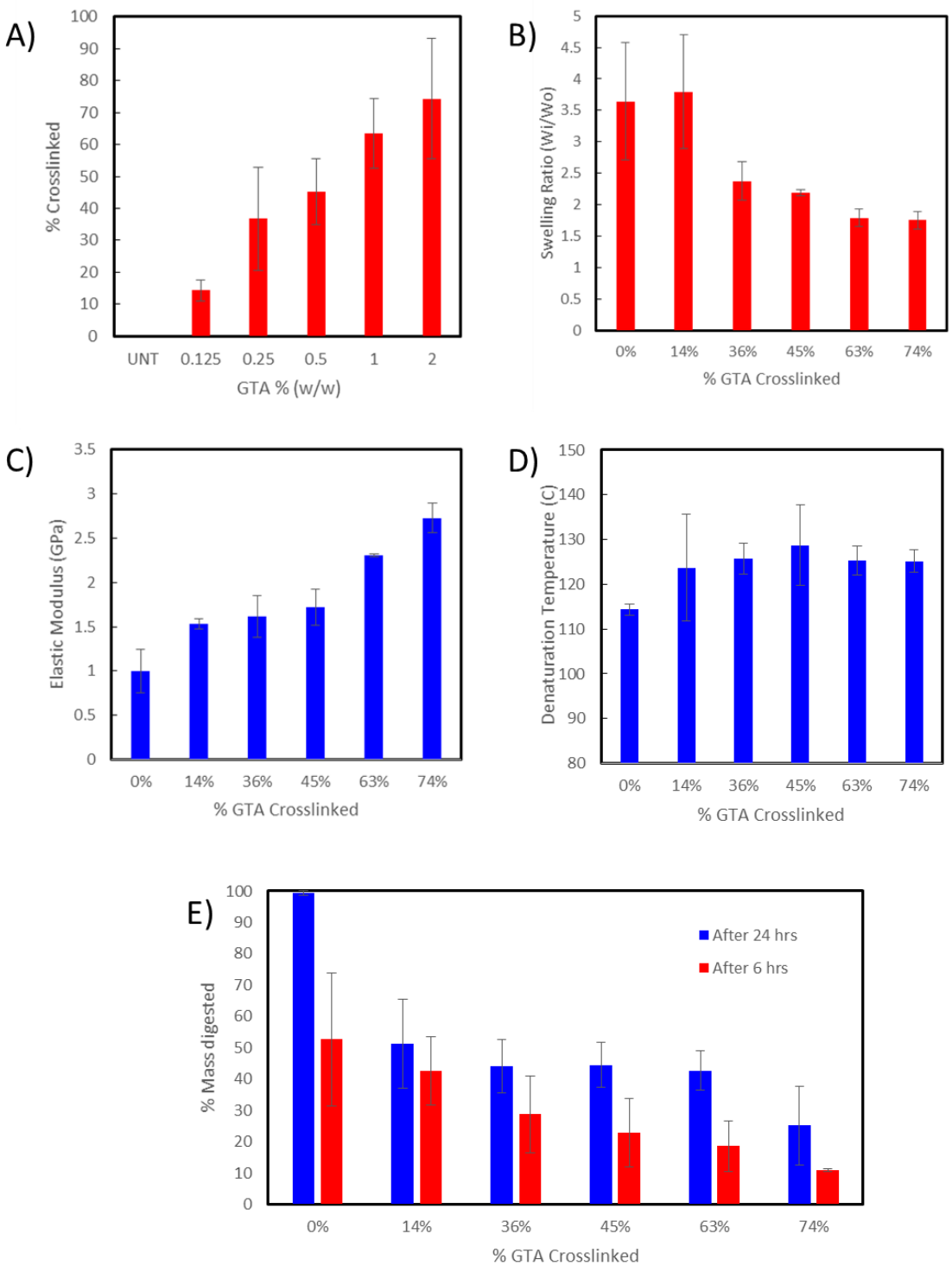

Figure 25. *(A) Relative percentage crosslink of GTA crosslinked collagen, (B) Swelling ratio of GTA crosslinked collagen films in PBS, (C) the elastic modulus vs. GTA% crosslinked samples, (D) Denaturation temperature vs. GTA%, (E) % Mass digested in collagenase vs. GTA%.*

4.2 GTA Crosslinking and TNBS Assay

Collagen crosslinking by GTA was studied in order to determine possible film property improvement in regards to flexible electronics. In order to compare different collagen films, it was first necessary to establish a quantitative comparison of relative crosslinking. There are a variety of assays to determine crosslinking, however, TNBS (trinitrobenzensulfonic acid) is one of the most popular spectroscopic methods [93]. Typically used in protein studies, TNBS is a fast method of measuring the amount of amine content available in a solution, which correlates with crosslinking since GTA crosslinking targets free amine groups on collagen molecules. When TNBS binds with amine groups on collagen, an orange/yellow solution derivative is formed, whose absorbance intensity correlates with the availability of amine sites or inversely the degree of crosslinking. The absorbance can readily be measured using a card reader, allowing for a large set of samples to be processed quickly. For this study, collagen films were first cross-linked in GTA/1X PBS solution concentrations ranging from 0.125% (w/w) to 2% (w/w) for incremental doubling incubation times of 15 minutes, 30 minutes, 1 hour, 2 hours, and finally 24 hours. Samples were washed two cycles of 1X PBS for 30 minutes and 30 minutes water.

Once cross-linked, the following protocol based on Grovel et al [85] and Castaneda et al. [93] was followed: the collagen films were cut into 1-3 mg samples and placed into a TNBS buffer solution and incubated for two hours at 40 °C. After TNBS incubation, samples were placed in 6M HCL to solubilize and incubated overnight at 60 °C. Samples were diluted in water and cooled down to room temperature. Sample absorbance was measured at 320 nm in 96 well cell plates using a BioTek Synergy H4 plate reader. Cross-linking degree % was calculated to be: (Abs_{GTA} -Abs_{unt})/

Abs_{unt})x100, where Abs_{unt} represents the absorbance intensity of untreated collagen after subtracting absorbance of a noise control sample. Abs_{GTA} similarly represents the absorbance intensity of GTA treated collagen. Relative crosslink percentage of collagen ranged from 74% crosslinked at 2% (w/w) GTA to 14% crosslinked at 0.125% (w/w) GTA as seen in Figure 25A where n =3.

4.3 FTIR analysis of crosslinked samples

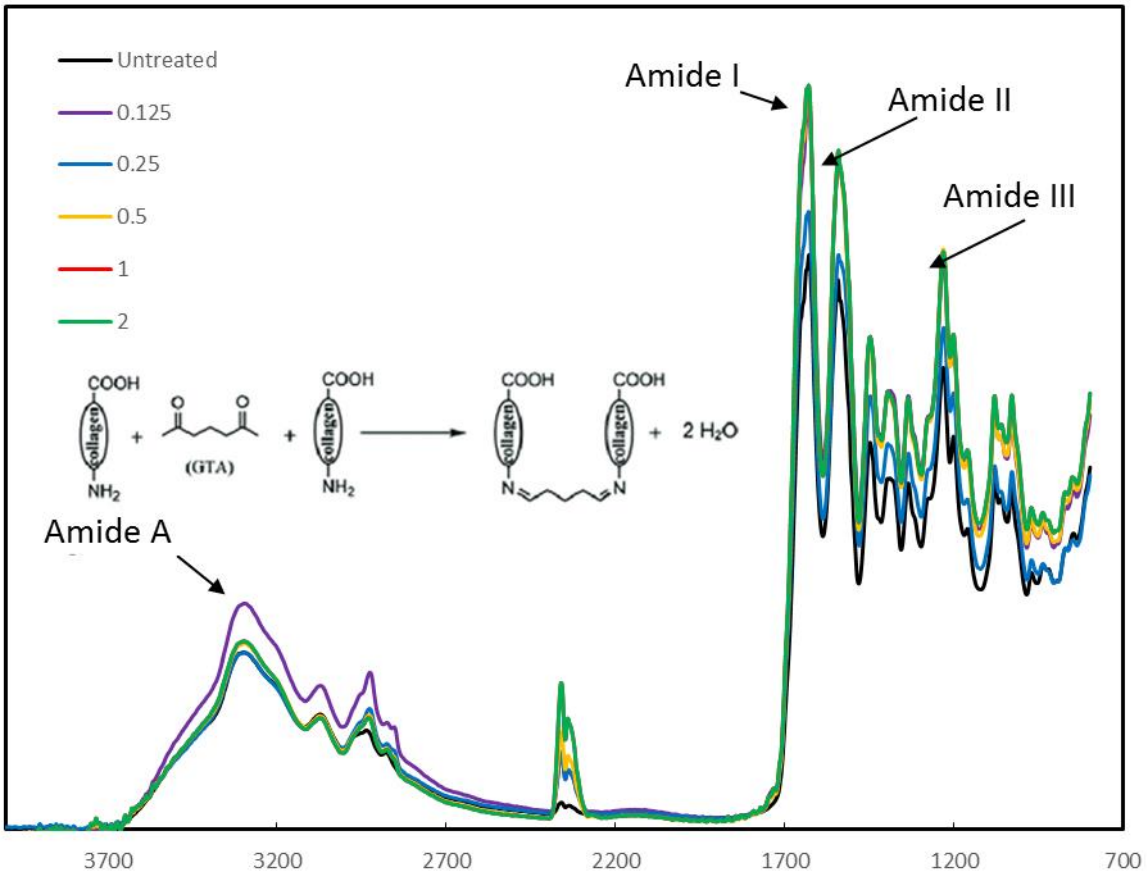

Figure 26. *FTIR analysis of % GTA crosslinked samples with GTA mechanism* [84].

In addition to TNBS, FTIR analysis was done to confirm relative crosslinking between collagen samples. Amide A at 3200 - 3500 cm^{-1} is the peak typically associated with the amine group N-H as well as hydroxyl group O-H, both of which are associated with hydrogen bonding and therefore

water swelling. With an increase in crosslinking, the expected trend would be a decrease in intensity in this peak, but when GTA crosslinks with amine in collagen, the carbonyl group C = O on GTA is replaced by an O - H group so there is no trend in regards to % crosslink with GTA. From 14% to 45% crosslinked, the intensity peak decreases, however, for 63%-74% the intensity peak increases. Amide I at ~ 1650 cm^{-1} is typically associated with the carbonyl group C = O, however, there is also an overlap with the C = N group [94], which results from the Schiff's based formed when GTA crosslinks with amine on collagen [84]. The overall trend in Amide I, II, and III is an increase with a percent increase in GTA crosslinking suggesting that the films are more crosslinked with each additional GTA treatment.

4.4 Crosslinked Swelling

Intermolecular and intramolecular bonds play a major role in collagen's stability, particularly at the molecular level [94]. As mentioned previously in Section 4.1, the collagen extraction process can damage the collagen molecule's terminal intramolecular bonds, which destabilizes it. Therefore, the structure is highly dependent on intramolecular hydrogen bonding from hydroxyl (OH) and amine (NH) groups on sidechains to maintain the triple helix structure. As a result of hydrogen bonding dependency, collagen films are highly susceptible to mechanical deformation in water. GTA crosslinking, which targets amine groups, can decrease the film's hydrophilicity and increase stability in aqueous environments. To observe this, collagen film samples were cut (approx. 15 mm × 15 mm, 30 - 40 mg) and placed into 1X PBS overnight. Films were removed from the PBS solution the next day and blotted with filter paper and immediately weighed. Swelling ratio was calculated as the swollen collagen weight divided by original weight, or

Ws/Wo as seen in Figure 25B. The untreated collagen can swell up to an average 3.6 times its own weight in 1X PBS. GTA crosslinked collagen ranges from 3.7 at 14% to 1.75 at 74% GTA crosslinked. In other words, untreated collagen swells by 260% its own weight, while 74% GTA crosslinked collagen swells by 75% weight, a 175% reduction, showing that GTA crosslinking helps stabilize collagen in aqueous environments and help with handling of films that often get stuck to themselves and are difficult to unfold without damaging.

4.5 Crosslinked Mechanical Properties

Increased intermolecular bonding should also increase the mechanical properties of collagen films as additional bonding can help transfer loads amongst collagen molecules. Tensile testing of GTA-treated collagen was done to observe this phenomenon. Samples 5 mm wide were glued on a cardboard frame with a 30 mm gauge length and 3 mm/min displacement. The elastic modulus was calculated from the resulting stress strain curves. The results are summarized in Figure 25C, showing an elastic modulus of ~ 0.9 GPa for an untreated collagen film. The elastic modulus for treated films ranged from ~1.53 GPa for 14% GTA crosslinked to ~2.7 GPa for 74% GTA crosslinked or a 272% increase in stiffness.

4.6 Crosslinked Thermal Stability

Differential Scanning Calorimetry (DSC) experiments were done on collagen crosslinked samples at rates of 5°C/min up to 300°C in a nitrogen environment. The denaturation temperature of an untreated sample was 112°C to 133°C for 14% GTA crosslinked, to 142°C for a 74% GTA crosslinked sample. Within certain variation, the trend was positive, with increasing percentage

crosslinks resulting in a more thermally stable collagen. Increased intramolecular bonds can be attributed to this increase in denaturation temperature. Denaturation temperature is when the triple helix structure unwinds irreversibly, therefore more intramolecular bonds increases the amount of energy needed to denature.

4.7 Crosslinked Collagenase Degradation

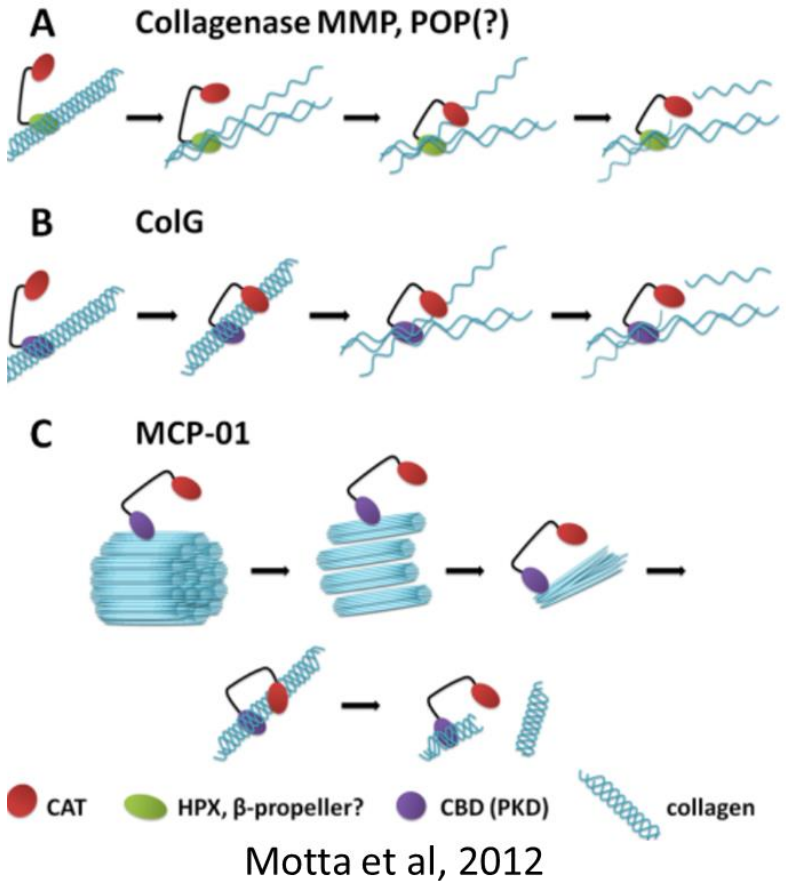

Figure 27. *(A) Mammalian Collagenase, (B) Collagenase derived from bacteria, (C) Serine-protease deseasin MCP-01 (mammalian)* [96].

As seen in Section 3.8, collagen once in the body is remodeled and digested by a variety of enzymes, one of which is collagenase. In Section 3.8, it was demonstrated that increasing the concentration of the collagen solution from 5 mg/mL to 10 mg/mL used to cast films can increase time it takes for collagen films to be 100% digested in collagenase by four fold. Fine control of

this digestion is of interest for a long term view on the application of implantable electronics with collagen as their substrate. The mechanism by which collagenase digests or unwinds collagen is known as the collagenolytic mechanism and varies by collagenase type [97]. Figure 27 shows the differences between mammalian and bacterial collagen. Mammalian collagenase typically unwinds the collagen triple helix as it passes through it and cleaves it at specific sites [98]. Bacterial collagenase hydrates itself and passes through the collagen triple helix and then cleaves it at specific sites [96]. Regardless of the mechanism, collagenase is highly dependent on the structural organization of collagen molecules as additional crosslinks between molecules as shown with fibers can slow down the degradation. In fibers, collagenase has to start from the outside of the fiber and digest inwards, slowing down the degradation rate for an equivalent mass of collagen that is not organize. Although still not fully understood, collagenase D, which is derived from bacteria, cleaves collagen at Y-Gly bonds, which are hyperactive sites in the Gly-X-Y collagen amino acid sequence. This characteristic of collagenase D has been studied on synthetic peptides [99]. Regardless of the specifics of the mechanisms, intramolecular and intermolecular bonding play a key role. In this sense, intermolecular crosslinking between collagen molecules can slow down the collagenolytic mechanism. Similarly, intramolecular crosslinking can slow down the unwinding of the collagen triple helix by mammalian collagenase. In either scenario, GTA crosslinks can be used to control this mechanism by varying relative crosslinking degree.

To study how GTA crosslinking can affect the rate of the collagenolytic mechanism, the crosslinked GTA samples were cut into 15 mm ×15 mm squares, 30 - 40 mg in weight and placed in 1 mL of 1 mg/mL of Collagenase D/HBSS. Two sets of films were pulled out and washed with

PBS and blotted at 6 and 24 hours and weighed. Figure 25E shows percentage mass digested during these incubation times. After six hours, untreated samples were 52% digested, where the crosslinked samples ranged from 42% for 14% GTA crosslinked to 10.8% for 74% GTA crosslinked samples. This means that for an incubation time of six hours, one can slow down collagen digestion by roughly 20 - 80% for 14% and 74% GTA crosslinked. For an incubation time of 24 hours, a similar trend is observed, with untreated samples completely digested and a range of 51% to 25% for 14% to 74% GTA crosslinked. The percentage mass loss is not linear across incubation times, and this can be attributed to the saturation as the one mL collagenase solution was constant during the experiment as switching out media to avoid

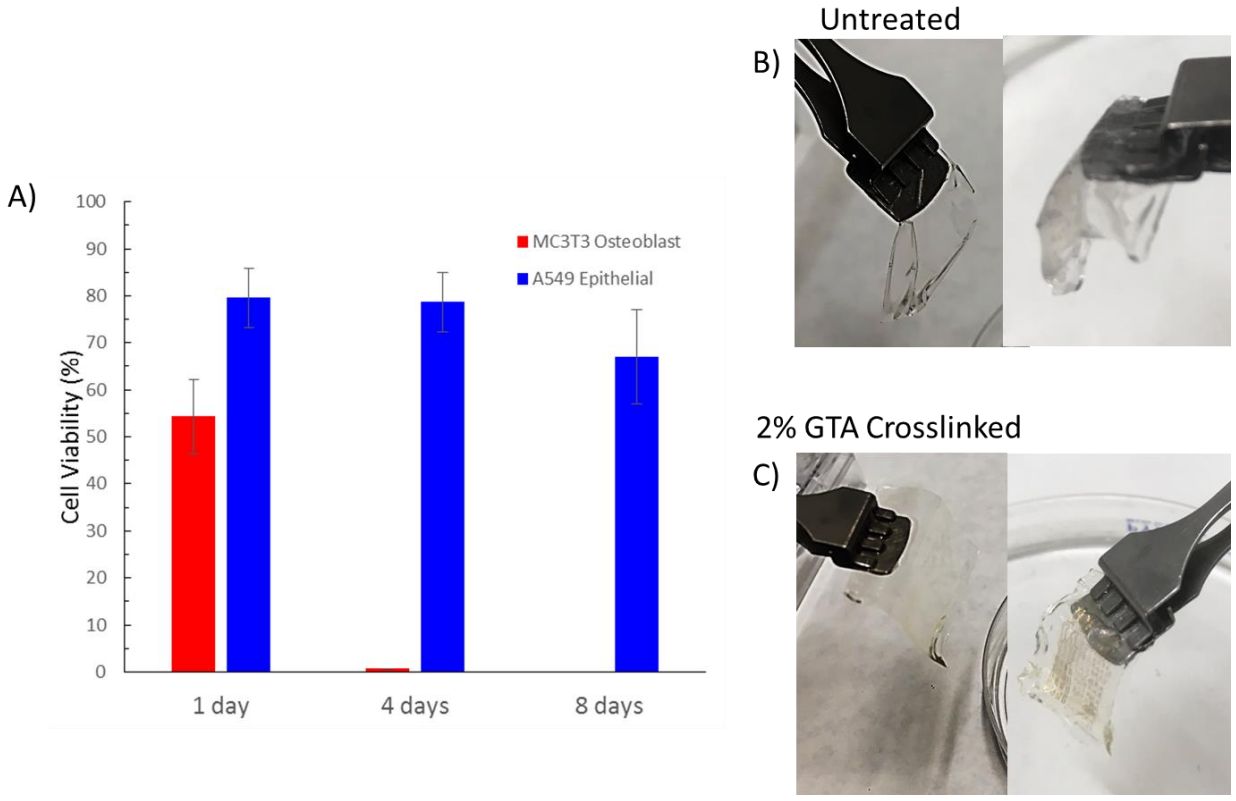

Figure 28. *(A) Cell viability of 0.25% GTA treated collagen samples (B) collagen film pulled out of a water vial, (C) 2% treated collagen film pulled out of a water vial.*

4.8 Conclusions

Towards the initial thesis hypothesis about demonstrating controllable degradation of collagen films for transient electronics, in Chapter 4 it was shown that it is possible. Controllable degradation was shown by crosslinking collagen with glutaraldehyde that can slow down the collagenase degradation process by 20 - 80%. Further work needs to be done to improve the biocompatibility of crosslinked samples as cell viability is demonstrably lower for GTA treated films as seen in Figure 28A. This is attributed more to the sterilization method used in cell culturing than to the crosslinking itself. Alcohol based sterilization can make GTA unstable and even more cytotoxic. Further exploration of sterilization strategies is needed, namely ethylene oxide gas to counter unreacted GTA residues in collagen without reacting with it similar to alcohol. GTA crosslinked films showed remarkable differences in water absorption, stiffness, and denaturation temperature. This makes devices more stable in aqueous environments. Collagen films with devices (crosslinked in the same manner after transferring) are much easier to handle as the untreated films fold into themselves. Figures 28B and C summarize these significant changes as the crosslinked film is demonstrably more stable and easier to handle after being pulled out of a water vial after a 24 hours. Higher percentage crosslinked films are also more amenable to the transfer printing process as less superficial cracks on parylene for GTA crosslinked collagen films are observed compared to the untreated collagen films as seen in Figure A21. Further work is needed to determine in vivo performance for these crosslinked films.

4.9 Materials and Methods

4.9.1 Collagen Crosslinking:

50% Glutaraldehyde (GTA) was diluted into % GTA in 1X PBS. Collagen Films were incubated as desired then washed as follows: 1X PBS 30 min, DI water 30 min, 1X PBS 30 min, DI water 30 min

The following treatments were used:

- 0.125% GTA solution for 15 minutes
- 0.25% GTA solution for 30 minutes
- 0.5% GTA solution for 1 hr
- 1% GTA solution for 2 hr
- 2% GTA solution for 24 hrs

4.9.2 Crosslinked Collagen Degradation via Collagenase:

For GTA crosslinked films, collagen was kept at a constant 5 mg/mL and the following protocol was used :

- Samples cut ~15mm x 15mm ~30 - 40mg samples
- Placed in 1 mg/mL Collagenase D in HBSS
- Films were blotted with filter paper and quickly weighed
- % Mass Digested $(M_f-M_o)/M_o$ x 100

  Where M_o is the control weight placed in 1X PBS, blotted, and weighed before treatment

4.9.3 TNBS Assay:

For TNBS Assay the following protocol was used:

Step 1

- 1-3 mg film in 0.5 mL of 4% (w/v) $NaHCO_3$
- Add 0.5 mL of 0.05% (w/v) TNBS
- Incubate for 2hr at 40 °C

Step 2

- Add 1.5 mL of 6 M HCL to solubilize
- Incubate for 90 min overnight at 60 °C

Step 3

- Add 2.5 mL of water to dilute and cool down samples
- 0.1 mL or 100 µL was drawn and placed in a 96 well cell plate
- Measure absorbance at 320 nm using a BioTek Synergy H4 plate reader

CHAPTER 5

OUTLOOK AND CONCLUSIONS

5.1 Towards Wireless Implantable Devices

In order to study the performance of implanted device fabricated on collagen, it is necessary to develop a wireless platform to power and communicate with the device with a rectifying circuit as demonstrated by Hwang et al [33], which is powered by an antenna as seen in Figure 29A. This circuit is called a half-wave rectifier with a smoothing capacitor as seen in Figure 29B. It was demonstrated in this dissertation, that it is possible fabricate capacitors and serpentine resistors on collagen, so only a diode with good rectification need to be developed and then integrated into a circuit design.

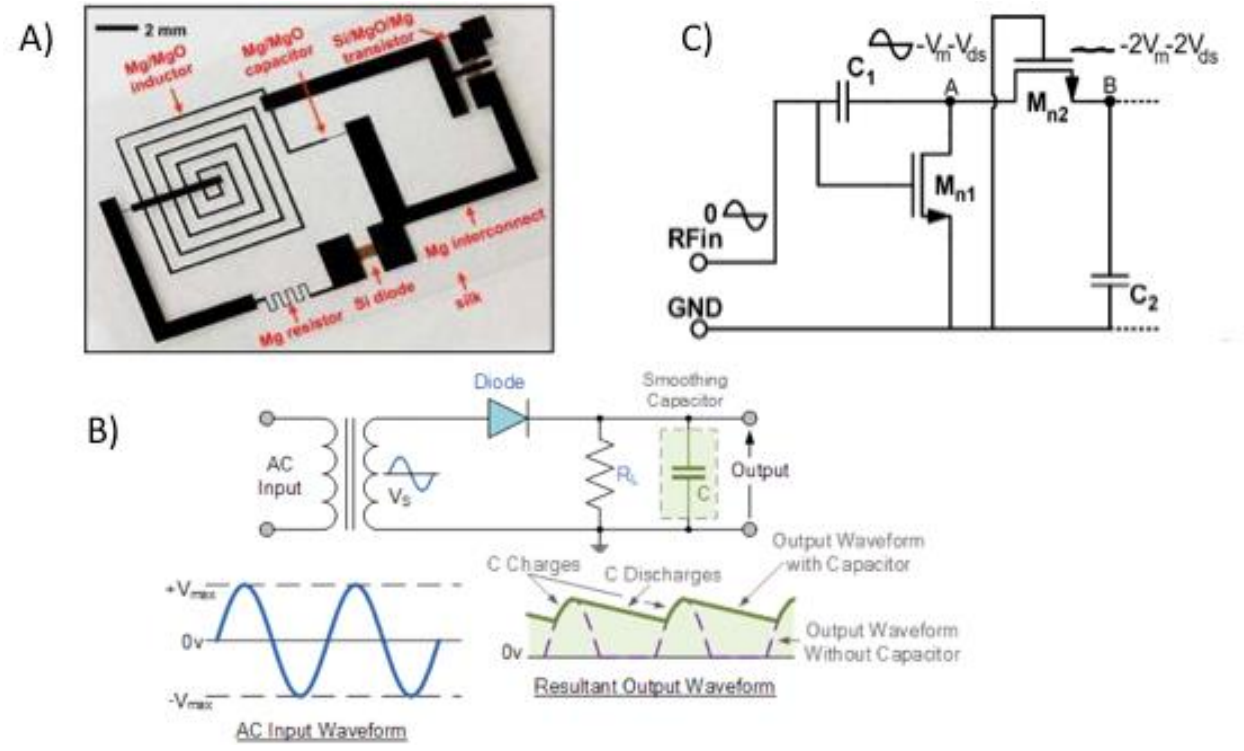

Figure 29. *(A) RF circuit on silk* [33]*, (B) half-wave rectifier* [100]*, (C) TFT-capacitor rectifier* [101].

5.2 Work progress towards rectifying circuit

Towards this end, current work involves working on a P-N junction diode based on nickel oxide or Schottky Indium Gallium Zinc Oxide (IGZO) with collaborators for a rectifying circuit. The nickel oxide device has been shown to work on shadow mask based designs with rectification orders of 5 magnitudes when comparing forward and reverse bias. As shown in Figure 30, current devices need further work with a new lithographic process to transfer onto collagen. The current iteration uses dry etching to complete the device and this hardens the patterning resin which is difficult to remove. Although lithography was done on the device, it is difficult to remove resin and therefore measure the device. An alternative strategy is to use liftoff to avoid etching, but finding a liftoff layer that can handle high temperature may prove to be difficult.

A rectifying circuit as designed in Section 5.1 was fabricated as shown in Figure 30B and Figure S23, showing that the semiconductor process protocol designed is compatible with all the different layers. However, the circuit did not show rectification when excited with an antenna nor when AC voltage was applied. This was attributed to the IGZO diode itself as measured after full fabrication. The IGZO diode after fabrication was no longer rectifying. Tracing back the progress made on the IGZO diode which uses platinum and aluminum as schottky and ohmic contacts respectively shows that shadow mask diodes have five orders of magnitude of rectification as demonstrated by Zhang et al [103]. Using a lithographic process, which involves acid etching to define vias to connect contacts, Figure 31A shows that the lithographic process shows only three orders of magnitude of rectification, less than a shadow mask diode design. This can be attributed to acid leaching and potentially damaging the IGZO layer. A more complex structure such as a rectifying

circuit and antenna has several acid etching layers that can potentially damage the IGZO layer until it shows no rectification. Typically sensitive semiconductor layers are protected by an insulator such as parylene, which was included in the rectifying design. Future work should focus on redesigning this insulating mask and adding additional mask layers to protect the semiconductor layer from acid leaching.

If neither diode process yields acceptable rectification from the diodes, it is possible to form a rectification circuit with transistors as seen in Figure 29C. Transistors and capacitors fabricated on a single chip simultaneously has already been demonstrated. In order to accommodate for this design, we would have to redesign the masks, but the layer stack would remain the same, so none of the process parameters would change. However, redesigning the masks can prove costly as the TFT's described in this study used 8 masks, so it should only be a last resort when designing a rectifying circuit. Once the circuit is fabricated, it would be possible to simulate sending a wireless signal by applying an AC voltage at the terminals and measure the rectified voltage at the outputs. This would be necessary until the correct inductor coil (antenna) is determined. The dimensions of the planar square coil were determined by calculating the inductance using the Grover method [102]. In order to account for possible errors, coils with more and less turns should be tested.

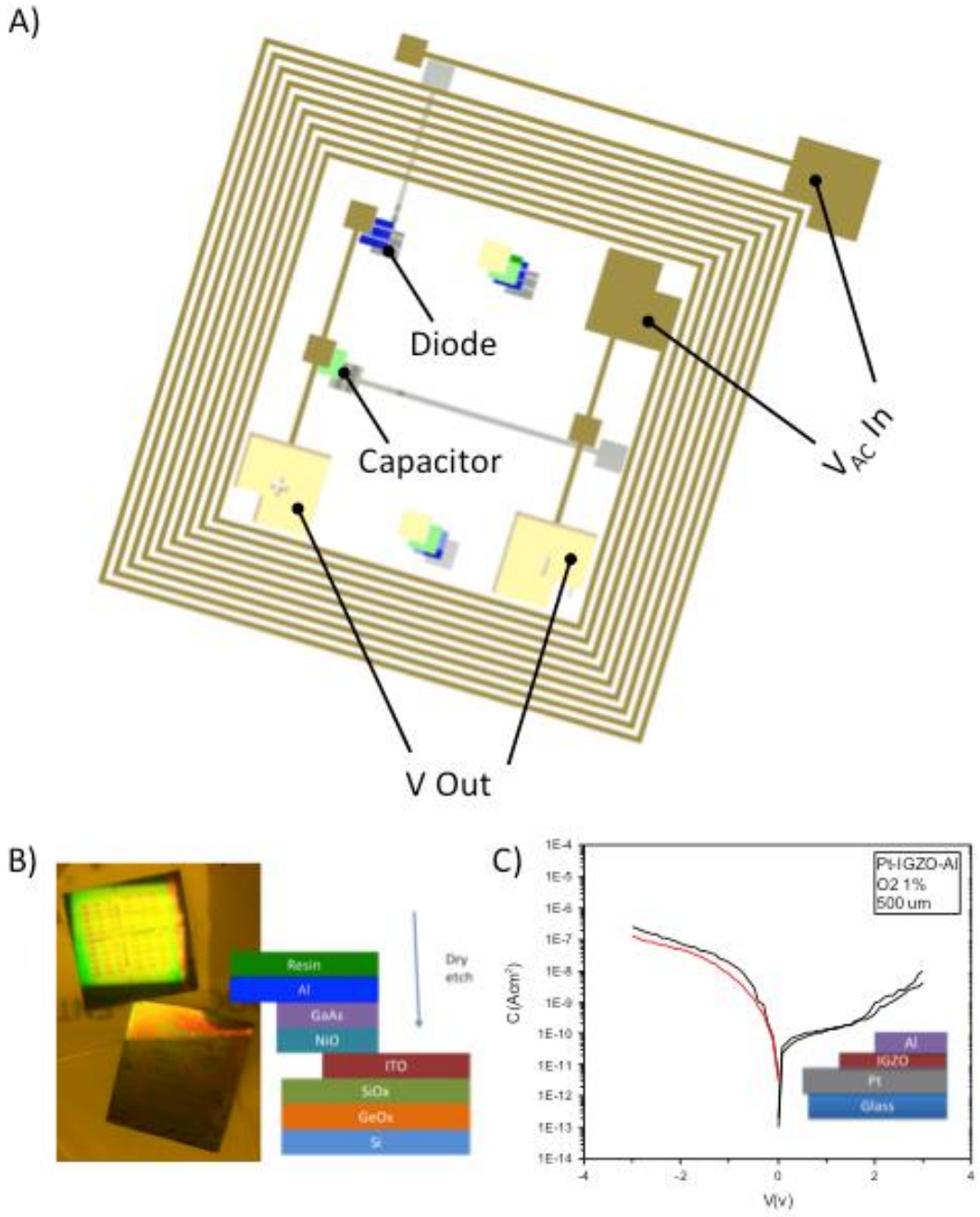

Figure 30. *(A) Proposed rectifier circuit with antenna, (B) Nickel Oxide diodes, (C) IGZO diode IV curve.*

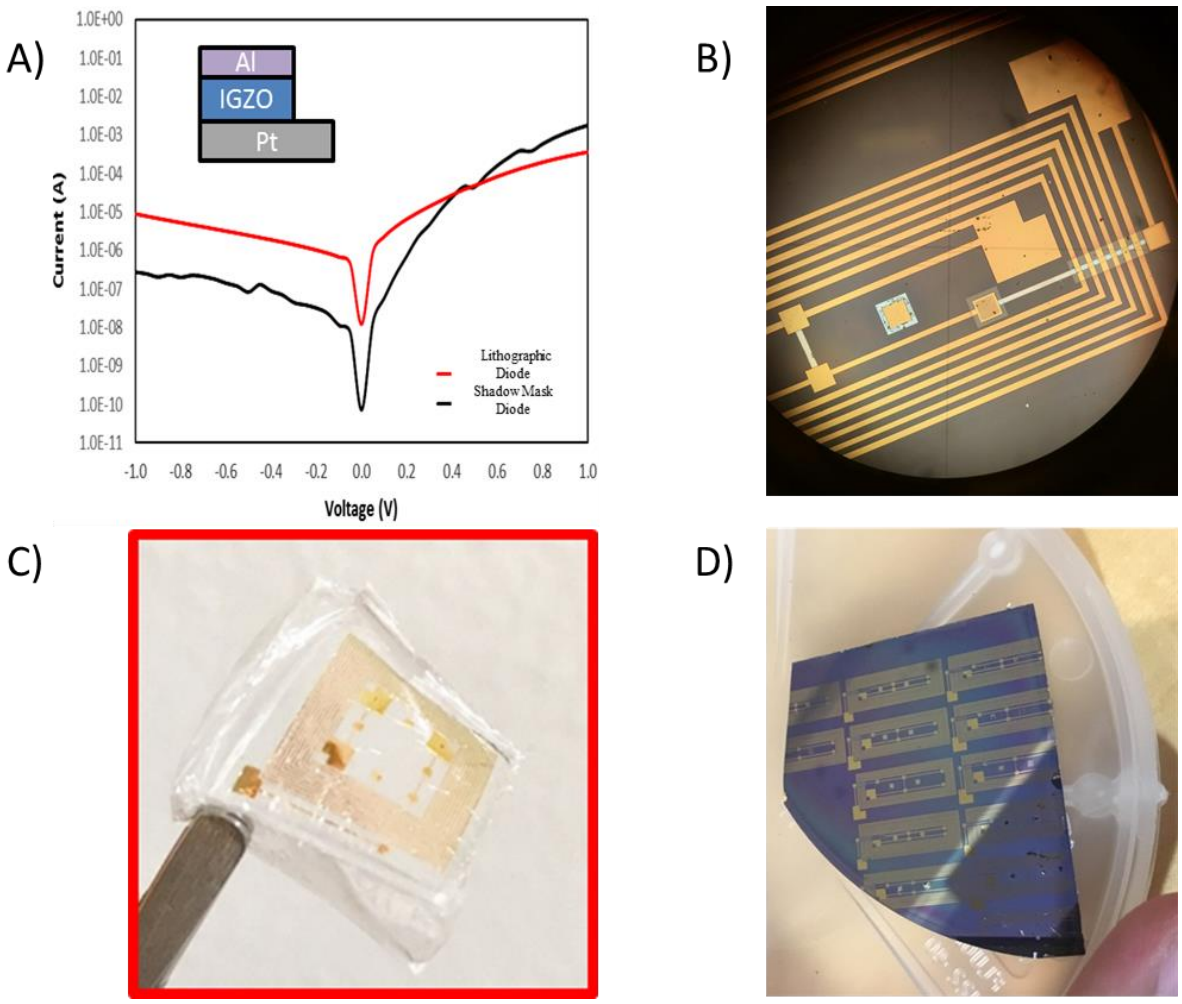

Figure 31. *(A) IGZO diodes by shadow mask and lithography, (B) Completed rectifying circuit on silicon, (C) Completed antenna circuit on collagen, (D) Antenna array with loop variations on silicon.*

5.3 Towards More Biocompatible Collagen Crosslinking and Controlled degradation

Glutaraldehyde crosslinks collagen, enhancing thermomechanical properties and preventing the digestion of collagen by collagenase, but it is highly cytotoxic. There are a variety of cross-linkers, but one prominent collagen cross-linker is riboflavin (Vitamin B2) [104], which is commonly used to treat keratoconus by cross-linking the corneal collagen. Riboflavin crosslinks

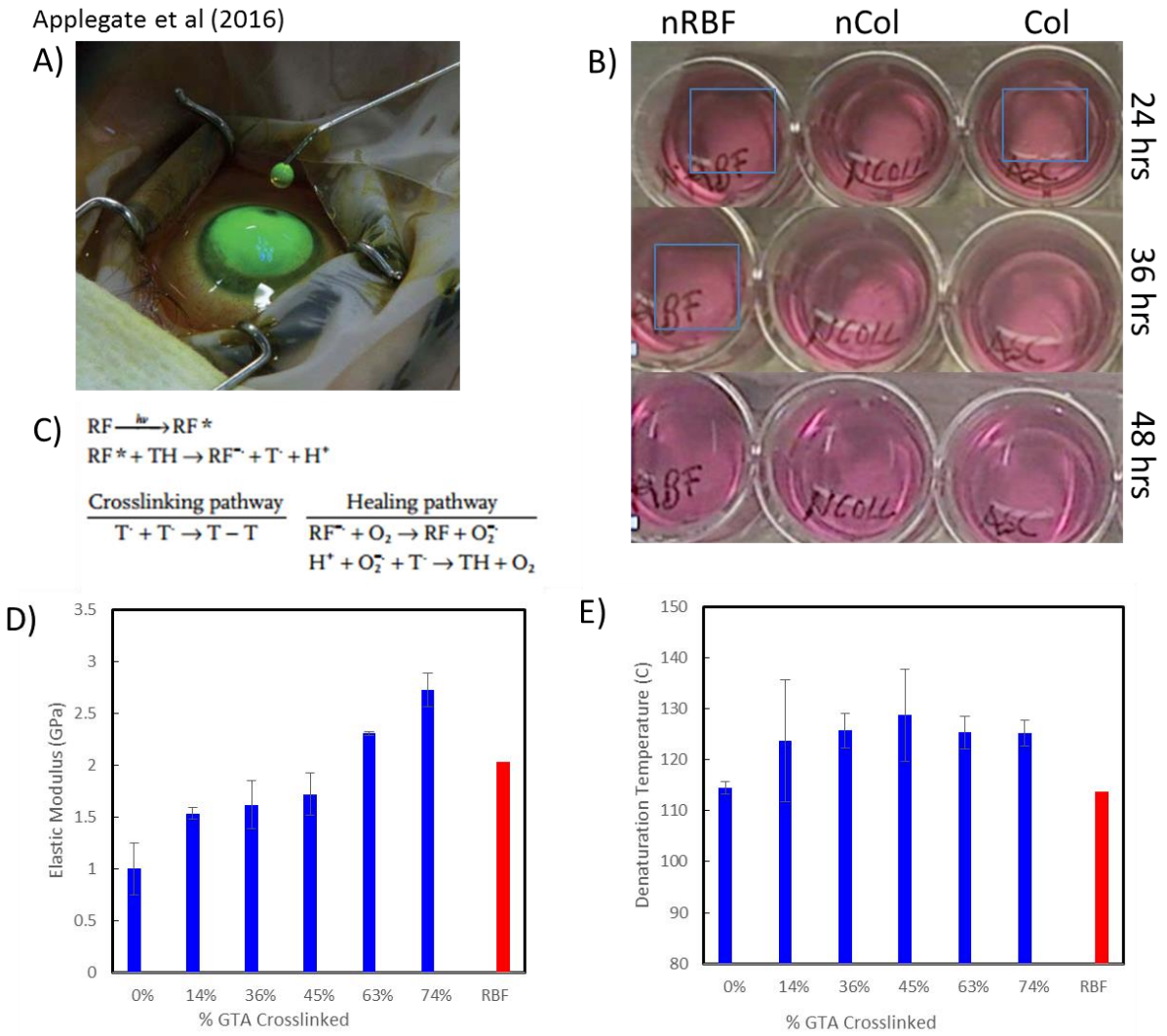

Figure 32. *(A) Riboflavin crosslinking eye cornea, (B) Collagenase degradation of riboflavin crosslinked films, (C) Riboflavin crosslinking mechanism.*

tyrosine [103] by UV-C excitation at 5.4 J/cm^2 as described in Figure 30. Collagen films crosslinked with riboflavin as shown in Figure A22 were incubated in collagenase and showed a 50% increase in degradation time at 0.01 mg/mL. These results are preliminary and further experiments are needed to determine if the trend continues for different collagenase concentration. The modulus increased by 100% as well with a minor increase in denaturation temperature when compared to as made collagen (110.2 °C to 113 °C). However, in order to crosslink collagen in riboflavin, the collagen solution used to prepare collagen needs to be neutralized, as riboflavin's metabolic activity is highly pH dependent. Further studies need to understand how this strategy

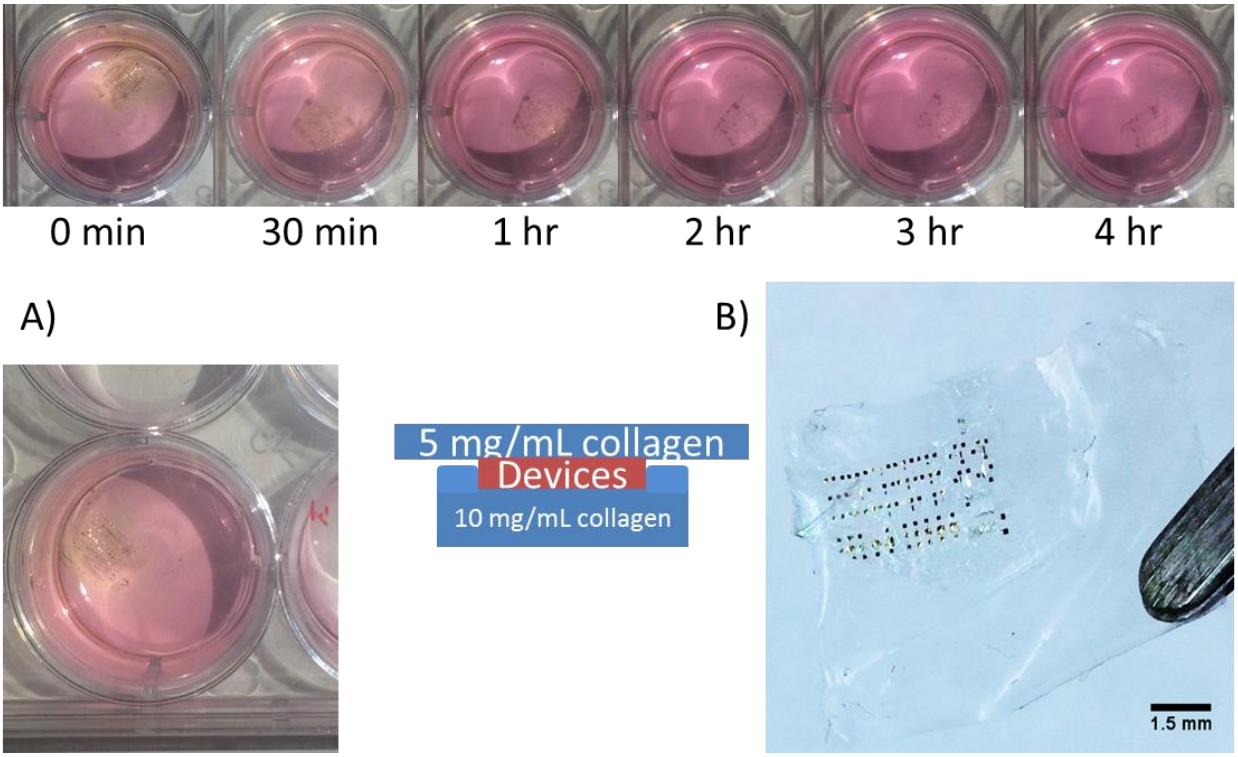

Figure 33. *(A) Collagen film demonstrating controllable degradation, (B) An array of transistors, inverters, capacitors, resistors on collagen.*

for fabricating collagen film fits into the transfer process of collagen. Collagen was crosslinked in riboflavin (0.2 mM in 1X PBS) at a constant UV irradiation of 5.4 J/cm^2, however, the effects of

dosage and riboflavin concentration needs to be further studied in regards to effects on mechanical properties and thermos stability. Stress strain tests will need to be conducted to see if there is any trend when increasing or decreasing a specific parameter to determine if it is possible to tune degradation of collagen in a controllable manner using riboflavin.

5.4 Conclusions

This study was the first demonstration of flexible electronics on collagen. Towards the thesis hypothesis of demonstrating controllable degradation of collagen for transient electronics, many of those principles have been demonstrated. In that regard, it is also the first demonstration of transient electronics on collagen as seen in Figure 33. Cell viability assays as seen in section 3.7 and collagenase degradation in 3.7 showed that collagen based devices are both biocompatible and biodegradable demonstrating the transient aspect of the hypothesis. Cell staining showed that cells recognize the amino acid sequences on collagen and attach to the collagen films showing enhanced biocompatibility.

After the initial exploration of direct fabrication of electronics on collagen in Chapter 2, transfer printing from silicon onto collagen was demonstrated in Chapter 3, which has many advantages over direct fabrication, since it is almost universally compatible with a variety of semiconductor processes. The sacrificial layer used in transfer printing is germanium oxide, which is encapsulated with silicon oxide to protect it during processes with a temperature range up to 650 °C. The germanium oxide sacrificial layer is removed after fabrication with water, and no toxic chemicals required. Collagen film is then cast onto the backside of the transferred device. This process

benefits from a stiffer transfer substrate as demonstrated in S24 with less superficial cracks in the protective parylene layer on kapton as compared to collagen. This suggests that a stiffer collagen would serve as a better substrate for this transfer.

Crosslinking of collagen by GTA as demonstrated in Chapter 4, overall enhances the properties of collagen such as the elastic modulus, swelling ratio, and thermal stability. Figure A21 shows that a 74% GTA cross-linked film has cracks in the protective parylene layer compared to the untreated collagen sample showing the benefit of a more stable collagen. Towards the demonstration of controllable collagen degradation, collagenase experiments showed that it is possible to slow down degradation by 20 - 80% for 14% and 74% GTA cross-linked collagen. This demonstrates that similar to silk, collagen film degradation can be modulated to change the lifetime for different transient electronic applications. Since a variety of processes are compatible with this transfer process, the next step would be to develop recipes for transient conductors, semiconductors, and dielectrics for a fully transient device from metals to substrate. A fully wireless platform as proposed in Section 4.1 would help isolate measurement issues with encapsulated device as well as help monitor devices implanted *in vivo*. Implanted collagen device experiments are still needed to demonstrated vascularization observed with collagen pericardial patches to fully demonstrate the potential of collagen based electronics.

APPENDIX

SUPPLEMENTARY INFORMATION

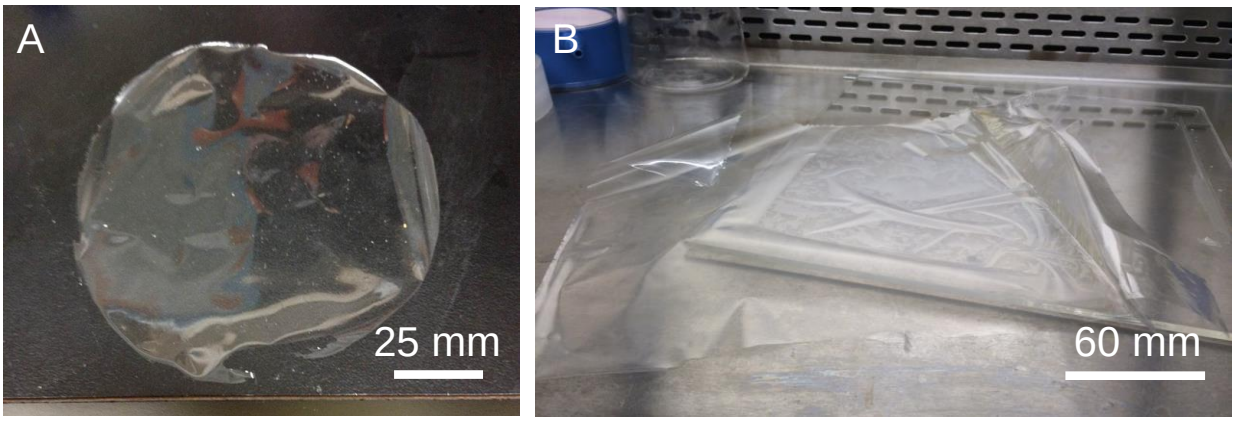

Figure A1. *(A) and (B) Large-scale uniform and transparent collagen films. Density of ~1.27 g/cm^3 was calculated from the weight and dimension of the dried films.*

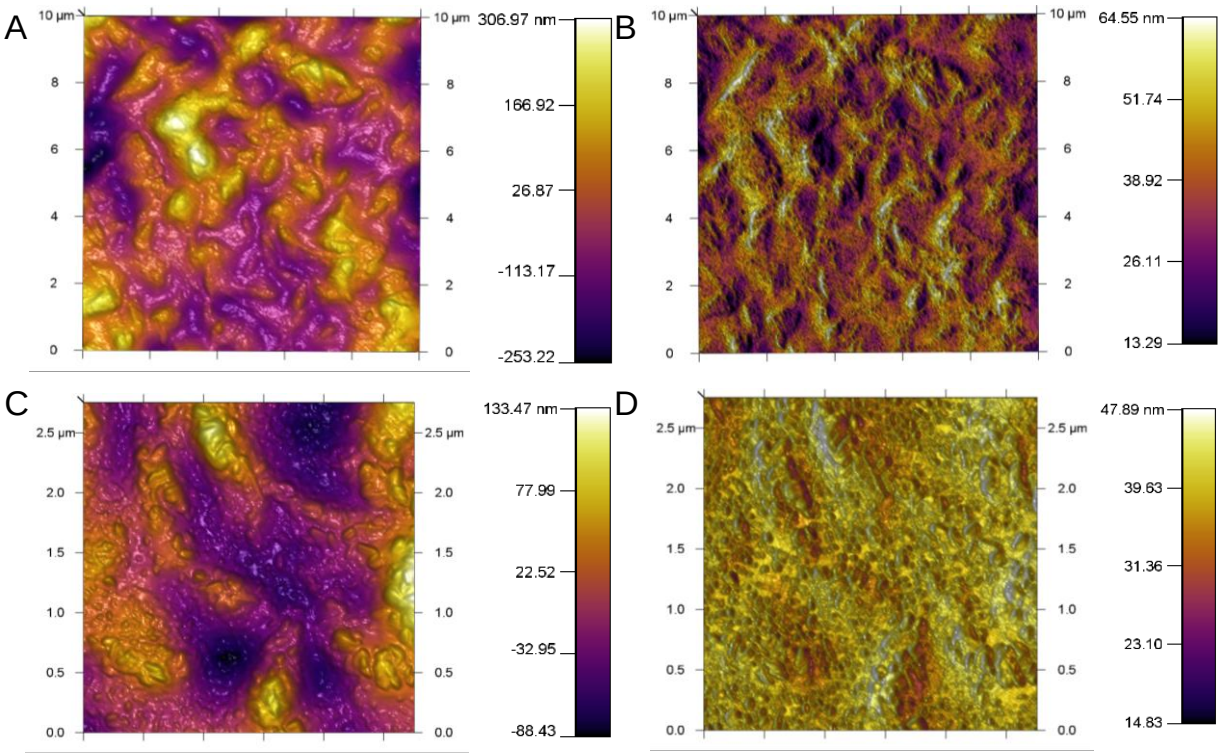

Figure A2. *AFM topography (A and C) and corresponding amplitude (B and D) images of collagen films. The filament nature of collagen film is particularly visible in the amplitude images. RMS surface roughness are ~81 nm and ~37nm for A and C topography images, respectively.*

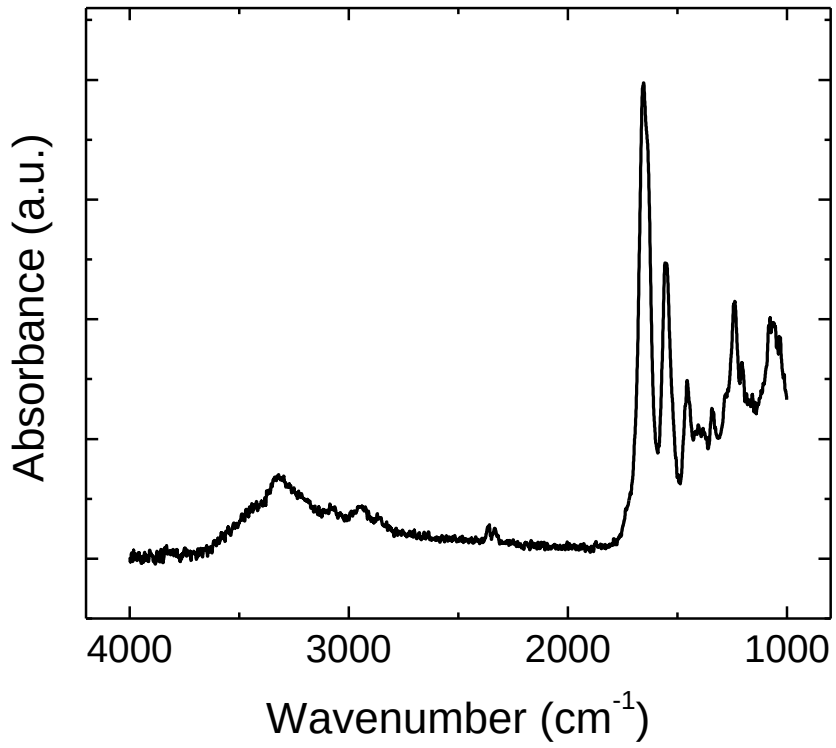

Figure A3. *FTIR spectra of collagen film. The peak between 3000 and 3500 is associated with Amide A band, which is mostly due to N-H stretching vibration.*

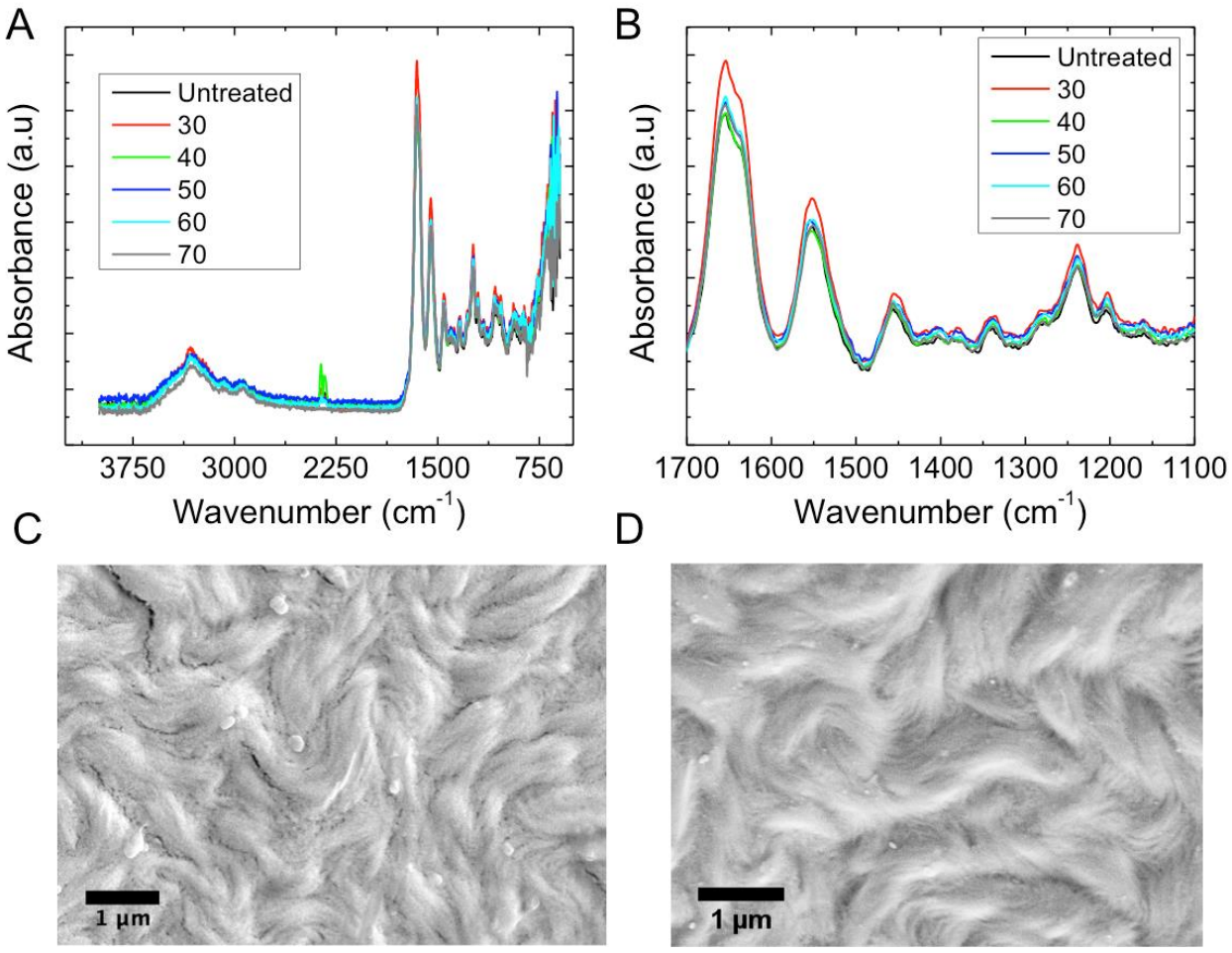

Figure A4. *(A) FTIR spectra of collagen film subjected to temperature in the range of 30 ˚C – 70 ˚C. (B) Zoomed-in view of (A) for the main peaks. C) SEM image of untreated (unheated) collagen film. D) SEM Image of film after 70C. Overall, the results show that there is no noticeable change in the FTIR spectra or the microstructure of collagen films within this temperature range.*

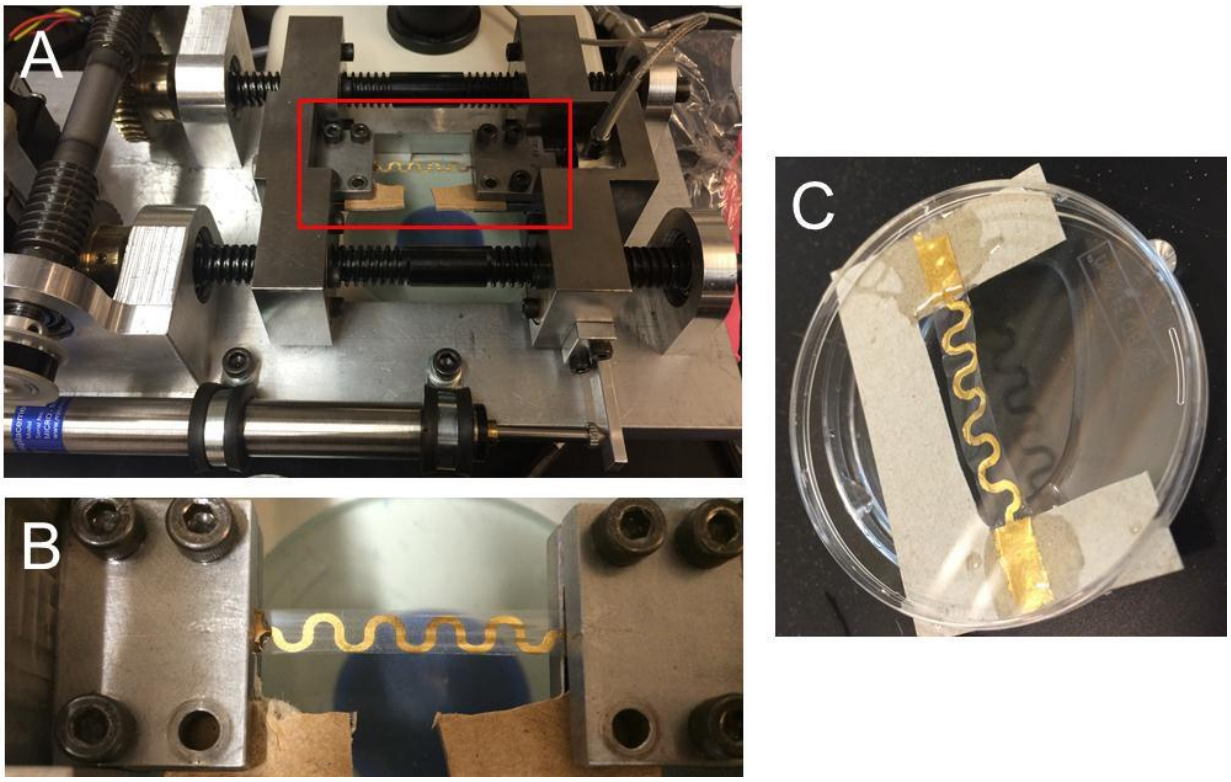

Figure A5. *(A) Micro-mechanical testing machine. Zoomed-in view of the boxed area in (A) shows the collagen specimen with a serpentine Au pattern under tension. (C) A specimen of collagen film with metal patterns prepared for tensile testing.*

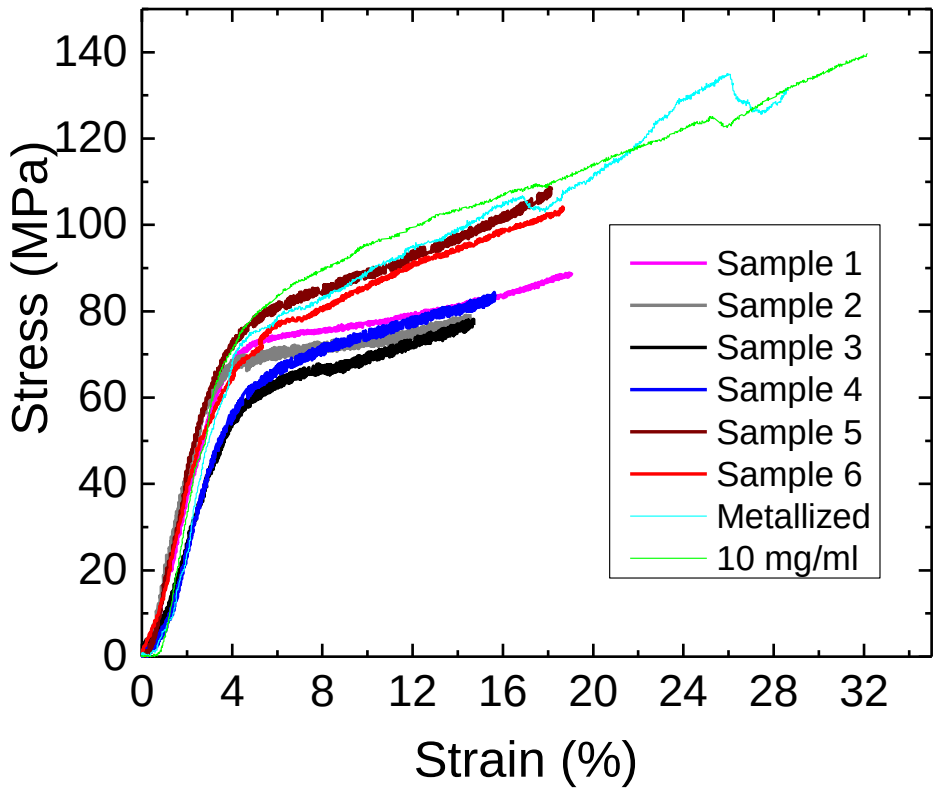

Figure A6. *Tensile test results for collagen samples.*

Table S1. *Detailed mechanical properties of the collagen films.*

Samples	Elastic modulus (GPa)	Yield strain ε_y (%)	Yield stress σ_y (MPa)	Fracture strain ε_f (%)	Failure strength σ_f (MPa)	Toughness (J/g)
Sample 1	2.0547	3.5566	63.49	18.9318	88.89	9.41
Sample 2	2.1682	2.932	60.11	14.5315	79.35	5.83
Sample 3	1.6285	3.7479	52.80	14.826	78.59	6.70
Sample 4	1.9028	3.628	52.78	15.6226	84.33	6.72
Sample 5	2.3891	3.1305	62.43	18.2106	108.92	12.44
Sample 6	2.0894	3.0007	54.38	18.6508	104.19	8.26
Average	**2.0387**	**3.3326**	**57.66**	**16.7956**	**90.71**	**8.23**
±SD	**±0.26**	**±0.35**	**±4.92**	**±2.02**	**±12.91**	**±2.43**
Metallized	2.1044	4.32	71.32	27.85	127.89	12.87
10 mg/ml	2.3753	3.781	69.372	32.159	139.72	25.58

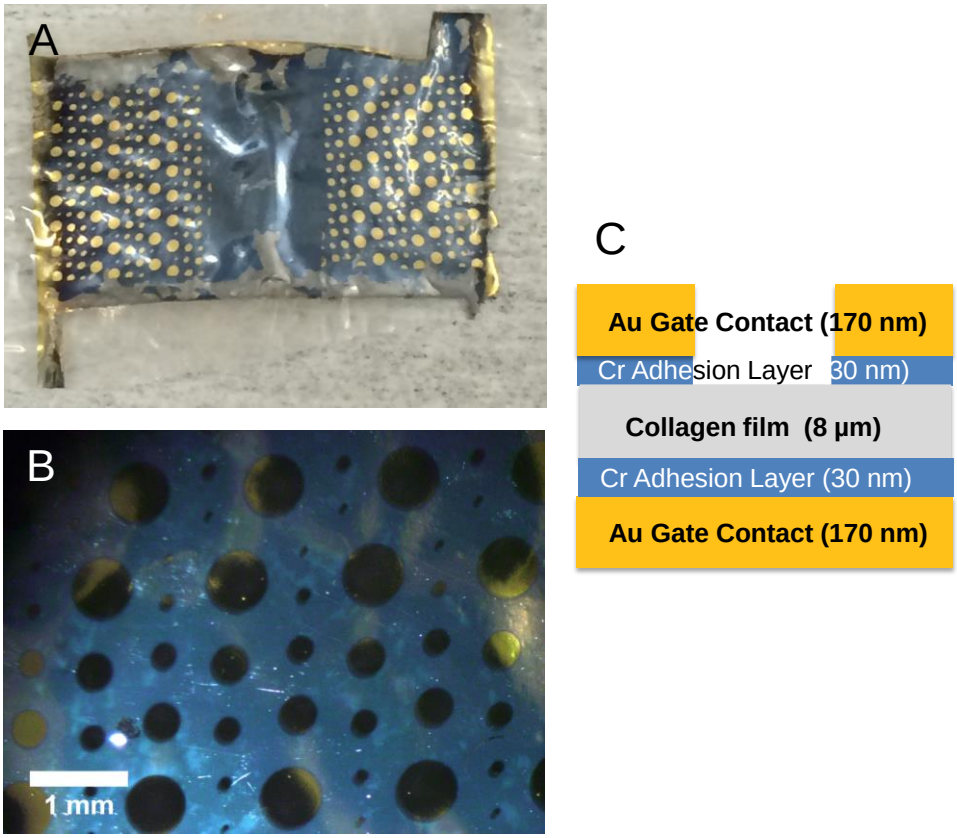

Figure A7. *(A) and (B) Optical images of capacitors fabricated on a collagen film for measurement of dielectric constant of collagen film. (C) Schematic of the structure and dimensions of the capacitors.*

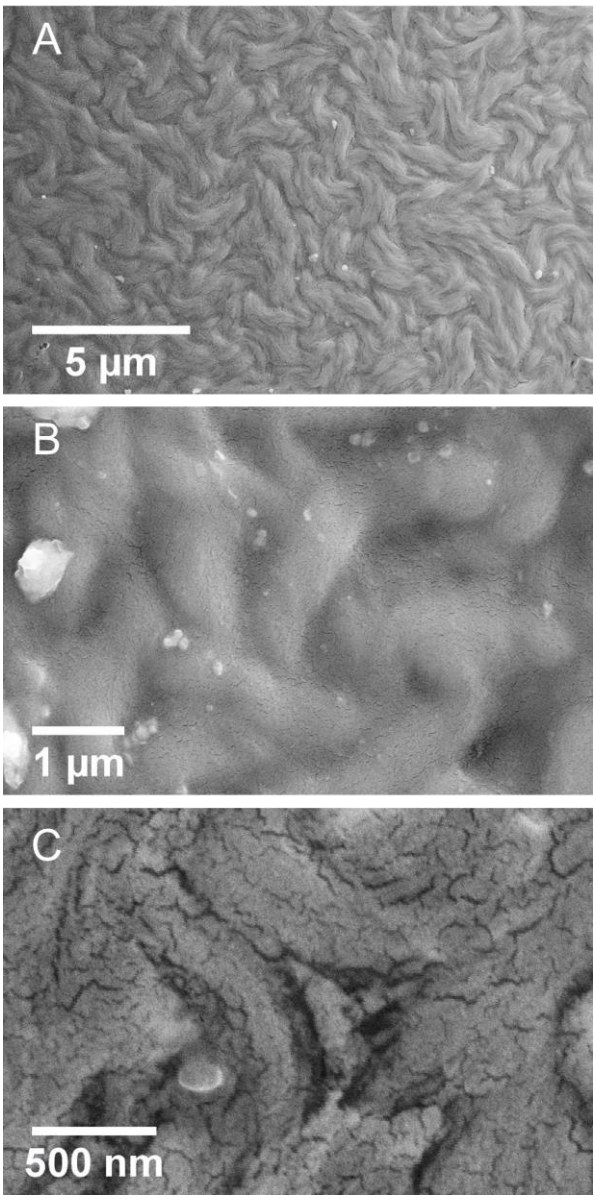

Figure A8. *(A) - (C) SEM images of collagen films after metal depostion. (B) Metal layer is conformal onto collagen film and the microstruture of collagen film is unaffected by metal depostion. Micro-crack in metal layer are apparent in high magnification image (C), which do not significantly affect the overall conductivity of the metal layer.*

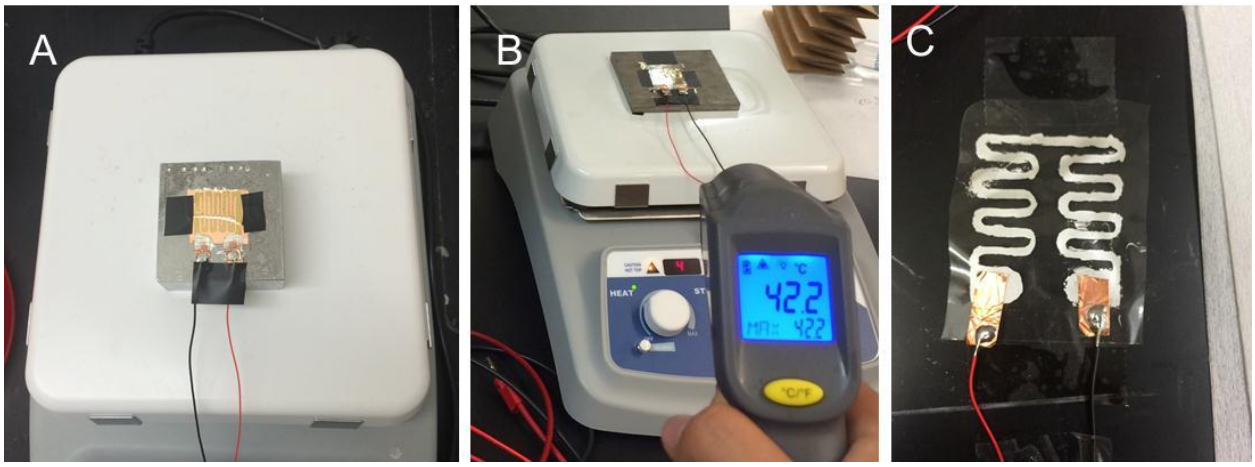

Figure A9. *(A) shows a temperature sensor on a metal sink placed on a hot plate for calibration. (B) IR gun temperature measurment of temperature sensor while being heated. (C) shows heater based on commercial etched heater design.*

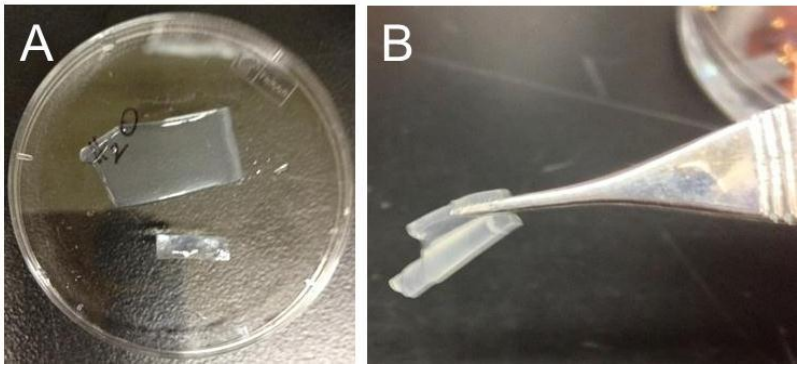

Figure A10*. (A) Collagen film hydrated in DI water. (B) The film after one hour held in forceps.*

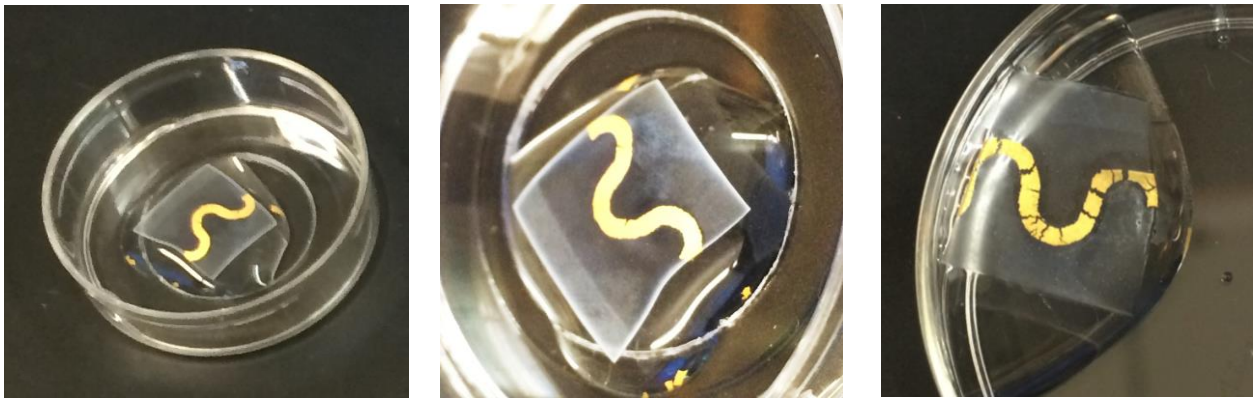

Figure A11. *Collagen films with exposed metal eletrode in PBS buffer.*

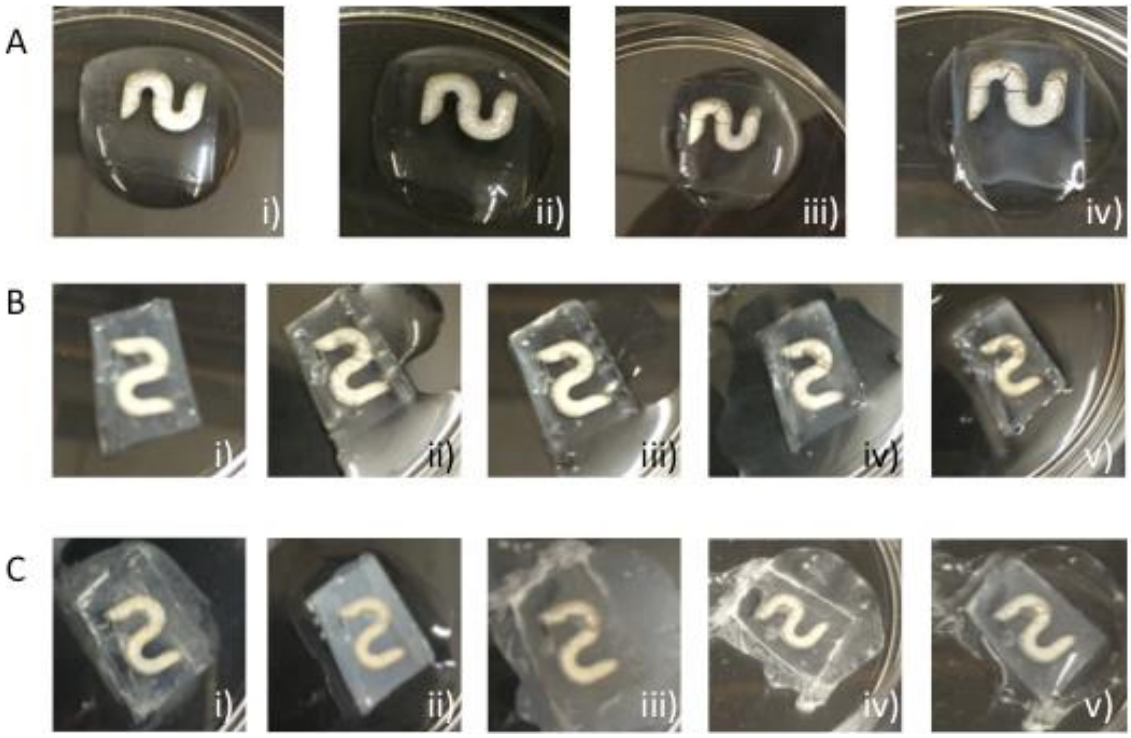

Figure A12. *(Ai-iv) shows a silver electrode without encapsulation in PBS, immediately after placement, 30 seconds, 5 minutes, and 15 minutes respectively. (Bi-v) shows a silver electrode in PBS solution encapsulated with a moist film, immediately after encapsulation, 5 minutes, 30 minutes, 1 hour, and 2 hours respectively. (Ci-v) shows the same silver electrode over long term placement in PBS. (Ci-v) shows the electrode dried out after 1 day, after addition of PBS to keep electrode in solution, after 1 week treatment in solution, dry state after 4 weeks in treatment, and after 4 weeks in treatment respectively. After 1 day, the electrode reaches an equilibirum which after 4 weeks seems that it can be extended indefinitely.*

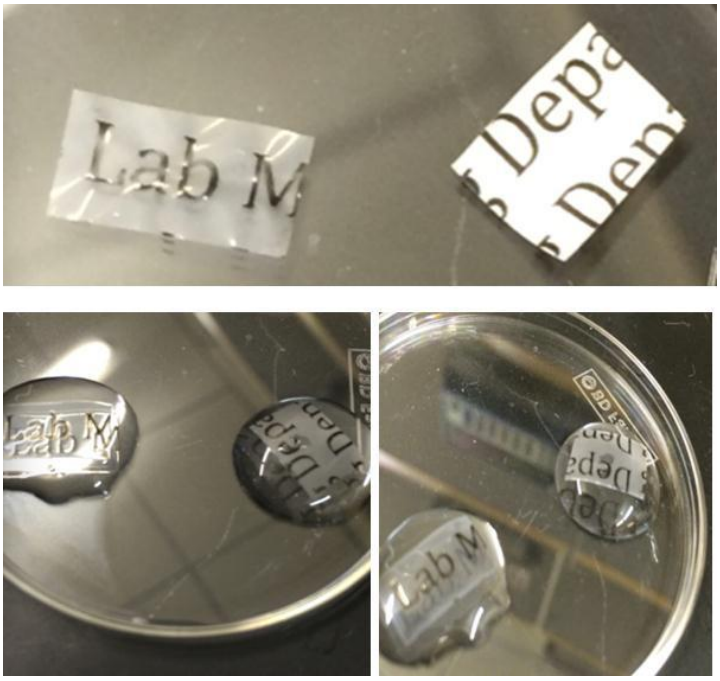

Figure A13. *Ink printed letters on collagen films using a desktop office printer. The printed film was placed inside water and PBS 1X solution. As shown, the printted letters are stable in the buffer and do not peel off form the film.*

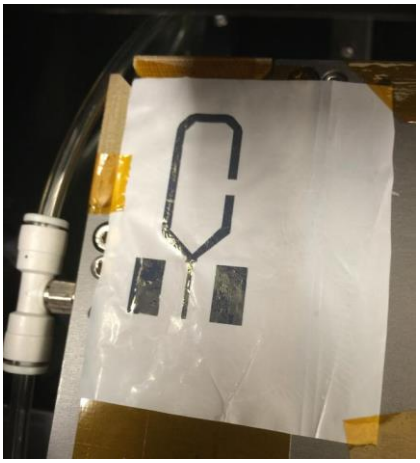

Figure A14. *Priting on a opaque collagen film using an ink jet printer. This collagen film was extracted from citric acid and hence was opaque. The printed feature the wireless antenna pattern shown in the main text.*

Calibration of strain sensor

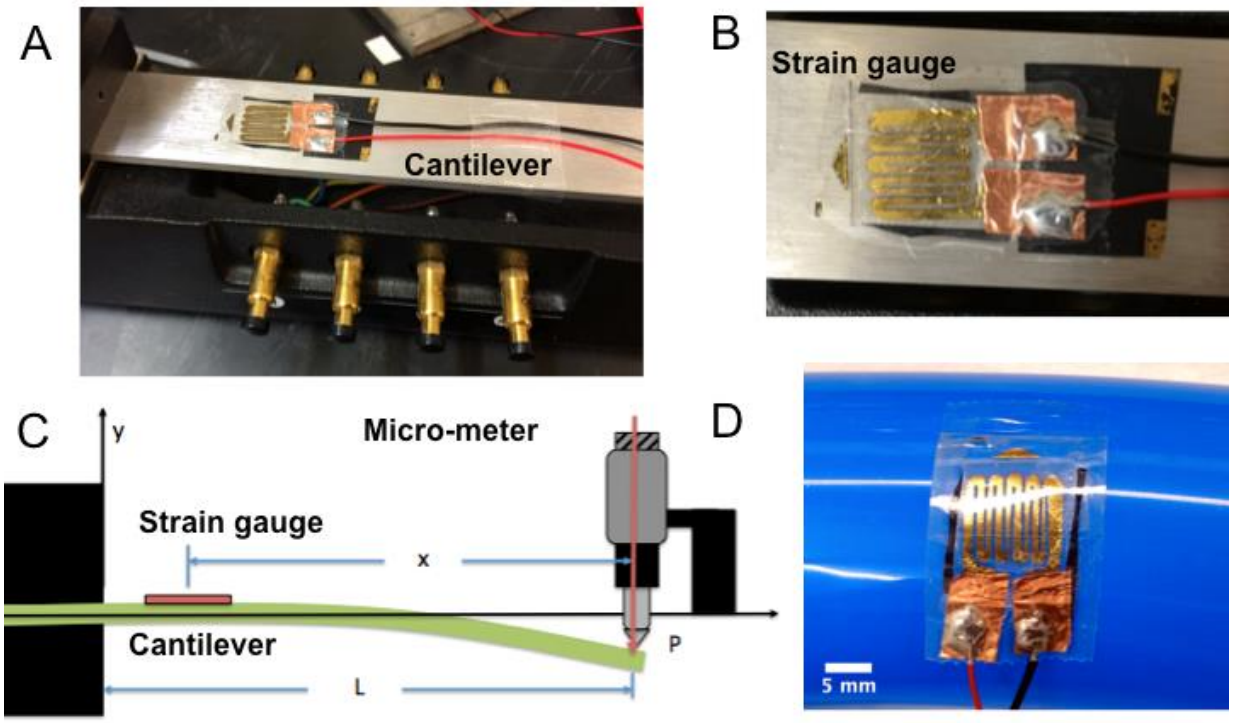

Figure A15. *(A) Experimental setup of the cantilever beam for calibration of the strain gauge. The strain gauge was mounted toward the cantilevered end of the beam. (C) The geometry of the setup used for the beam bending theory. (D) Strain gauge mounted on an inflated balloon experiencing hoop stress.*

The strain sensor was calibrated on a fixed beam deflected by a known distance using a micrometer at a distance L from the fixed point and distance x from the center of the strain gauge. From the beam theory, the bending stress is $\sigma=Mc/I$, where I is the moment of inertia of the beam about its neutral axis, M is the applied moment, and c is the distance between the cantilever surface to the neutral axis of the beam or $t/2$, with t being the thickness of the beam. From the Hooke's Law, strain is $\varepsilon=\sigma/E$, and hence $\varepsilon=Mc/(EI)$. Moment along the beam at any point x can be determined as $M=Px$ where P is the applied load such that strain can now be expressed as $\varepsilon=Pxc/(EI)$. Given

that maximum deflection for a fixed cantilever beam is $\delta=PL^3/(3EI)$, one can solve for applied load $P=\delta 3EI/L^3$. Substituting P into ε results in $\varepsilon=3xc\delta/(L^3)$ or given that $c=t/2$:

$$\varepsilon = \frac{3tx}{2L^3}\delta$$

Since strain is directly a function displacement δ measured by the micrometer, it is possible to calibrate the strain gauge by measuring the change in resistance as a result of strain at location x on the cantilever.

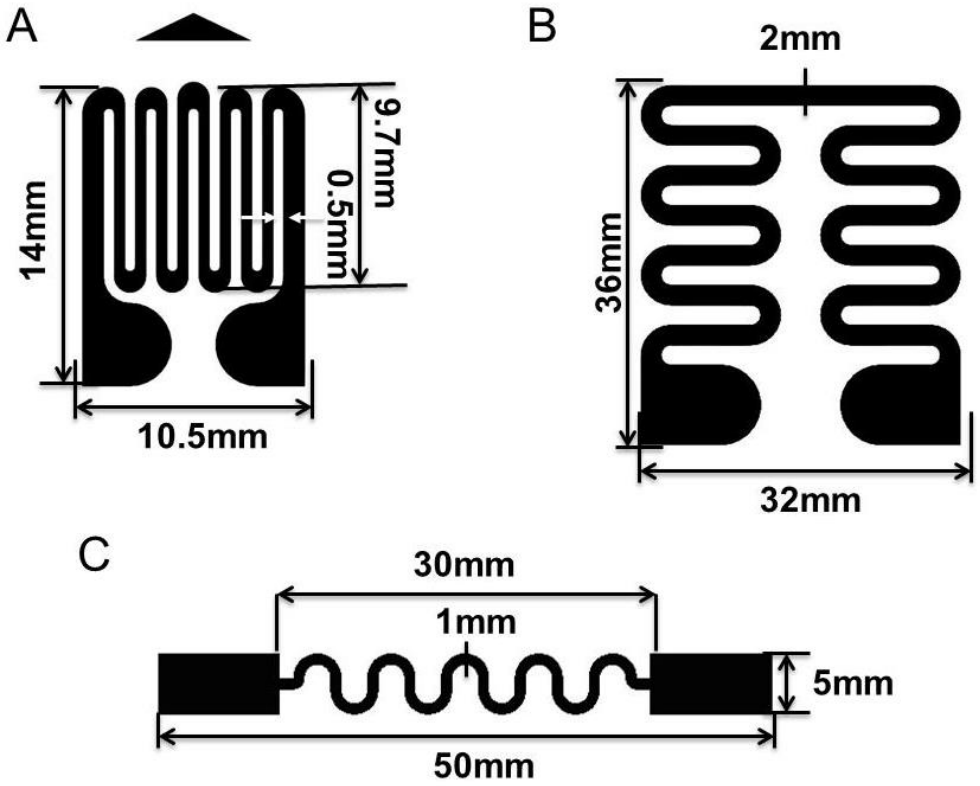

Figure A16. *(A)-(C) Schematics of the various shadow masks design used for the e-beam evaporation of metal on collagen films for fabrication of strain gauge, temperature sensors and serpentine patterns on collage films.*

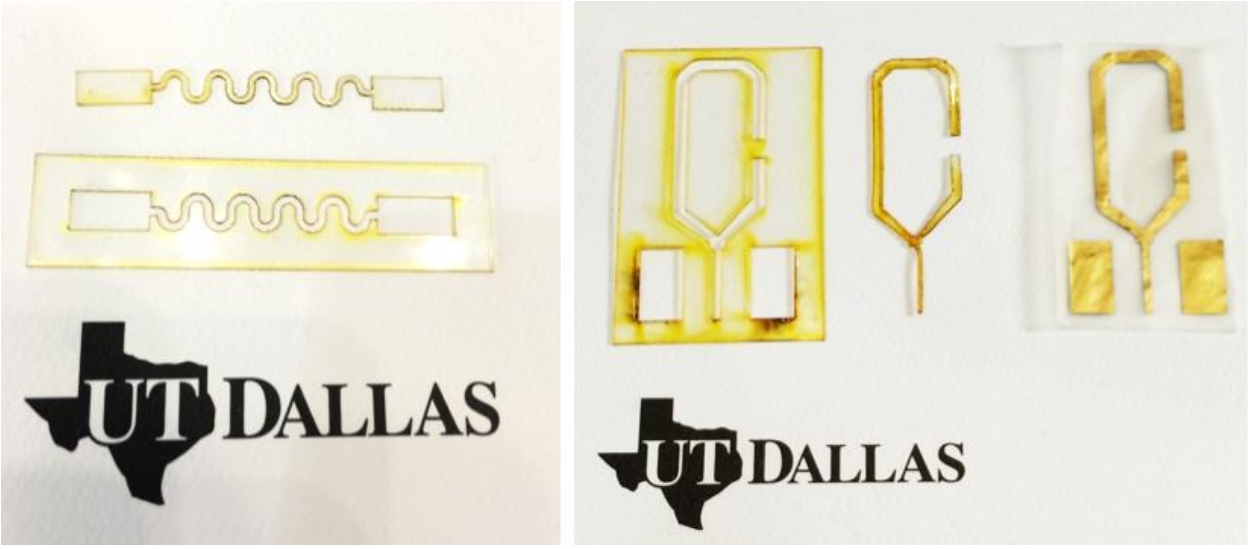

Figure A17. *Shadow masks for metal depostion fabricated using a laser engraver.*

Radius of Curvature Mechanical Analysis

The flexure test apparatus moves the crossheads inward ΔL, buckling the collagen film (Length L) and results in an out-of-plane displacement $w(x)=A[1+\cos(2\pi x/L)]/2$ as shown in Figure A17. For plane-strain analysis ($\varepsilon_{22}=0$), the membrane energy and bending energy as relating to the curvature can be minimized to give the amplitude A as:

$$A = \frac{2}{\pi}\sqrt{L \cdot \Delta L - \frac{\pi^2 t_{kapton}^2}{3}} \approx \frac{2}{\pi}\sqrt{L \cdot \Delta L}$$

This approximation holds when compression of the film causes it to buckle since the value is significantly larger than its critical value $\pi^2t^2/(3L)$ required to initiate buckling. As such, the radius of curvature can be determined as: $R=|(1+w'^2)^{3/2}/w''|$ where $w'(x)=-/2(2\pi/L)\sin(2\pi x/L)$ and $w''(x)=-A/2(2\pi/L)^2\cos(2\pi x/L)$. The radius of curvature at its center, where it is at its minimum, is determined when $x=0$. As the crossheads move inward, buckling the film, it is possible to measure

the resistance of change of resistors deposited on the films at different approximated radii of curvature.

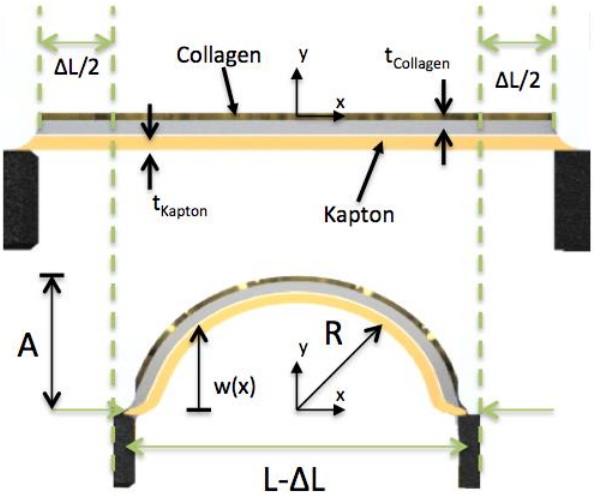

Figure A18. *Schematic of the model used for flexure experiment. Adapted from* [24].

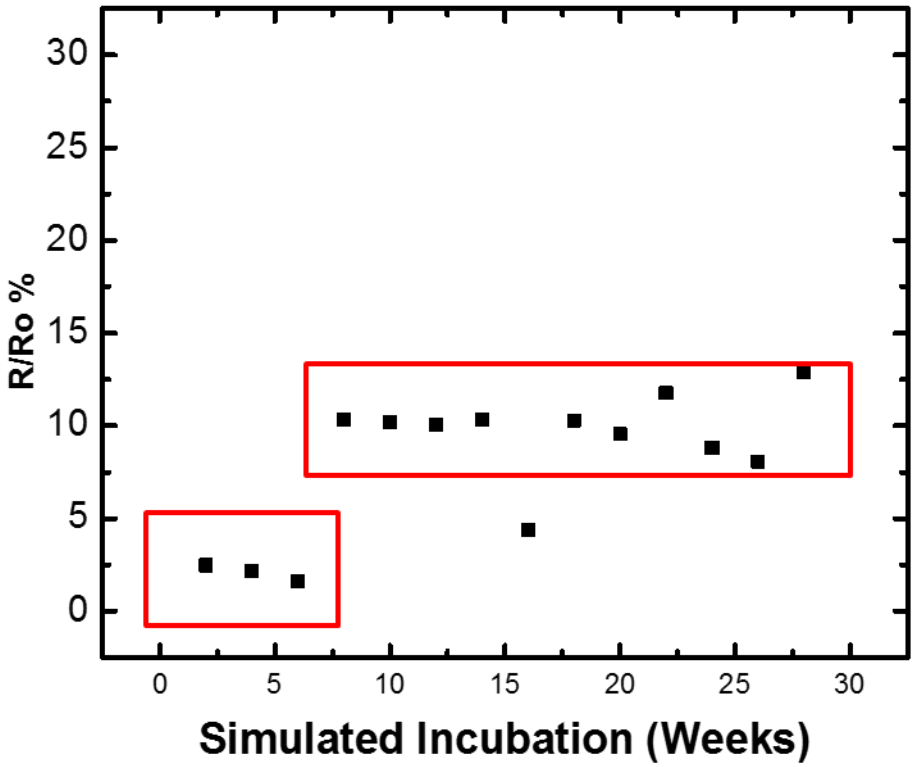

Figure A19. *Simulated incubation over 28 weeks with highlighted sections.*

HOLISTA COLLTECH

OVICOLL 95 - AMINO ACID PROFILE

		g/100g protein
Aspartic Acid	ASP	5.68
Glutamic acid	GLU	9.04
Hydroxyproline	HYP	12.98
Serine	SER	3.13
Glycine	GLY	22.5
Histidine	HIS	0.99
Arginine	ARG	8.94
Threonine	THR	2.07
Alanine	ALA	8.76
Proline	PRO	12.52
Tyrosine	TYR	0.48
Valine	VAL	2.37
Methionine	MET	1.09
Isoleucine	ILE	1.45
Leucine	LEU	2.80
Phenylalanine	PHE	1.37
Lysine	LYS	3.82

Figure A20. *Ovine Collagen Amino acid profile as provided by manufacturer Holista CollTECH.*

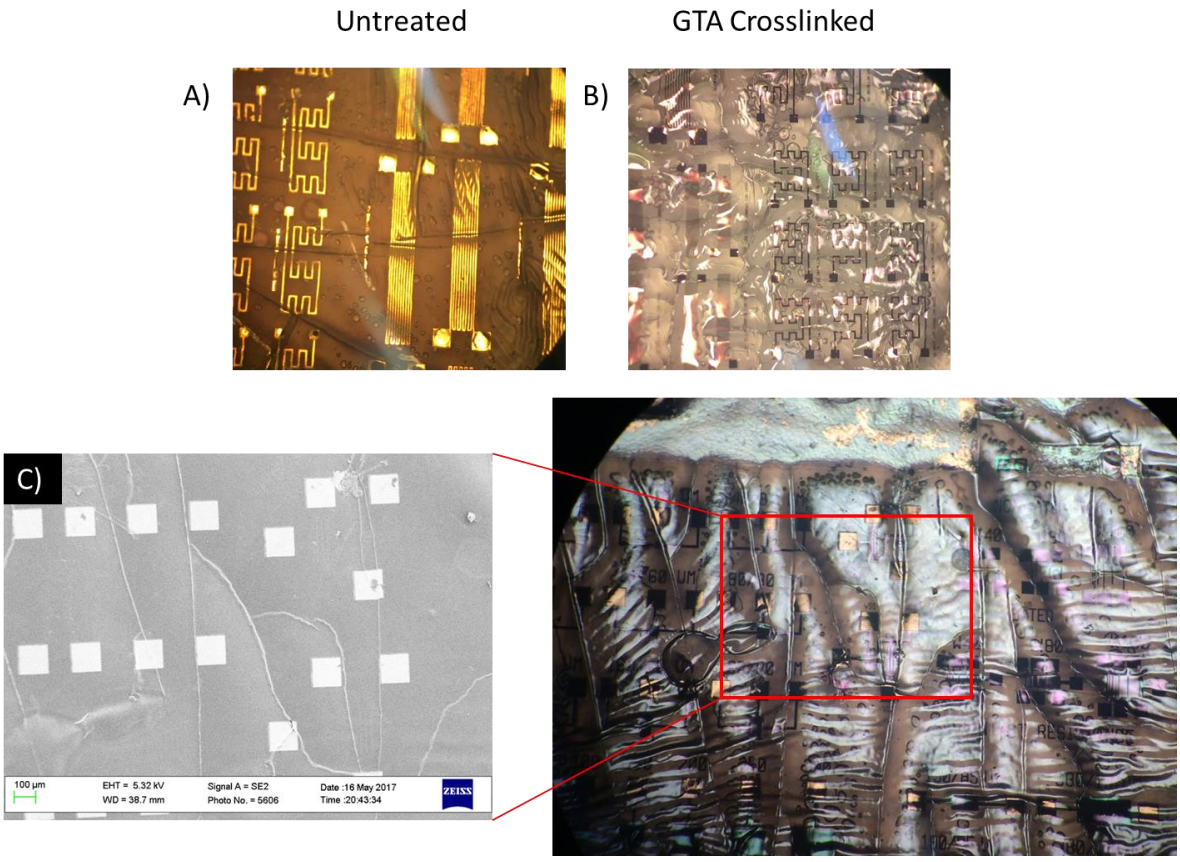

Figure A21. *(A) Untreated sample with parylene cracks, (B) GTA Crosslinked sample with no parylene cracks, (C) Superficial cracks on parylene via SEM compared to optical images.*

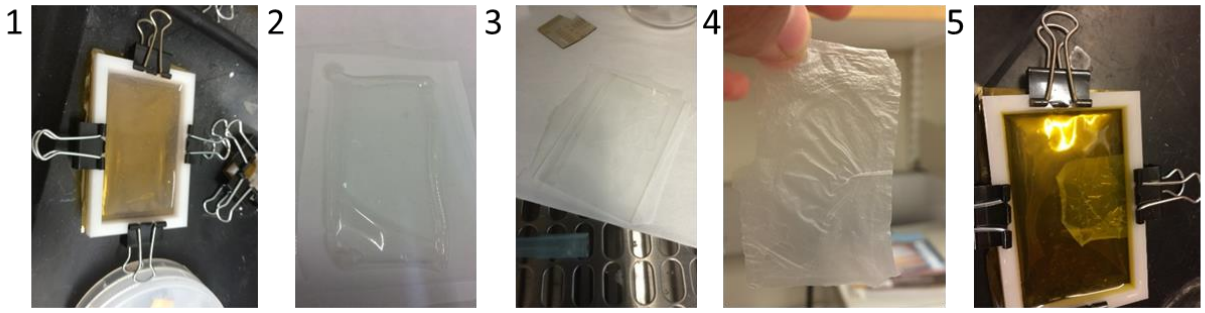

1. Neutralize solution at 4C
2. Incubate solution at 37C and form gel
3. Use plastic compression and filters to squeeze gel into film
4. Remove film from filter without damaging film
5. Crosslink in RBF under UV light at 5.4 J/cm

Figure A22. *(A) Crosslinking process for Riboflavin collagen films.*

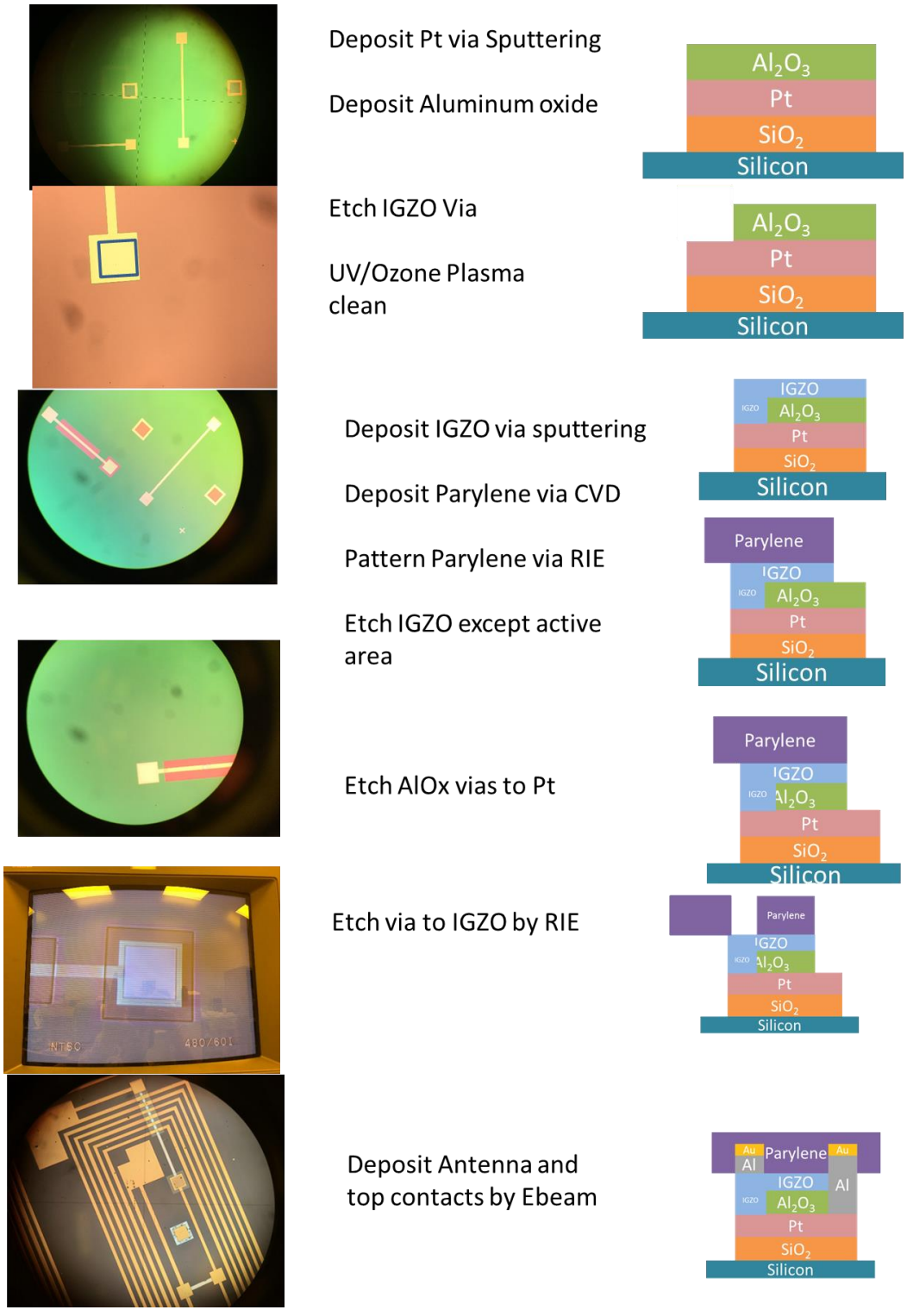

Figure A23. *Antenna Semiconductor Process Protocol.*

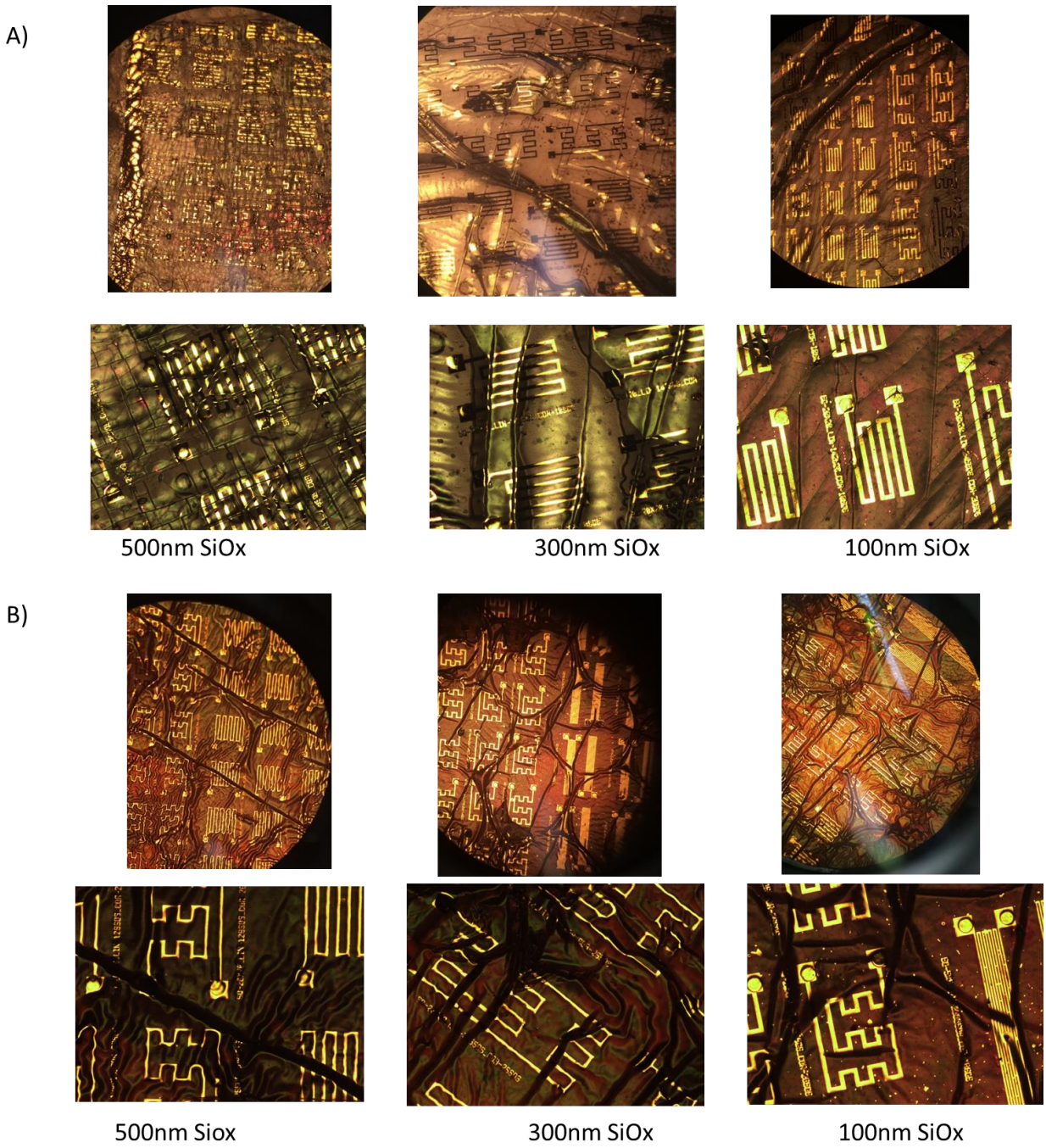

Figure A24. *(A) Resistors transferred onto collagen with varying degrees of Silicon oxide bottom layers, (B) Resistors transferred onto Kapton with varying degrees of Silicon oxide.*

REFERENCES

[1] D. -H. Kim and al., "Dissolvable films of silk fibroin for ultrathin conformal bio-integrated electronics.," *Nat Mater,* vol. 6, no. 9, pp. 511-517, 2010.

[2] A. Najafabadi and al., "Biodegradable Nanofibrous Polymeric Substrates for Generating Elastic and Flexible Electronics," *Advanced Materials,* no. 26, pp. 5823-5830, 2014.

[3] H. Tao and al., "Silk-based resorbable electronic devices for remotely controlled therapy and in vivo infection abatement," *PNAS,* vol. 111, no. 49, pp. 17385-17389, 2014.

[4] M. A. Danielle and al., "Sweet Substrate: A Polysaccharide Nanocomposite for Conformal Electronic Decals," *Advanced Materials,* vol. 27, no. 9, pp. 1600-1606, 2014.

[5] I. Minev and al., "Electronic dura mater for long-term multimodal neural interfaces. Science, 2015," *Science,* vol. 347, no. 6218, pp. 159-163, 2015.

[6] J. Norton and al., "Soft, curved electrode systems capable of integration on the auricle as a persistent brain–computer interface," *PNAS,* vol. 112, no. 13, pp. 3920-3925, 2015.

[7] C. Liao and al., "Flexible Organic Electronics in Biology: Materials and Devices. Advanced Materials," *Advanced Materials,* vol. 27, no. 46, pp. 7493-7527, 2014.

[8] T. Kelley and al., "Recent Progress in Organic Electronics: Materials, Devices, and Processes. Chemistry of Materials," *Chemistry of Materials,* vol. 16, no. 23, pp. 4413-4422, 2004.

[9] M. Roberts and al., "Flexible, plastic transistor-based chemical sensors," *Organic Electronics,* vol. 10, no. 3, pp. 377-383, 2009.

[10] A. Briseno and al., "High-Performance Organic Single-Crystal Transistors on Flexible Substrates. Advanced Materials," *Advanced Materials,* vol. 18, no. 17, pp. 2320-2324, 2006.

[11] J. Rogers and al., " Paper-like electronic displays: Large-area rubber-stamped plastic sheets of electronics and microencapsulated electrophoretic inks," *PNAS,* vol. 98, no. 9, pp. 4835-4840, 2001.

[12] T. Someya and al., "Conformable, flexible, large-area networks of pressure and thermal sensors with organic transistor active matrixes," *PNAS,* vol. 102, no. 35, pp. 12321-12325, 2005.

[13] G. Kushto and al., "Flexible organic photovoltaics using conducting polymer electrodes," *Applied Physics Letters,* vol. 86, no. 093502, 2005.

[14] A. Dey and al., "CMOS TFT Op-Amps: Performance and Limitations," *IEEE Electron Device Letters,* vol. 32, no. 5, pp. 650-652, 2011.

[15] D. Mao and al., "Ferroelectric random access memory based on one-transistor–one-capacitor structure for flexible electronics," *Organic Electronics,* vol. 14, no. 2, pp. 505-510, 2013.

[16] D. Mao and al., "Hybrid CMOS thin-film devices based on solution-processed CdS n-TFTs and TIPS-Pentacene p-TFTs," *Organic Electronics,* vol. 13, no. 12, pp. 3045-3049, 2012.

[17] R. Gross and B. Kalra, "Biodegradable Polymers for the Environment," *Science,* vol. 297, no. 5582, pp. 803-807, 2002.

[18] H. Tamai and al., "Initial and 6-Month Results of Biodegradable Poly-l-Lactic Acid Coronary Stents in Humans," *Circulation,* vol. 102, no. 4, pp. 399-404, 2000.

[19] J. Middleton and A. Tipton, "Synthetic biodegradable polymers as orthopedic devices.," *Biomaterials,* vol. 21, no. 23, pp. 2335-2346, 2000.

[20] E. Fortunato and al., "High-Performance Flexible Hybrid Field-Effect Transistors Based on Cellulose Fiber Paper," *Electron Device Letters, IEEE,* vol. 29, no. 9, pp. 988-990, 2008.

[21] K. Yong-Hoon and al., "Organic TFT array on a paper substrate," *Electron Device Letters, IEEE,* vol. 25, no. 10, pp. 702-704, 2004.

[22] D. Khodagholy and al., "In vivo recordings of brain activity using organic transistors," *Nature Communications,* vol. 4, no. 1575, pp. 1-7, 2012.

[23] J. Reeder and al., "Mechanically Adaptive Organic Transistors for Implantable Electronics," *Advanced Materials,* vol. 26, no. 29, pp. 4967-4973, 2014.

[24] C. Dagdeviren and al., "Conformal piezoelectric energy harvesting and storage from motions of the heart, lung, and diaphragm," *PNAS,* vol. 111, no. 5, pp. 1927-1932, 2014.

[25] Y. Jung and al., "High-performance green flexible electronics based on biodegradable cellulose nanofibril paper," *Nature Communications,* vol. 6, no. 7170, pp. 1-11, 2015.

[26] N. Lu and D.-H. Kim, "Flexible and Stretchable Electronics Paving the Way for Soft Robotics," *Soft Robotics,* vol. 1, no. 1, pp. 53-62, 2013.

[27] D.-H. Kim, N. Lu and al., "Epidermal Electronics," *Science,* vol. 333, pp. 838-843, 2011.

[28] R. Feiner and T. Dvir, "Tissue–electronics interfaces: from implantable devices to engineered tissues," *Nature Reviews Materials,* vol. 3, no. 17076, pp. 1-16, 2017.

[29] C. Wilson and al., "Mediation of Biomaterial–Cell Interactions by Adsorbed Proteins: A Review," *Tissue Engineering,* vol. 11, pp. 1-17, 2005.

[30] R. Weigert, "Dissecting Fibrosis," *Nature Biomedical Engineering,* vol. 1, no. 0016, pp. 1-2, 2017.

[31] M. Fishbein and al., "The histopathologic evolution of myocardial infarction," *Chest,* vol. 73, pp. 843-849, 1978.

[32] V. Poliko and al., "Response of brain tissues to chemicall implanted neural electrodes," *J. Neurosci,* vol. 148, pp. 1-18, 2005.

[33] S.-W. Hwang and al., "A Physically Transient Form of Silicon Electronics, With Integrated Sensors, Actuators and Power Supply," *Science,* vol. 337, no. 6102, pp. 1640-1644, 2012.

[34] A. Sorushanova, "The Collagen Suprafamily: From Biosynthesis to Advanced Biomaterial Development," *Advanced Materials,* vol. 31, no. 1801651, pp. 1-39, 2019.

[35] P. Yadav and al., "Biomedical Biopolymers, their Origin and Evolution in Biomedical Sciences: A systematic review," *Journal of Clinical and Diagnostic Research,* vol. 9, no. 9, pp. 21-25, 2015.

[36] S. Canelon and J. Wallace, "β-Aminopropionitrile-Induced Reduction in Enzymatic Crosslinking Causes In Vitro Changes in Collagen Morphology and Molecular Composition," *PLOS ONE,* vol. 11, no. 11, p. e0166392, 2016.

[37] M. Minary and al., "Uncovering Nanoscale Electromechanical Heterogeneity in the Subfibrillar Structure of Collagen Fibrils Responsible for the Piezoelectricity of Bone," *ACS Nano,* vol. 3, no. 7, pp. 1859-1863, 2009.

[38] Z. Zhou and al., "Molecular Mechanism of Polarization and Piezoelectric Effect in Super-Twisted Collagen," *ACS Biomaterials Science & Engineering,* vol. 2, pp. 929-936, 2016.

[39] P. Fratzl, Collagen structure and mechanics, an introduction, in Collagen: Structure and Mechanics, New York: Springer, 2008.

[40] H. Lodish and al., Molecular Cell Biology, New York: Freeman, 2004.

[41] J. Cavallaro and al., "Collagen fabrics as biomaterials," *Biotechnology and Bioengineering,* vol. 43, no. 8, pp. 781-791, 1994.

[42] G. Karp, Cell and Molecular Biology: Concepts and Experiments 5th edition, Hoboken, NJ: John Wiley & Sons, 2007.

[43] J. Anson and E. Marchand, "Bovine Pericardium for Dural Grafts: Clinical Results in 35 Patients," *Neurosurgery,* vol. 39, no. 4, pp. 764-768, 1996.

[44] X. Li and al., "Pericardial patch angioplasty heals via an Ephrin-B2 and CD34 positive cell mediated mechanism.," *PLoS One,* vol. 7, no. 6, p. e38844, 2012.

[45] S. Dimitrijevich, "Pericardial anti-adhesion patch". USA Patent 6599526, 29 7 2003.

[46] A. Thomas and al., "A BRIEF COMMUNICATION : Collagen Fragments Modulate Innate Immunity," *Experimental Biology and Medicine,* vol. 232, pp. 406-411, 2007.

[47] M. Torculas and al., "Protein-Based Bioelectronics," *ACS Biomaterials Science & Engineering,* vol. 2, no. 8, pp. 1211-1223, 2016.

[48] S. Sofia and al., "Functionalized silk-based biomaterials for bone formation," *Journal of Biomedical Materials Resarch,* vol. 54, no. 1, pp. 138-148, 2001.

[49] A. Alves and al., "Study of tensiometric properties, microbiological and collagen content in nile tilapia skin submitted to different sterilization methods.," *Cell Tissue Bank,* vol. 19, pp. 373-382, 2018.

[50] R. Wasylyk, "A valve for saving your heart," Clemson University, 2012. [Online]. Available: http://glimpse.clemson.edu/2366/. [Accessed 2019].

[51] T. Nagai and N. Suzuki, "Isolation of collagen from fish waste material — skin, bone and fins," *Food Chemistry,* vol. 68, no. 3, pp. 277-281, 2000.

[52] G. Chandrakasan and al., "Preparation of Intact Monomeric Collagen from Rat Tail Tendon and skin and the structrue of the nonhelical ends in solution," *Journal of Biological Chemistry,* vol. 251, no. 19, pp. 6062-6067, 1976.

[53] J. Snowden, "Collagen and Method for producing same". Australia Patent WO 03/097694 A1, 27 11 2003.

[54] K. Payne and A. Veis, "Fourier transform ir spectroscopy of collagen and gelatin solutions: Deconvolution of the amide I band for conformational studies," *Biopolymers,* vol. 27, no. 11, pp. 1749-1760, 1988.

[55] N. Camacho and al., "FTIR microscopic imaging of collagen and proteoglycan in bovine cartilage," *Biopolymers,* vol. 62, no. 1, pp. 1-8, 2001.

[56] B. de Campos Vidal and M. Mello, "Collagen type I amide I band infrared spectroscopy," *Micron,* vol. 42, no. 3, pp. 283-289, 2011.

[57] M. Minary and M.-F. Yu, "Nanomechanical heterogeneity in the gap and overlap regions of ypye I collagen fibrils with implications for bone heterogeneity," *Biomacromolecules,* vol. 10, pp. 2565-2570, 2009.

[58] J. Caves and al., "Elastin-like protein matrix reinforced with collagen microfibers for soft tissue repair," *Biomaterials,* vol. 32, no. 23, pp. 5371-5379, 2011.

[59] R. Newnham, Properties of materials: anisotropy, symmetry,structure, Oxford: Oxford University Press, 2005.

[60] X. Huang and al., "Biodegradable Materials for Multilayer Transient Printed Circuit Boards," *Advanced Materials,* vol. 23, pp. 7371-7377, 2014.

[61] Y. Li and al., "RFID Tag and RF Structures on a Paper Substrate Using Inkjet-Printing Technology," *IEEE Transactions on Microwave Theory and Techniques,* vol. 55, no. 12, pp. 2894-2901, 2007.

[62] M. Drack and al., "An Imperceptible Plastic Electronic Wrap," *Advanced Materials,* vol. 27, no. 1, pp. 34-40, 2015.

[63] D. Son and al., "Multifunctional wearable devices for diagnosis and therapy of movement disorders," *Nature Nano,* vol. 9, no. 5, pp. 397-404, 2014.

[64] I. Mejia and M. Estrada, "Characterization ofPolymethyl Methacrylate (PMMA) Layers for OTFTs Gate Dielectric. in Devices, Circuits and Systems," *Proceedings of the 6th International Caribbean Conference,* 2006.

[65] Y. Kato and al., "Mechanical properties of collagen fibres: a comparision of reconstituted and rat tail tendon fibres," *Biomaterials,* vol. 10, no. 1, pp. 38-42, 1989.

[66] M. Wenger and al., "Mechanical Properties of Collagen Fibrils," *Biophysical Journal,* vol. 90, no. 4, pp. 1255-1263, 2007.

[67] S. Moreno and al., "Biocompatible Collagen Films as Substrates for Flexible Implantable electronics," *Advanced Electronic Materials,* no. 1500154, pp. 1-8, 2015.

[68] R. Lakra and al., "Fabrication of homobifunctional crosslinker stabilized collagen for biomedical application," *Biomedical Materials,* vol. 10, no. 6, p. 065015, 2015.

[69] C. Knight and al., "Identification in Collagen Type I of an Integrin α2β1-binding Site Containing an Essential GER Sequence," *Journal of Biological Chemistry,* vol. 273, pp. 33287-33294, 1998.

[70] A. Munnelly and al., "Porcine vena cava as an alternative to bovine pericardium in bioprosthetic percutaneous heart valves," *Biomaterials,* vol. 33, no. 1, pp. 1-8, 2012.

[71] S. MacNeil, "Biomaterials for tissue engineering of skin," *materialstoday,* vol. 11, no. 5, pp. 26-35, 2008.

[72] H. Tao and al., "Silk-Based Conformal, Adhesive, Edible Food Sensors," *Advanced Materials,* vol. 24, no. 8, pp. 1067-1072, 2012.

[73] S. Jin and al., "Water-Soluble Thin Film Transistors and Circuits Based on Amorphous Indium–Gallium–Zinc Oxide," *ACS Applied Materials & Interfaces,* vol. 7, no. 15, pp. 8268-8274, 2015.

[74] S. Jin and al., "Water-Soluble Thin Film Transistors and Circuits Based on Amorphous Indium–Gallium–Zinc Oxide," *ACS Applied Materials & Interfaces,* vol. 7, no. 15, pp. 8268-8274, 2015.

[75] C. Lee and al., "Peel-and-Stick: Mechanism Study for Efficient Fabrication of Flexible/Transparent Thin-film Electronics," *Scientific Reports,* vol. 3, no. 2917, pp. 1-6, 2013.

[76] K. Addae-Mensah and al., "Poly(vinyl alcohol) as a structure release layer for the microfabrication of polymer composite structures," *Journal of Micromechanics and Microengineering,* vol. 17, no. 7, 2017.

[77] T. Sameshima and al., "Poly(vinyl alcohol) as a structure release layer for the microfabrication of polymer composite structures," *Japanese Journal of Applied Physics,* no. 17, pp. N42-46, 2005.

[78] A. Almuslem and al., "Water soluble nano-scale transient material germanium oxide for zero toxic waste based environmentally benign nano-manufacturing," *Applied Physics Letters,* vol. 110, no. 7, p. 074103, 2017.

[79] T. Sameshima and al., "Germanium Oxide Layers Used for Forward Transfer of Electrical Circuits to Foreign Plastic Substrates," *Japanese Journal of Applied Physics,* vol. 44, no. 9A, pp. 6421-6424, 2005.

[80] J. Nam and al., "Transfer Printed Flexible and Stretchable Thin Film Solar Cells Using a Water-Soluble Sacrificial Layer," *Advanced Energy Materials,* vol. 6, no. 21, p. 1601269, 2016.

[81] H. Charkhkar and al., "Development and demonstration of a disposable low-cost microelectrode array for cultured neuronal network recording," *Sensors and Actuators B: Chemical,* vol. 161, no. 1, pp. 655-660, 2012.

[82] R. Chapman and al., "Quantum Confinement and Interface States in ZnO Nanocrystalline Thin-Film Transistors," *IEEE Transactions on Electron Devices,* vol. 65, no. 5, pp. 1787-1795, 2018.

[83] A. Garcia-Sandoval and al., "Chronic softening spinal cord stimulation arrays," *Journal of Neural Engineering,* vol. 15, no. 045002, pp. 1-17, 2018.

[84] S. Gorgieva and V. Kokol, "Collagen- vs. Gelatine-Based Biomaterials and Their Biocompatibility: Review and Perspectives," in *Biomaterials Applications for Nanomedicine*, IntechOpen, 2011, p. DOI: 10.5772/24118.

[85] S. Gao and al., "Comparison of glutaraldehyde and carbodiimides to crosslink tissue engineering scaffolds fabricated by decellularized porcine menisci," *Materials Science and Engineering C*, no. 71, pp. 891-900, 2017.

[86] C. Grover and al., "Crosslinking and composition influence the surface properties, mechanical stiffness and cell reactivity of collagen-based films," *Acta Biomaterialia*, no. 8, pp. 3080-3090, 2012.

[87] S. Jus and al., "Cross-linking of collagen with laccases and tyrosinases," *Materials Science and Engineering C*, vol. 31, no. 5, pp. 1068-1077, 2011.

[88] A. Toricai and H. Shibata, "Effect of ultraviolet radiation on photodegradation of collagen," *Journal of Applied Polymer Science*, vol. 73, no. 7, pp. 1259-1265, 1999.

[89] J. Labout, "Gamma-radiation in Collagen Solutions Influence of Solutes on the Gelatin Dose," *International Journal of Radiation Biology*, vol. 21, no. 5, pp. 483-492, 1972.

[90] D. Cheung and al., "Mechanism of Crosslinking of Proteins by Glutaraldehyde III . Reaction With Collagen in Tissues," *Connective Tissue Research*, vol. 13, no. 2, pp. 109-115, 1984.

[91] Z. Zhou and al., "A simulation study on the significant nanomechanical heterogeneous properties of collagen," *Biomechanics and Modeling in Mechanobiology*, vol. 14, no. 3, pp. 445-457, 2015.

[92] L. Hapach and al., "Manipulation of in vitro collagen matrix architecture for scaffolds of improved physiological relevance," *Physical Biology*, vol. 12, no. 061002, 2015.

[93] W. Neethling, "Sterilzation process". USA Patent US20160287748A1, 6 10 2016.

[94] L. Castaneda and al., "Collagen Cross-Linking with Au Nanoparticles," *Biomacromolecules*, vol. 9, no. 12, pp. 3383-3388, 9 Biomacromolecules 2008.

[95] J. Coates, "Interpretation of Infrared Spectra, A Practical Approach," in *Encyclopedia of Analytical Chemistry*, Hoboken, John Wiley & Sons, 2006, pp. 1-23.

[96] M. Shoulders and R. Raines, "Collagen Structure and Stability," *Annual Review of Biochemistry,* no. 78, pp. 929-958, 2009.

[97] F. Motta and al., "DEGRADATION OF TYPE I COLLAGEN AND PATHOGENESIS OF INFECTIOUS DISEASES," in *Type I Collagen: Biological Functions, Synthesis and Medicinal Applications*, Hauppauge, Nova Publishers, 2012, pp. 1-26.

[98] Y.-Z. Zhang and al., "Diversity, Structures, and Collagen-Degrading Mechanisms of Bacterial Collagenolytic Proteases," *Applied and Environmental Microbiology*, vol. 81, no. 18, pp. 6098-6107, 2015.

[99] S. Han and al., "Molecular Mechanism of Type I Collagen Homotrimer Resistance to Mammalian Collagenases," *Journal of Biological Chemistry,* vol. 285, no. 29, pp. 22276-81, 2010.

[100] H. Van Wart, "Clostridium collagenases," in *Handbook of Proteolytic Enzymes 2nd edition,* London, Elsevier, 2004, pp. 416-419.

[101] "Power Diodes and Rectifiers," Electronics Tutorials, [Online]. Available: https://www.electronics-tutorials.ws/diode/diode_5.html.

[102] M. Ebrahimian and al., "Enhanced RF to DC CMOS rectifier with capacitor-bootstrapped transistor," *Proceedings of 2010 IEEE International Symposium on Circuits and Systems,* no. 11463389, 2010.

[103] S. life.augmented, "AN2866 Application note: How to design a 13.56 MHz customized antenna," ST, 2019.

[104] J. Zhang and al., "Flexible indium–gallium–zinc–oxide Schottky diode operating beyond 2.45 GHz," *Nature communications*, vol. 6, no. 7561, pp. 1-7, 2015.

[105] G. Snibson and al., "Collagen cross-linking: a new treatment paradigm in corneal disease - a review," *Clinical Experimental Ophthalmol,* vol. 38, no. 2, pp. 141-53, 2010.

[106] M. Applegate and al., "Photocrosslinking of Silk Fibroin Using Riboflavin for Ocular Prostheses," *Advanced Materials,* vol. 28, no. 12, pp. 2417-20, 2016.

BIOGRAPHICAL SKETCH

A Dallas, Texas native, hailing from local schools Science and Engineering Magnet and UT Dallas (BS' 2014), Salvador continued as a mechanical engineer (MS' 2015) for his graduate career. In 2015, Salvador was accepted into the PhD program in Mechanical Engineering at The University of Texas at Dallas. In the same year, Salvador was the recipient of the National Science Foundation Graduate Research Fellowship and the McDermott Graduate Fellowship for the work in this dissertation on collagen-substrate based flexible electronics.

During the doctorate program, Salvador additionally received an NSF GROW (Graduate Research Opportunities Worldwide) award in collaboration with the Science Foundation of Ireland (SFI) to study in Dublin with a focus on collagen derived from fish scales. Additionally, he was awarded an internship at NanoRanch under the NSF GOALI program to study manufacturing.

CURRICULUM VITAE

Salvador Moreno

PhD Candidate

Department of Mechanical Engineering

University of Texas at Dallas

800 W Campbell Road

Richardson, TX 75080

Education:

2015-2019 (Expected)PhD. in Mechanical Engineering

The University of Texas at Dallas, Richardson, TX

Concentration: Manufacturing and Design Innovation

Nanobio Lab

Advisor: Dr. Majid Minary

Research Topic: Collagen films as Substrates for Flexible Implantable Electronics

2014-2015 M.S. in Mechanical Engineering

The University of Texas at Dallas, Richardson, TX

Concentration: Manufacturing and Design Innovation

GPA: 3.84

2010-2014 B.S. in Mechanical Engineering

The University of Texas at Dallas, Richardson, TX

Capstone Project: Design, Development, and Manufacturing of a Micro-Tensile Tester for In Situ AFM/Optical Microscopy Applications

GPA: 3.86

Work Experience:

2018-2019 NSF INTERN

NANORanch/UHV Technologies, Fort Worth, TX

- Collaboration in 3D printing, metal manufacturing, electrochemistry

2017-2018 NSF GROW/ SFI Marie Skłodowska-Curie Fellow

University College Dublin, Dublin, Ireland

- Research in biomaterials, tissue culturing, cell assays, Piezoelectric force microscopy,

2015-2019 NSF Graduate Research Fellow

The University of Texas at Dallas, Richardson, TX

- Research in nanofibers, nanomaterials, biomaterials and flexible electronics

2014-2015 Teacher Assistant

The University of Texas at Dallas, Richardson, TX

- Statics and Dynamics

2010-2014 Tutor, Academic Bridge Program

The University of Texas at Dallas, Richardson, TX

- Algebra-Calculus III, Differential Equations, Linear Algebra, Chemistry, Physics

Publications:

1. Yang, E, Xu, Z, Baniasadi, M, Moreno, S., Yi, H., Di, J., Baughman, R., Minary, M., Tensile fatigue behavior of single carbon nanotube yarns, J Mater Sci (2018), pp 1-7

2. Serna, M.I., Hasan, S. M. N., Nam, S., El Bouanani, L., Moreno, S., Choi, H., Alshareef, H., Minary-Jolandan, M., Quevedo-Lopez, M.A., Low-Temperature Deposition of Layered SnSe2 for Heterojunction Diodes, Adv. Mater. Interfaces 2018, 1800128

3. Morsali, S., Daryadel, S., Zhou, Z., Behroozfar, A., Baniasadi, M., Moreno, S., Qian, D., and Minary-Jolandan, M., Multi-physics simulation of metal printing at micro/nanoscale using meniscus-confined electrodeposition: Effect of nozzle speed and diameter, Journal of Applied Physics, 2017, 121, 214305

4. Yang, E., Xu, Z., Chur, L., Behroozfar, A., Baniasadi, M., Moreno, S., Huang, J., Gilligan, J., and Minary-Jolandan, M., Nanofibrous Smart Fabrics from Twisted Yarns of Electrospun Piezo Polymer, ACS Applied Materials Interfaces, 2017, 9(28):24220-24229

5. Huang, J., Xu, Z., Moreno, S., Morsali, S., Zhou, Z., Daryade, S., Baniasadi, M., Qian, D., Minary-Jolandan, M., Lamellar Ceramic Semicrystalline-Polymer Composite Fabricated by Freeze Casting, Advanced Engineering Materials, 2017:1700214

6. Baniasadi, M., Xu, Z., Moreno, S., Daryadel, S., Cai, J., Naraghi, M., Minary-Jolandan. M., Effect of thermomechanical post-processing on chain orientation and crystallinity of electrospun P(VDF-TrFE) nanofibers, Polymer, 118:223-235

7. Daryadel, S., Behroozfar, A., Morsali, S.R., Moreno, S., Baniasadi, M., Bykova, J., Bernal, R.A., and Minary-Jolandan, M., Localized Pulsed Electrodeposition Process for Three-Dimensional Printing of Nanotwinned Metallic Nanostructures, Nanoletters, 18: 208-214

8. Behroozfar, A., Daryadel, S., Morsali, S.R, Moreno, S., Baniasadi, M., Bernal, R.A., Minary Jolandan, M., Microscale 3D Printing of Nanotwinned Copper, Advanced Materials, 2018, 30:1705107

9. Xu, Z., Bykova, J., Baniasadi, M., Moreno, S., Zhou, Z., Das, N., Bandi, S., Xi, Y., Qian, D., Baughman, R. H. and Minary-Jolandan, M. Bioinspired Multifunctional Ceramic Platelet-Reinforced Piezoelectric Polymer Composite. Advanced Engineering Materials, 2016,

10. Xu, Z., Baniasadi, M., Moreno, S., Cai, J., Naraghi, M., Minary-Jolandan, M., Evolution of electromechanical and morphological properties of piezoelectric thin films with thermomechanical processing, Polymer, 2016, 106: p. 62-71

11. Serna, M. I., Moreno, S., Higgins, M., Choi, H., Minary-Jolandan, M. and Quevedo-Lopez, M. A. Growth parameter enhancement for MoS2 thin films synthesized by pulsed laser deposition. Physica Status Solidi C, 2016, p. 1-7

12. Serna, M., Yoo, S., Moreno, S., Xi, Y., Oviedo, J., Choi, H., Alshareef, H., Kim, M., Minary-Jolandan, M., and Quevedo-Lopez, Q., Large-Area Deposition of MoS2 by Pulsed Laser Deposition with In Situ Thickness Control, ACS Nano, 2016, 10 (6): p. 6054-6061

13. Moreno, S., Baniasadi, M., Mohammed, S., Mejia, I., Chen, Y., Quevedo-Lopez, M., Kumar, N., Dimitrijevich, D., & Minary-Jolandan, M., Biocompatible Collagen films as Substrates for Flexible Implantable Electronics, Advanced Electronic Materials, 2015, 1 (9)

14. Baniasadi, M., Huang, J., Xu, Z., Moreno, S., Yang, X., Chang, J., Quevedo-Lopez, M., Naraghi, M., & Minary-Jolandan, M., High-Performance Coils and Yarns of Polymeric Piezoelectric Nanofibers, ACS Applied Materials Interfaces, 2015, 7 (9): p. 5358-536

15. Hernandez-Como, N., Moreno, S., Mejia, I., Quevedo-Lopez, M., Low-temperature processed ZnO and CdS photodetectors deposited by pulsed laser deposition, Semiconductor Science and Technology, 2014, 29 (085008)

Under Preparation

Moreno, S., Keshtkar, J., Rodriguez Davila, R.A., Bazaid, A., Mejia, I., Rodriguez, B., Dimitrijevich, S., Quevedo-Lopez, M., Minary-Jolandan, M., Biocompatible Integrated Electronics onto Collagen by Transfer Printing

Presentations:
Salvador Moreno, Biocompatible Integrated Electronics by Transfer Printing onto Collagen, Gordon Research Conference: Frontiers of Science, Ventura CA, January 14-19, Poster

Salvador Moreno, Biocompatible Integrated Electronics by Transfer Printing onto Collagen, 2018 Materials Research Society Spring Meeting, Phoenix AZ, April 1-5, Oral

Moreno, S., Baniasadi, M., & Minary-Jolandan, M., (2015)," Biocompatible Collagen films as Substrates for Flexible Implantable Electronics"2015 ASME IMECE, Houston, TX, (Technical Presentation. IMECE2015-52069)

Moreno, S., Baniasadi, M., Mohammed, S., Mejia, I., Chen, Y., Quevedo-Lopez, M., Kumar, N., Dimitrijevich, D., & Minary-Jolandan, M., Collagen Films as Substrate for Flexible Implantable Electronics, 2015 Society of Engineering Science Annual Technical Meeting, College Station, TX, (Poster Presentation)

Moreno, S., Keshtkar, J., Rodriguez Davila, R.A., Bazaid, A., Mejia, I., Rodriguez, B., Dimitrijevich, S., Quevedo-Lopez, M., Minary-Jolandan, M., Biocompatible Integrated Electronics onto Collagen by Transfer Printing, 2018 ASME IMECE Conference, Pittsburgh, PA Technical Presentation

Activities and Awards

- Fellow, National Science Foundation Graduate Research (2015-present)
- Fellow, Eugene McDermott Graduate Fellow Program (2015-present)
- Fellow, NSF GROW/ SFI Marie Skłodowska-Curie Fellow (2017-2018)
- Fellow, Carl Storm Underrepresented Minority Program (GRC) (2017)
- Student Member, Phi Kappa Phi Honor Society
- Member, American Chemistry Society (ACS)
- Student Member, American Society for Mechanical Engineering (ASME)
- Student Member, Society of Hispanic Professional Engineers (SHPE)
- Student Member, Academic Bridge Program
- Academic Excellence Scholarship (2010-2014)
- Certificate of Academic Achievement in Mechanical Engineering (2014)
- 2nd place in UT Design Senior Student competition